



CHALMERS



Modelling of dynamic track forces generated by tram vehicles

Master Thesis in Applied Mechanics

EJDER EKEN

ROBERT FRIBERG

Department of Applied Mechanics
Division of Dynamics
CHALMERS UNIVERSITY OF TECHNOLOGY

Master Thesis

Modelling of dynamic track forces
generated by tram vehicles

EJDER EKEN
ROBERT FRIBERG

Department of Applied Mechanics
Division of Dynamics
CHALMERS UNIVERSITY OF TECHNOLOGY
Gothenburg, Sweden 2015

Modelling of dynamic track forces generated by tram vehicles.
EJDER EKEN
ROBERT FRIBERG

© EJDER EKEN
ROBERT FRIBERG, 2015

Master's Thesis 2015:75
ISSN 1652-8557
Department of Applied Mechanics
Division of Dynamics
Chalmers University of Technology
SE-412 96 Göteborg
Sweden
Telephone: +46(0)31-722 1000

Cover:
Tram models M31(to the right) and M32 (to the left) at Rantorget in Gothenburg, Sweden

Printing: Chalmers University of Technology
Gothenburg, Sweden 201

Abstract

Analysis of dynamic train-track interaction is a significant and fundamental ingredient in many railway engineering sub-disciplines. Examples of consequences of the dynamic interaction are track forces, derailment risk, curving behaviour, wear/fatigue on wheels and track, vibrations and noise, ride comfort and motion sickness. Due to the increasing amount of tram operations in the city of Gothenburg, the need for simulation models to improve the understanding of these issues has been identified by Trafikkontoret (TK, in charge of infrastructure) and Göteborgs Spårvägar (GS, in charge of rolling stock).

The task of this thesis project is to develop a dynamic model of the interaction between tram and track using the train-track interaction software GENSYS. In more detail, the purpose is to achieve useful models that later can be used to study effects of different combinations of vehicle and rail parameters and how these affect the dynamic track forces. After consultation with TK and GS it was decided that the work should focus on modelling the behaviour of the two most recent trams (M31 from ABB and M32 from AnsaldoBreda) in sharp curves on grooved rails.

Validation is an important part of the project in order to verify that the models built in GENSYS agree with the actual behaviour in field. One validation case is included in the project and was performed as part of the thesis work.

The studies show that the GENSYS models seem to capture the dynamic behaviour of the trams. Tram model M32 has a stiffer bogie design compared to tram model M31. This leads to higher magnitudes of track forces, especially in the lateral direction. When negotiating a curve, the wheels of the leading bogie of M32 oscillate in the lateral direction, creating a lateral “hammering” force on the rail affecting ride comfort and wear. An overall conclusion is that the bogie design is a key element influencing the magnitude of the dynamic track forces.

Parameter studies are performed to investigate and compare the performance of the different tram vehicles and to investigate the influence of various design, maintenance and operational parameters, such as primary and secondary suspension stiffness, passenger load, wheel and rail profiles and vehicle speed. The analyses are limited to small radius curves, which have been identified as a key problem area by TK and GS.

In future work, it is suggested to use the models in GENSYS to predict wheel and rail wear and to optimise the primary and secondary suspensions to reduce track forces and improve ride comfort. The curving noise is also a well-known problem in Gothenburg. This could be investigated as a follow-up study in which the curving behaviour obtained from GENSYS is used as input to a separate noise calculation model.

Keywords: tram, dynamic model, track, Gothenburg, M31, M32, GENSYS, track forces

Preface

This thesis work is the final part of our Master of Science degree. The work has been carried out in cooperation with ÅF, Göteborgs Spårvägar and Trafikkontoret in Gothenburg. The thesis work of 30 credit points is one part of the Masters Program Applied Mechanics at Chalmers University of Technology.

We would like to thank Florencio Garcia at Göteborgs Spårvägar for his time participating in this thesis work. His good support and assistance has been an enormous help in providing input data and arranging access to vehicles and measurements.

We would also like to thank Ingemar Persson at DEsolver for his support and guidance on the modelling work. We are grateful for the quick answers to the obstacles met during the project.

Thanks to Robert Ström at ÅF who carried out the validation measurements at Rantorget.

Thanks to Dr Rickard Nilsson at SL for providing us with the Miniprof rail measuring equipment used during the thesis work and for valuable inputs and discussions.

We would also like to thank Mats Larsson at Trafikkontoret, who initiated the work and for his continued support during the study.

We would like to thank our examiner Professor Jens Nielsen for inputs and finally our supervisor at ÅF Dr Anders Frid for his involvement and his belief in this work.

We wish you all a pleasant and interesting reading.

Göteborg, June 2015

Ejder Eken
Robert Friberg

Glossary

A34:	A low floor tram vehicle operating in Stockholm. Built by Bombardier in-between years 2006-2011.
AnsaldoBreda:	AnsaldoBreda is an Italian rail transport engineering company. AnsaldoBreda develops and produces tram vehicles. One of their models is operating in Gothenburg.
ASEA/ABB:	ASEA/ABB is an engineering company, operating in robotics, power and automation technology areas. They have developed and constructed at least one of the tram models operating in Gothenburg.
Bogie:	A frame under the vehicle car body. It consists of one or more wheel sets and suspension components.
Bombardier:	Bombardier is a Canadian-based multinational aerospace and transport company. Bombardier develops and produces tram vehicles. At least one of their model is operating in Stockholm
CAD:	Computer-aided design. A computer software used for creating, modifying and constructing mechanical components.
Cg:	Centre of gravity. The centre of mass for a component.
Dof:	Degrees of freedom. The number of independent variables needed to describe a component's position.
GENSYS:	A software program used for modelling three-dimensional general multibody-dynamic problems.
GS:	Göteborgs spårvägar is the tram operator in Gothenburg city and is in charge of the rolling stock.
High-pass filter:	An electronic filter that allows signals with a frequency higher than a given value to pass.
Low-pass filter:	An electronic filter that allows signals with a frequency lower than a given value to pass.
M31:	A tram model originally delivered by ASEA/ABB in 1984-1992 as a two-car tram called M21. The model was rebuilt to its current form in 1998-2003 and renamed M31. The model consists of three car bodies, two motor bogies and two trailer bogies.

M32:	An Italian low floor tram model delivered by AnsaldoBreda in 2004-2012. The model consists of five car bodies, two motor bogies and one trailer bogie.
MATLAB:	MATLAB is a computer software used for calculations, visualization and calculations.
MiniProf:	A mechanical device to measure wheel and rail profiles.
ODE:	Ordinary differential equation. An equation consisting of a function of one independent variable and its derivative.
Pitch:	A rotational movement about the lateral direction.
Primary coupling:	Components connecting bogie and wheel sets, transferring loads.
Roll:	A rotational movement about the longitudinal direction.
Secondary coupling:	Components connecting car body and bogie, transferring loads.
SIMPACK:	A general multi-body simulation software used for dynamic analysis of mechanical systems, for example tram vehicles.
SP:	Sveriges Provnings- och Forskningsinstitut. SP is a research institute conducting technical studies, research and investigations.
Trafikkontoret:	Trafikkontoret is an infrastructure administration office for the city of Gothenburg.
Trelleborg AB:	Trelleborg AB is Swedish company that specializes in designing and manufacturing of elastic suspension components.
Yaw:	A rotational movement about the vertical direction.

List of notations

A table of notations used in this thesis work is presented below.

Symbol	Significance	Units
a	acceleration	m/s^2
a	length	m
A	area	m^2
b	width	m
c	viscous damping	Ns/m
C	damping matrix	
d	diameter	m
D	diameter	m
E	Young's modulus	N/m^2
E_r	error ratio	
f_0	frequency	$1/\text{s}$
F	force	N
F	force matrix	
g	gravitational acceleration	m/s^2
G	shear modulus	N/m^2
h	time step	s
H	height	m
I	unit matrix	
J	mass moment of inertia	kgm^2
J	Jacobian matrix	
k	stiffness	N/m
K	stiffness matrix	
l	spring length	m
L	length	m
m	mass	kg
M	moment	Nm
M_y	flexibility value	Nm/rad
M	mass matrix	
n	step number	
Q	vertical contact force between wheel and rail	N
R	wheel radius	m
S_r	steering ratio	
t	time	s
v	speed	m/s
v_z	speed	m/s
W_{el}	The total stored elastic energy	Nm
W_u	external work	Nm
X	longitudinal coordinate direction	
Y	lateral coordinate direction	
Z	vertical coordinate direction	

Symbol	Significance	Units
α	angle between lateral direction and car body	rad
β	angle between lateral direction and lower frame	rad
β	geometrical constant	
β	flange angle	rad
Δ	difference	
ζ	ratio of critical damping	
λ	coil angle	rad
μ	friction coefficient	
ν	Poisson's ratio	
ρ	density	kg/m ³
φ	roll	rad
χ	pitch	rad
ψ	yaw	rad

Table of Contents

Abstract	I
Preface	III
Glossary	V
List of notations	VII
1. Introduction	1
1.1 Background	1
1.2 Purpose	1
1.3 Research questions	2
1.4 Limitations	2
1.5 Description of the tram models	2
1.5.1 Tram vehicle M31	2
1.5.2 Tram vehicle M32	6
2. Theory	8
2.1 Literature study	8
2.2 The curving behaviour of tram models M31 and M32	9
2.2.1 Tram vehicle M31	10
2.2.2 Tram vehicle M32	12
2.3 The software GENSYs	14
2.3.1 Two-dimensional mathematical model	14
2.3.2 Time-domain integrator	16
2.3.3 Wheel and rail contact model	19
3. Methods	21
3.1 Modelling description	21
3.1.1 Types of couplings used in the GENSYs modelling	22
3.1.2 Tram model M31	24
3.1.3 Tram model M32	25
3.2 Debugging of the vehicle models	26
3.2.1 Graphical check	26
3.2.2 Check of abnormal data	26
3.2.3 Time-domain integration check	26
3.2.4 Stability check	26
4. Field measurements and validation	27

4.1	MiniProf wear measurements on tram wheels and rails.....	27
4.2	Validation of tram models	29
5.	Results	36
5.1	Parameter study	36
5.1.1	Nominal dynamic track forces	36
5.1.2	Comparison of track forces for worn and nominal profiles	44
5.1.3	Influence of M31 car body on wheel set misalignment angle.....	50
5.1.4	Empty and fully loaded tram vehicle	52
5.1.5	Primary springs stiffnesses.....	57
5.1.6	Secondary suspension stiffnesses.....	59
5.1.7	Derailment study	61
5.1.8	Track forces as function of vehicle speeds and curve radii.....	62
5.1.9	Nominal wheel profiles used on tram vehicle A34 in Stockholm.....	65
6.	Discussion	71
6.1	Modelling.....	71
6.2	Validation	72
6.3	Results	73
7.	Conclusions and future work.....	74
	References	77
	Appendices	

1. Introduction

In this chapter an introduction of the thesis will be presented, which includes a background followed by the purpose of the project. Furthermore, research questions and established limitations of the project will be presented. Finally the tram vehicles treated in this thesis work will be described.

1.1 Background

Trams are the oldest and most common way of public transportation in Gothenburg. The Gothenburg city tram network has existed since 1879. In the beginning, the tram vehicles were horse-drawn and in 1902 the first electrical trams were introduced. Since then many different tram models have been operated in the city [1]. The two newest are the tram vehicles M31 and M32. The older of these two, M31 is a Swedish design tram model originally delivered by ASEA/ABB as a two-car vehicle in the years 1984-1992. The model was later rebuilt to its current three-car form and was delivered in-between years 1998-2003. In year 2004 the city invested in a new tram model called M32. The vehicle is an Italian tram model delivered by AnsaldoBreda during the years 2004-2012 [2]. These two tram models will be treated in this master thesis work.

At present time there are various problems with the models M31 and M32 regarding dynamic train-track interaction that are of high importance. Analysis of dynamic train-track interaction is a significant and fundamental ingredient in many railway engineering sub-disciplines. Examples of consequences of the dynamic interaction are track forces, derailment risk, curving behaviour, wear/fatigue on wheels and track, vibrations and noise, ride comfort and motion sickness. Understanding of the dynamic train-track interaction is thus a prerequisite for solving and mitigating these consequences for an improved system performance.

Today, there is a lack of computer aided models at Trafikkontoret (TK, in charge of infrastructure) and Göteborgs Spårvägar (GS, in charge of rolling stock) for the prediction of dynamic behaviour of trams. Due to the increased amount of tram operations in the city the need for a method dealing with these issues was identified and GENSYS [3] seen as a potential software tool for this purpose.

1.2 Purpose

The task is to develop dynamic models of the interaction between a tram and rail for vehicles M31 and M32. This will be done by using the train-track interaction software GENSYS. In more detail, the purpose is to achieve useful baseline models that can later be used to study effects of different combinations of vehicle and rail parameters and how these affect the dynamic track forces. The dynamic models are an important step for clarifying existing problems with the tram vehicles and evaluating methods to solve them.

1.3 Research questions

The questions that will be answered in this thesis are the following:

- Is there enough input data available to develop the dynamic tram-track interaction models?
- Can a model in the train-track interaction software GENSYS be built and adjusted to represent the real vehicles M31 and M32?
- Is there any difference in dynamic behaviour between the model M31 and M32?
- What can the dynamic tram models be used for in further studies?

1.4 Limitations

There are four tram models operating in Gothenburg city today. The tram models M31 and M32 will only be analysed in this project. The reason for this is that these are the two newest and most relevant. The older ones, M28 and M29, are expected to be phased out in a few years from now. Also, the M31 and M32 vehicles are the ones Göteborgs spårvägar has the most problems with.

The studies and validations in this report will only treat simulations of curves with small curve radius and grooved street rails as this was identified as a high priority case in early discussions with TK and GS.

There are different computer software that can be used to build the tram vehicle models. Some of these railway engineering software are GENSYS, DIFF, NUCARS and VAMPIRE. Also general software as ADAMS and SIMPACK have railway modules [4]. In this project the tram vehicles will only be modelled with the software GENSYS [3].

1.5 Description of the tram models

In this subchapter, detailed descriptions of the tram models M31 and M32 will be presented. The components that are necessary for the modelling are described in more in detail. This is significant to understand before explaining the modelling work. The wheel profiles of the two tram models and rail profile are presented and discussed in *Appendix 1*.

1.5.1 Tram vehicle M31

Tram model M31 consists of three car bodies as can be seen in figure 1.1 below. The middle part has a low floor while the other parts have high floors. It is possible to walk through from one car to another.

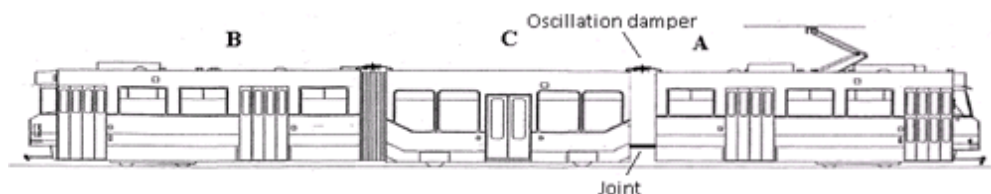
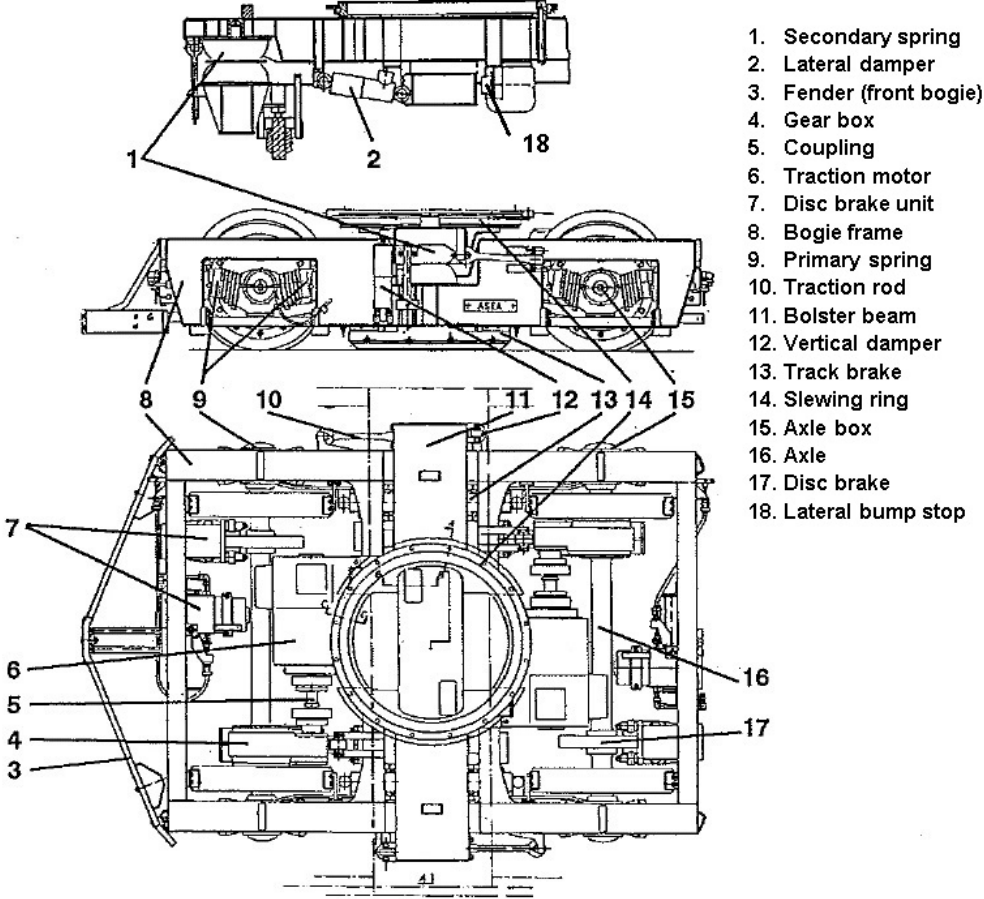


Figure 1.1 – Tram model M31. The bellow between car body A and car body C is taken off to show principle sketches of the joint and oscillation damper.

The car bodies are coupled together by a joint and a lateral oscillation damper, which are also illustrated in figure 1.1. The joint is constructed such that it can carry loads also in the vertical direction and is constrained so that only a rotation about the vertical direction is possible. The oscillation damper is mounted on the roof to prevent large difference in lateral movement of the cars relative to each other.

Car bodies A and B are resting on car body C by the joints. Furthermore, the car bodies are resting on two motor bogies and two trailer bogies. The tram is driven by the motor bogies, one under each car body A and B. A detailed illustration of the motor bogie is presented in figure 1.2 below. The following text with numbers included will refer to figure 1.2.

The motor bogie consists of a framework (8) with four wheels and two axles (16) driven by two traction (electric) motors (6). The bogie controls the movements of the car body and will be explained here. The slewing ring (14) is attached to the car body and allows yaw rotation between the bogie and the car body but transfers loads to the bolster beam (11) in all other directions.



- 1. Secondary spring
- 2. Lateral damper
- 3. Fender (front bogie)
- 4. Gear box
- 5. Coupling
- 6. Traction motor
- 7. Disc brake unit
- 8. Bogie frame
- 9. Primary spring
- 10. Traction rod
- 11. Bolster beam
- 12. Vertical damper
- 13. Track brake
- 14. Slewing ring
- 15. Axle box
- 16. Axle
- 17. Disc brake
- 18. Lateral bump stop

Figure 1.2 – Representation of components attached to the motor bogie. The figure is copied from [5].

There is one secondary spring (1) of the type hour glass spring on each side of the bogie. The springs are capable of handling loads in all directions. These are coupled between the bogie frame and the bolster beam. The task of the secondary springs is to transfer the loads smoothly from the bolster beam to the bogie frame. There is also one traction rod (10) and one hydraulic vertical damper (12) on each side of the bogie that are coupled between the bolster beam and bogie frame. The rods are placed in the longitudinal direction so that yawing motion of the beam is decreased. The vertical damper decreases the large vertical loads from the car body in order to protect the secondary springs from shock loads and also reduces the rolling movement of the car body. One hydraulic lateral damper (2) is also placed to reduce shock loads in the lateral direction and restrain the lateral movement of the bolster beam. Additionally a lateral bump stop (18) is placed to restrict the lateral movement of the bolster beam and hence the car body.

The bogie frame is coupled to the two axles via primary springs (9) and axle boxes (15). There are four primary springs called chevron springs. These springs are capable of handling loads in all directions and they also have damping effects.

In summary, the forces that arise from the weight of the car bodies are transferred by the slewing ring to the bolster beam and then to the bogie frame by the secondary springs. The loads are then transferred to the tracks by the primary springs and wheel sets. An illustration of a wheel set can be seen in figure 1.3.

There are four wheels in a motor bogie and they are constructed with a wheel ring and a hub. A stiff rubber ring is mounted in between, which gives a damping effect and decreases the wheel squeal. All the wheels in the tram model have the same nominal profile. The difference is that the wheels in the motor bogies have a diameter of 680 mm while the wheels under car body C have a diameter of 590 mm [5]. These are nominal wheel diameters, which mean that there is no wear. The profile of the wheels is an important factor in the modelling and is described more in detail in *Appendix 1*.

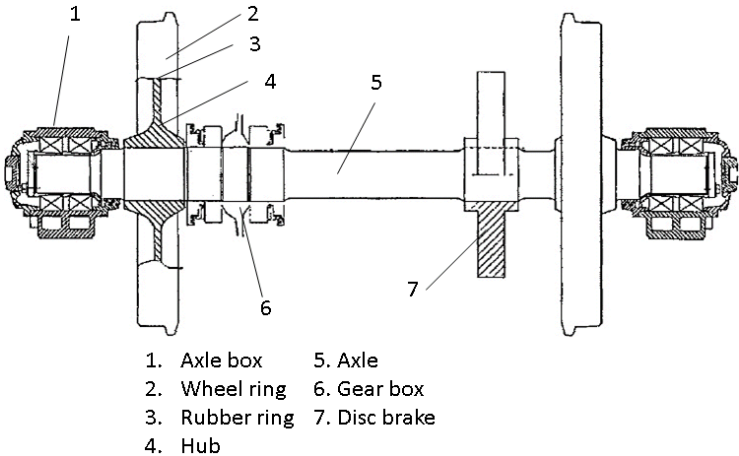


Figure 1.3 – Wheel set on the motor bogie [5].

Car body C is resting on two trailing bogies without driving equipment such as motors and gear boxes. A detailed illustration of the trailer bogie is shown in figure 1.4. The wheel sets are specially constructed in this case. A frame (9) with four secondary springs (1), two hydraulic vertical dampers (3), two traction rods (4), one hydraulic lateral damper and two anti-pitch bars (2) are connected to the car body. This frame is connected to a lower frame (8) by a coupling (10). This coupling only allows yaw rotation between the frames relative to each other. This is a type of a stiff slewing ring.

The wheels are connected to the lower frame (8) by stiff primary springs and are not connected by an axle. The wheels can rotate freely independent of each other, unlike the wheel sets under car bodies A and B, where the rotation of the wheels are constrained by the axles.

For this particular case, the secondary springs are coil springs and have helical structures with circular threads. The vertical dampers have the same functions as before. The anti-pitch bars are constructed such that the pitch movement of the car body is restrained. It should be noted that nothing is fully constrained in reality, hence a minor movement will occur. There are also lateral bump stops (7) to restrict the lateral movement of the car body. The wheel sets are coupled by a mechanical coupling (5) to car bodies A and B. The steering of the wheels is mechanically controlled by car body A or B. See *Appendix 2* for a more detailed description.

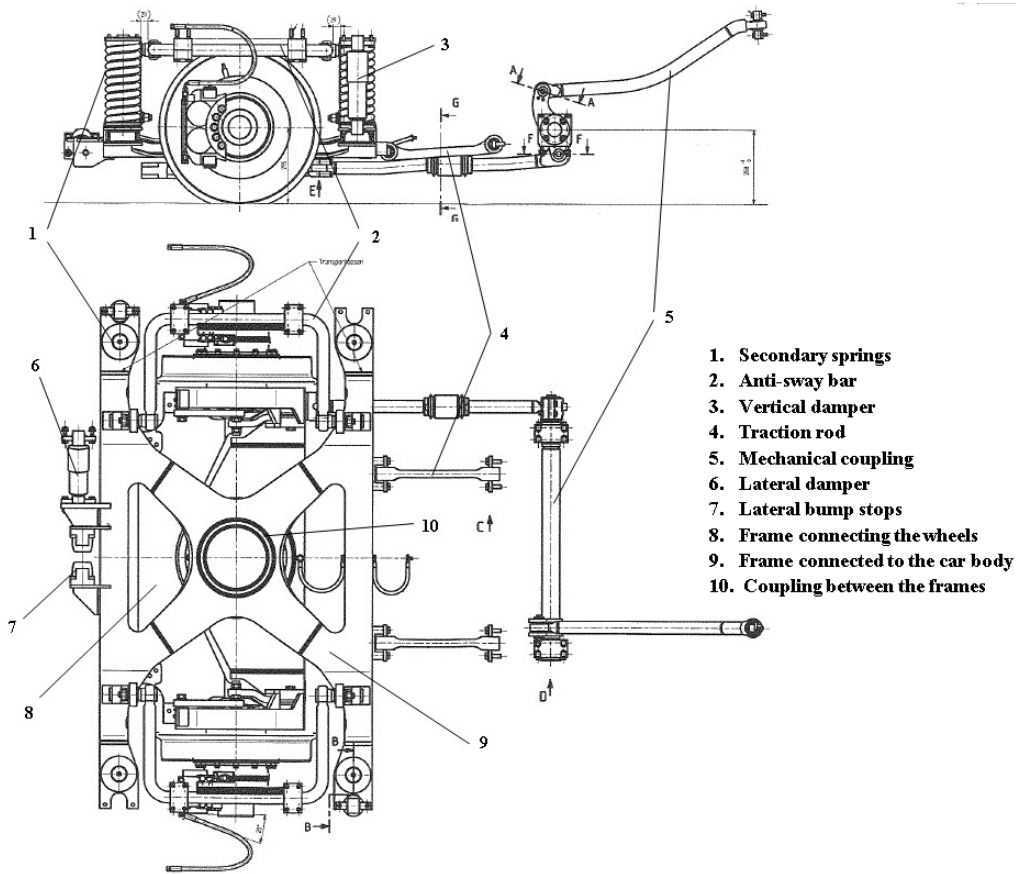


Figure 1.4 – One of the trailer bogies under car body C.

1.5.2 Tram vehicle M32

Tram model M32 was manufactured by the Italian company AnsaldoBreda and was delivered to GS with start in year 2004. The model consists of five car bodies as can be seen in figure 1.5 below. This construction will reduce the sweep surface of the car bodies in the traffic when negotiating a curve compared to M31. All the car bodies have low floors and it is possible to walk through from one car to another.

The car bodies have been labelled from A to E, where A is the front car and E the last car. The car bodies are coupled together with two joints, an illustration is shown in figure 1.5.

The joints are constructed such that they can carry loads also in the vertical direction and are constrained so that only a rotation about the vertical direction (yaw) is possible. Car body B is resting on car bodies A and C by these joints while car body D is resting on car bodies C and E. Furthermore, the car bodies A and E are resting on motor bogies, while car body C is resting on a trailer bogie, which will be explained in detail in the following pages.

The tram is driven by the motor bogies under car bodies A and E. A detailed illustration of this bogie is presented in figure 1.6. The following text with numbers included refers to figure 1.6. The car bodies are resting on the secondary springs (1), which are attached between bogie and car body. The secondary suspension in the motor bogies were originally coil springs but these were changed to cylindrical rubber blocks to reduce high lateral accelerations at the front and rear ends of the tram [6].

Furthermore, there are four hydraulic vertical dampers (5), two hydraulic lateral dampers (2) and two hydraulic longitudinal dampers (8). In short, the vertical dampers will reduce the roll and pitch movement of the car body and the longitudinal dampers will reduce the yawing movement of the car body. However as explained before, the main task of the dampers is to control and reduce the shock loads that can appear on the springs while the tram is in motion.

The primary springs (3) for this tram model differs from the ones in the tram model M31. The springs consist of cylindrical rubbers. There are a total of eight primary springs on each bogie,

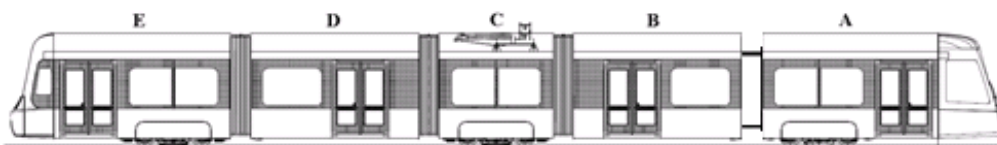


Figure 1.5 – Tram model M32. The bellow between car body A and car body B is taken off to show principal sketches of the joint.

The wheels are individually attached to a beam (12) with a stiff journal box (11) and can freely rotate relative to each other. One motor (4) controls two wheels by an axle (10). The transmission of the torque from the electric motors to the wheels is distributed differently with a differential depending on the appearance of the track.

Car body C is resting on a trailer bogie. The difference between a motor bogie and a trailer bogie is that there is no driving equipment such as motors and gear boxes.

Two parallel coupled coils springs are used as secondary springs in the trailer bogie. These have stiffer characteristics compared to the springs in the motor bogies. The calculation of these spring stiffnesses can be seen in *Appendix 3*.

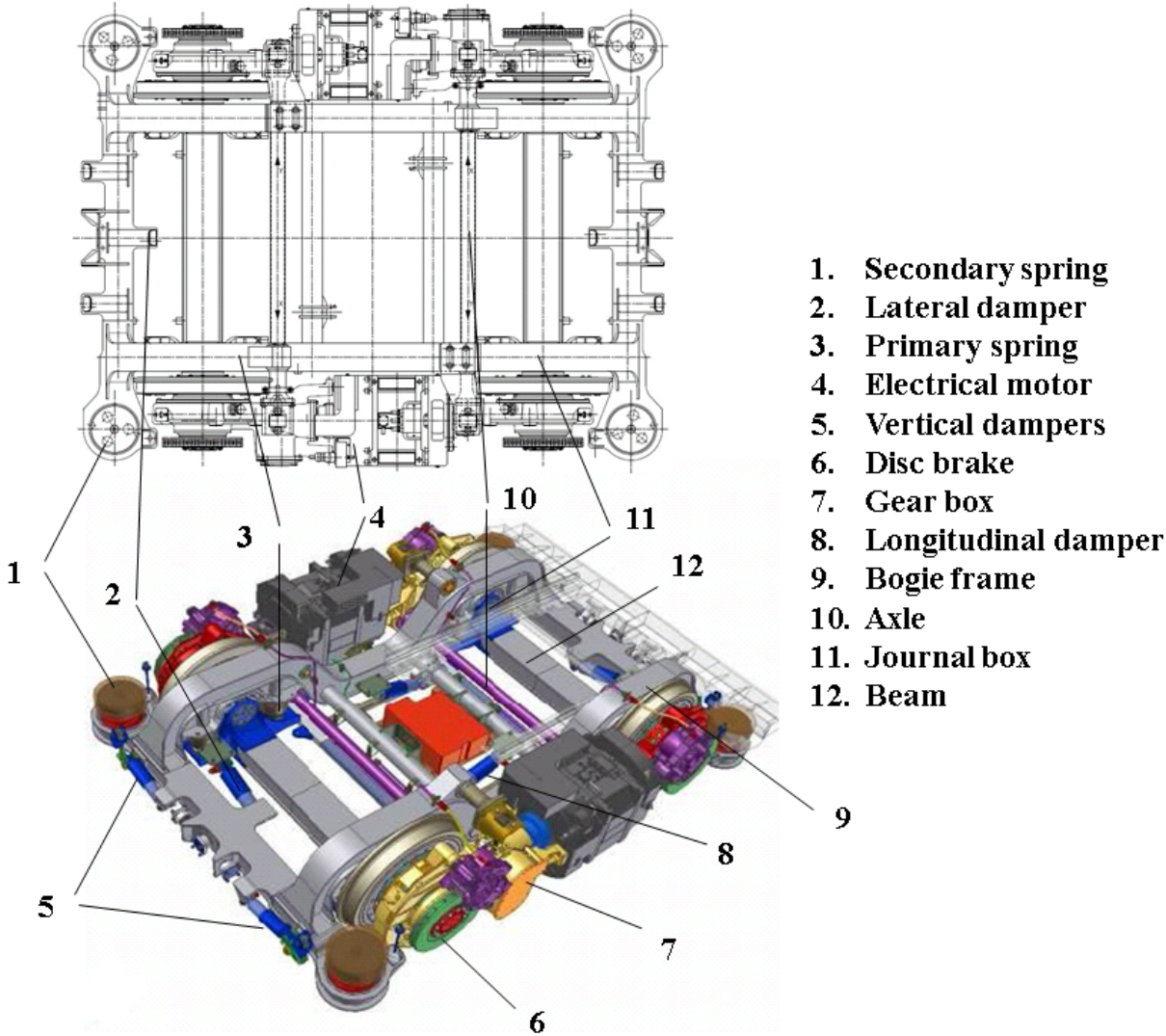


Figure 1.6 – Motor bogie on tram model M32. The figure has been copied from [7] and numbering of components has been added.

2. Theory

In this chapter a literature study will be presented followed by a discussion of the curving behaviour of the two tram models. The behaviour is of high importance to understand because it will be simulated and validated later. Also the theory used to model the dynamic system and solve the equations of motion will be presented and discussed. This theory will provide the basis to the thesis work and is considered significant for further understanding of the results.

2.1 Literature study

A literature study was performed to find references that have relevance to this thesis work. In this chapter the results of the study will be presented. Some conclusions from literature will be presented and how these can be beneficial to this thesis work will be discussed. A total of five interesting reports have been found.

The first work treats simulation of rail wear on the Swedish light rail line Tvärbanan [8]. In this work simulations of rail wear have been done with GENSYS in combination with a wear calculation program developed in MATLAB. The main result and conclusion from this report is that simulated and measured wear results do not agree too well. The simulated rail wear is more extensive than the measured one. However, the shapes of the simulated rail profiles are similar to the measured profiles. The work gives some hints of how a tram model can be built and simulated in GENSYS. This information is considered to be beneficial to this thesis work. Also a method used to calculate the wear is presented and discussed. This method can be investigated more and may be used for future wheel/rail wear calculations for the tram vehicles in Gothenburg.

In the second report an investigation of possible causes of wheel squeal on Roslagsbanan in Stockholm is presented [9]. Simulation of the dynamics for vehicles negotiating curves was carried out in GENSYS. Also this report links to the tasks that will be performed in this thesis work, where one of the purposes is to simulate the two tram models negotiating curves. A conclusion from this work is that curves below a radius of 300 m cannot be negotiated without wheel squeal for the specific vehicle investigated in the report and this leads to that curves tighter than 300 m need to be lubricated. This specific result is not that important for this thesis work but as mentioned some advice can be obtained of how a model can be built in GENSYS. Also a method used to investigate wheel squeal is presented that can be useful if a future study of wheel squeal is done.

The third report treats determination of tramway wheel and rail profiles to minimise risk of derailment [10]. The report investigates many different rail and wheel combinations of vehicles and rails in UK. The report concludes why some wheel and rail combinations give higher derailment risk than others and lists different factors that influence the derailment risk. Many steps of the report are linked to the results in this thesis work, where also here a dynamic vehicle model has been developed and simulated. Some of the results in this report have been an inspiration source for the parameter studies and results in this thesis work. Examples are derailment risks and wheel-rail combinations for tram models M31 and M32 operating in Gothenburg.

The fourth report treats rail corrugation growth on curves [11]. This report has provided theoretical foundation of how well different bogie designs negotiate curves. As will be presented later the bogie design on model M31 is not similar to model M32. This will lead to a different curving behaviour. The curving behaviour is presented in the next chapter. The simulation results presented here are also validated against the theory presented in this report.

A dynamic model has previously been done for a Sirio tram, closely related to model M32, in the software SIMPACK. Some results and stiffness/damping characteristics of bump stops and dampers are presented in the document *Simulation of dynamic behaviour of the new low floor tram Sirio for Milan* [12]. The document is written by AnsaldoBreda and the given values are used for the GENSYS modelling in this thesis work. The document is not that detailed and a whole tram vehicle could not be modelled with only the information from this document.

Some other literature, documents and reports are used to back up the theory, results and discussions about the GENSYS models. These sources are referred to throughout this report.

2.2 The curving behaviour of tram models M31 and M32

In this section the curving behaviour of tram models M31 and M32 will be presented. It should be noted that the curving behaviour of the two tram models behaves significantly different to each other. The steering of the trams is not controlled by the driver but is steered mechanically by difference in rolling radii of the inner and outer wheels, due to the positioning on the track and the coned wheels. Furthermore, the flanges of the wheels improve the lateral guiding and are a further assistance of the steering. An illustration of no flange and flange contact can be seen in figure 2.1.

When a railway vehicle enters a curve, creep forces will be developed in the wheel-rail contacts. The magnitudes of the creep forces depend on many factors, some of these are

- Running gear design of the vehicle bogies, such as stiffnesses in the primary suspension.
- Curve entering speed, curve radius and track cant.
- Track irregularities.
- Curve lubrication i.e. the friction between wheel and rail.

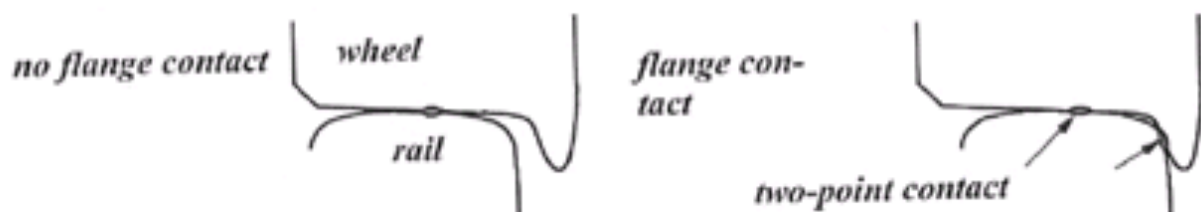


Figure 2.1 – One-point contact and two-point contact between wheel and rail. The figure is copied from [4] with permission from the authors.

The tangential force acting between wheel and rail can be divided into two force components. One that acts in the longitudinal direction and one that acts in the lateral direction. This is true for each contact point. From simple mathematics, the magnitude of the force resultant F_R and the phase angle θ of the tangential contact forces can be calculated as:

$$F_R = \sqrt{F_x^2 + F_y^2} \quad \text{and} \quad \theta = \arctan\left(\frac{F_x}{F_y}\right) \quad (2.1)$$

where F_x is the creep force in the longitudinal direction and hence F_y is the creep force in the lateral direction. These creep forces will start to develop as soon as the wheels are displaced from their equilibrium position. A typical example of this is when the vehicle enters a curve [4], [9], [11].

2.2.1 Tram vehicle M31

Tram model M31 consists of two-axle motor bogies with flexible suspended wheel sets and two wheel sets with independently rotating wheels. The behaviour of the tram negotiating a right-handed curve can be seen in figure 2.2 below. Note that only the lateral forces on the wheels are shown.

This is a typical curving behaviour for tram model M31 at normal operating speed. The wheels will have contact with the rails either at one point or two points. The flange contacts are denoted with red circles in figure 2.2. The wheels with the green force arrows have two-point contact, while the wheels with the blue force arrows have one-point contact. A typical illustration of the contacts is shown in figure 2.1.

Due to the chevron springs coupled between the motor bogie and wheel axles, flexible wheelset guidance will be obtained during a curving operation. The flexibility obtained from the primary springs will give the curving behaviour shown in figure 2.3.

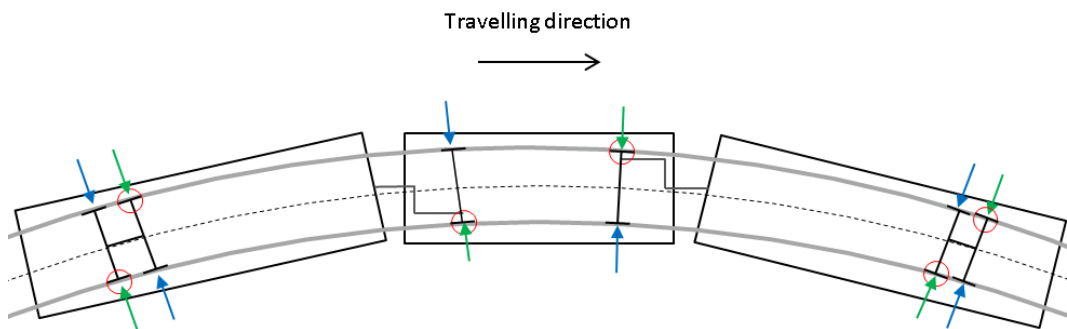


Figure 2.2 – A typical curving behaviour for tram model M31. Flange contacts are marked with red circles. The arrows represent lateral track forces, where green arrows denote two-point contact and blue arrows denote one-point contact.

The primary suspension will to some degree allow the wheel sets and axles to steer around the curve as can be seen in figure 2.3. This construction allows the vehicle to run “smoother” in a curve compared to a stiffer bogie construction. The smaller angle of attack for the leading wheel set leads to lower guiding forces on the wheels [4], [9], [11].

The wheel sets under car body C have a special steering. The steering is controlled mechanically by car body A or B. An illustration of one wheel set and the mechanical steering mechanism can be seen in figure 2.4. The wheel sets can yaw relative to car body C. When car body A enters the curve a rotation of an angle α relative to car body C will take place. This will push the mechanical coupling between car body A and the leading wheel set under car body C. The coupling will result in a yaw motion of the wheel set.

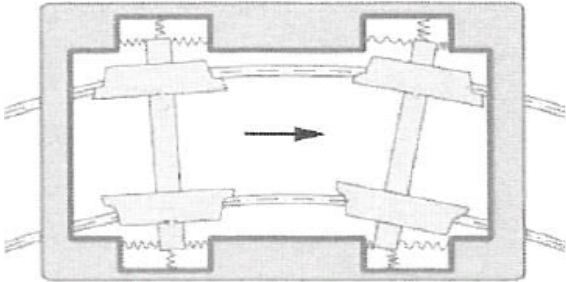


Figure 2.3 – Motor bogie on M31 with flexible wheel set guidance. The figure is copied from [4] with permission from the authors.

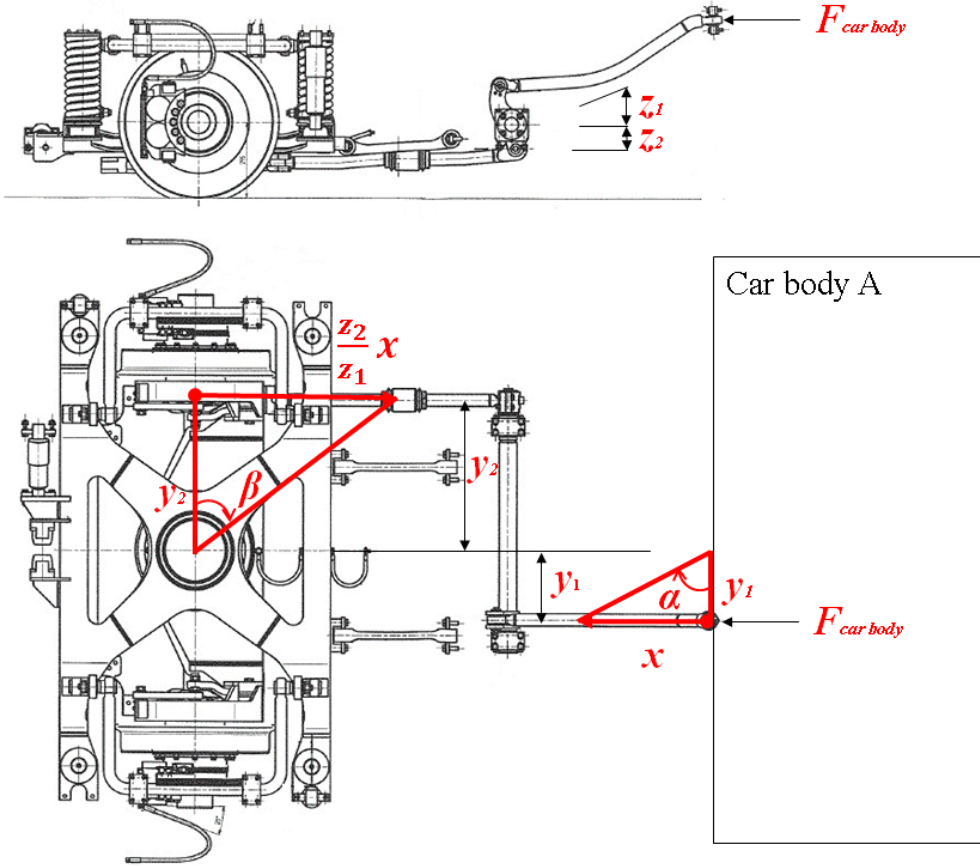


Figure 2.4 – Mechanical coupling, steering angles for car body A (or B) and wheel set.

There is also a mechanical coupling between car body B and the trailing wheel set under car body C. With simple calculations, the angle difference between car body and wheel set can be obtained. With that a resulting steering ratio that explains how much the frame will steer relative to the car body can be attained. The calculated steering ratio is 0.29, which means that the frame will be angled with 0.29 degree for every degree that the car body A or B is angled. The calculations can be seen in *Appendix 2*.

This mechanism can in some cases cause problems. The reason for this is due to that the wheel sets in car C are dependent on car bodies A and B. When car body A enters a curve it will make the leading wheel set in car body C to turn even if these wheels are still on a tangent track. This is also true for the trailing wheel set connected to car body B. Although, now the wheel set will enter the curve before car body B. This can give unwanted flange contact between the wheels and rail. This will lead to wheel/rail wear and also unwanted vibrations and wheel squeal.

2.2.2 Tram vehicle M32

Tram model M32 has stiff wheel set guidance and independently rotating wheels. The behaviour of the tram negotiating a right-handed curve with normal operating speed can be seen in figure 2.5.

The wheels will have contact with the rails either at one point or two points. The flange contacts are denoted with red circles in figure 2.5. The wheels with the green force arrows have two-point contacts, while the wheels with the blue force arrows have one-point contact. The stiff construction will lead to excessive flange contact in curves with a hammering movement. In other words, the wheel flange will be hammering on the rail when negotiating the curve. An illustration of the stiff wheel set guidance in a curve can be seen in figure 2.6.

The stiff construction will lead to higher forces on wheels and rails, especially the lateral guiding forces will be much higher compared to the bogie design used on tram model M31. This behaviour is mainly due to that this type of bogie construction will give a higher angle of attack for the leading wheels. The stiff guidance with independently rotating wheels also increases the risk of derailment through flange climbing in certain critical conditions compared to the design on tram vehicle M31. The reason for this is the increased lateral flange forces which will increase the lateral/vertical (Y/Q) value [4], [9], [11]. The benefit with this design is that the construction allows for a low floor tram vehicle.

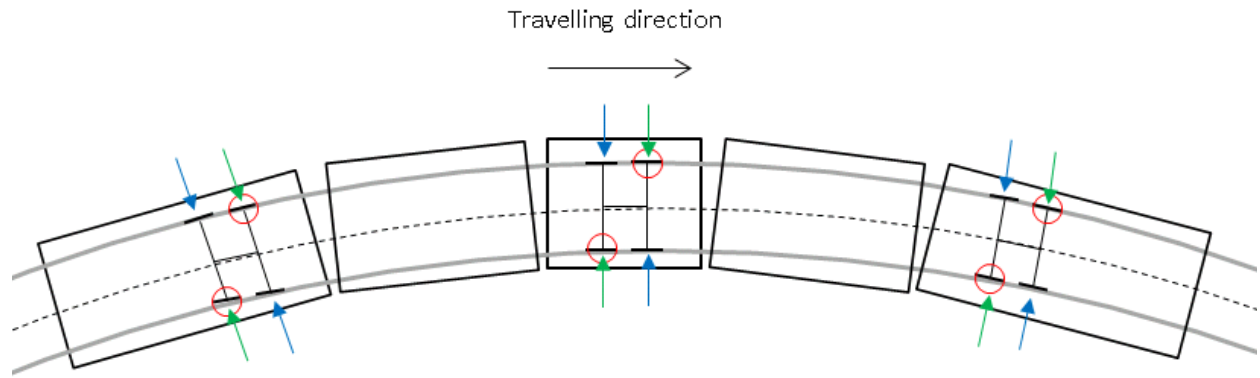


Figure 2.5 – A typical curving behaviour for tram model M32. Flange contacts are denoted with red circles. The arrows represent lateral track forces, where green arrows denote two-point contacts and blue arrows denote one-point contact.

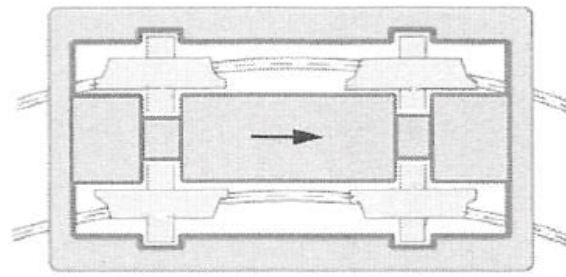


Figure 2.6 – Motor and trailer bogie on M32 with stiff wheel set guidance. The wheels can rotate independently. The figure is copied from [4] with permission from the authors.

2.3 The software GENSYS

GENSYS is a three-dimensional general multipurpose software for modelling of mechanical problems. The development of GENSYS began in 1992 due to strong demands of a three-dimensional modelling software for vehicles running on rails. There are four main calculation programs in GENSYS and these are:

- TSIM is a time-domain integrator for simulating the running behaviour of vehicles.
- QUASI program is used for quasistatic analysis.
- MODAL is used for modal analysis, where eigenfrequencies and eigenmodes of the vehicle can be determined.
- FRESP is a program for doing frequency-response analysis.

In GENSYS, the vehicle models can be considered as a collection of rigid bodies (here called components) with masses acting at each body centre. The rigid bodies are then interconnected by massless spring and damper elements resulting in a complete vehicle model. Due to the software's focus on rail vehicle dynamics, factors such as track irregularities, interaction between worn wheels and rail, critical speed, derailment risk and ride comfort can be studied [3].

2.3.1 Two-dimensional mathematical model

The dynamic railway vehicle simulations performed by GENSYS are based on mathematical models. Even if the software generates and solves the equations of motion for the user it is important to understand the theory behind this. In this subchapter a mathematical model of a simple two-dimensional tram vehicle describing the vertical dynamics will be presented. The purpose with this theory is to get a better understanding of the equations of motion and how GENSYS solves these. Also simple models are very useful and relatively fast for checking results from simulations.

A simple model of a tram vehicle or a bogie can be seen in figure 2.7. The model consists of a car body with the mass denoted with m and the moment of inertia denoted with J . Two wheels with masses m_{w1} and m_{w2} are attached to the car body by mathematical dampers and springs. The right figure shows the internal and external forces acting on the system.

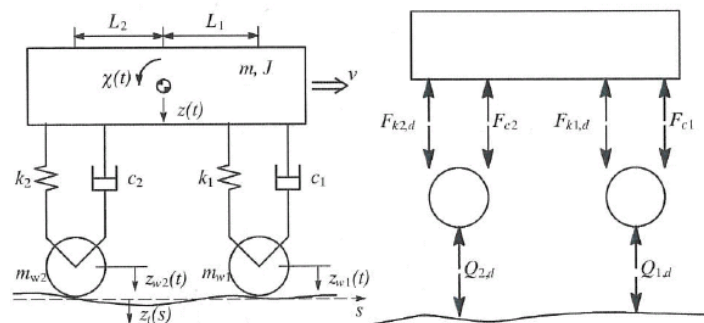


Figure 2.7 – Simple model of a tram vehicle. The left figure shows defined variables and constants. The right figure shows the internal and external forces acting on the system. The figure is copied from [4] with permission from the authors.

For the theoretical model the following assumptions are made:

- The tram is moving on a tangent track at constant speed. It is assumed that only vertical track irregularities act on the vehicle.
- Rail and wheels are rigid, do not lose contact and the wheels are perfectly round.
- Dampers and springs are assumed to have linear characteristics.

By using force and moment equilibrium for the car body the equations of motion can be written as (see figure 2.7):

$$\begin{cases} m\ddot{z} = -F_{k1,d} - F_{c1} - F_{k2,d} - F_{c2} \\ J\ddot{\chi} = F_{k1,d}L_1 + F_{c1}L_1 - F_{k2,d}L_2 - F_{c2}L_2 \end{cases} \quad (2.2)$$

It is assumed that the forces from the springs and dampers act at the same distance (L_i) from the mass centre. Force equilibrium can also be written for the two wheels on the system. The results are:

$$\begin{cases} m_{w1}\ddot{z}_{w1} = F_{k1,d} + F_{c1} - Q_{1,d} \\ m_{w2}\ddot{z}_{w2} = F_{k2,d} + F_{c2} - Q_{2,d} \end{cases} \quad (2.3)$$

The internal forces can be substituted with a displacement/velocity times the spring/damping constants if assuming linear characteristics for these components. Using this in the equations above gives the result below:

$$\mathbf{M}\ddot{\mathbf{x}} + \mathbf{C}\dot{\mathbf{x}} + \mathbf{K}\mathbf{x} = \mathbf{F} \quad (2.4)$$

This is the equations of motion for the bogie in matrix form where:

$$\mathbf{M} = \begin{bmatrix} m & 0 \\ 0 & J \end{bmatrix} \quad (2.5)$$

$$\mathbf{C} = \begin{bmatrix} c_1 + c_2 & -c_1L_1 + c_2L_2 \\ -c_1L_1 + c_2L_2 & c_1L_1^2 + c_2L_2^2 \end{bmatrix} \quad (2.6)$$

$$\mathbf{K} = \begin{bmatrix} k_1 + k_2 & -k_1L_1 + k_2L_2 \\ -k_1L_1 + k_2L_2 & k_1L_1^2 + k_2L_2^2 \end{bmatrix} \quad (2.7)$$

$$\mathbf{F} = \begin{bmatrix} c_1\dot{z}_{w1} + c_2\dot{z}_{w2} + k_1z_{w1} + k_2z_{w2} \\ -c_1\dot{z}_{w1}L_1 + c_2\dot{z}_{w2}L_2 - k_1z_{w1}L_1 + k_2z_{w2}L_2 \end{bmatrix} \quad (2.8)$$

$$\ddot{\mathbf{x}} = \begin{bmatrix} \ddot{z} \\ \ddot{\chi} \end{bmatrix}, \quad \dot{\mathbf{x}} = \begin{bmatrix} \dot{z} \\ \dot{\chi} \end{bmatrix}, \quad \mathbf{x} = \begin{bmatrix} z \\ \chi \end{bmatrix} \quad (2.9)$$

Where the time derivatives of the wheel displacement due to a harmonic track irregularity can be expressed as:

$$\begin{cases} \dot{z}_w = z'_t v \\ \ddot{z}_w = z''_t v^2 \end{cases} \quad (2.10)$$

A dot notation for a variable is referring to a time derivative whereas a prime denotes derivatives of the position in the equations. The equations of motion in matrix form is a

system of second-order ordinary differential equations (2nd ODE). These equations can be solved more easily by reducing the equations to a first order ODE. This is done by introducing a new variable $v_z = \dot{z}$ and hence transforming the second order equations into a set of first order differential equations.

$$\begin{cases} \boldsymbol{\theta} = \begin{bmatrix} z \\ v_z \end{bmatrix} \\ \dot{\boldsymbol{\theta}} = \mathbf{J}\boldsymbol{\theta} + \mathbf{F}_{\text{ext}} \end{cases} \quad (2.11)$$

This set of equations can then be solved with help of numerical methods. This will be discussed in more detail in the next subchapter. Observe that the matrix \mathbf{J} is the Jacobian matrix and not the moment of inertia J for the bogie. As mentioned earlier this is only a simplified model of a tram vehicle, a model in GENSYS is a three-dimensional representation of a vehicle and may have 50 or more degrees of freedom. This kind of model is not easy to solve by hand. Basically the same method is used when the software algorithm solves the more realistic model in GENSYS, but the number of equations is greater [3], [4].

2.3.2 Time-domain integrator

Tram vehicle simulations of the running behaviour are of high importance. This is done in GENSYS with the time-domain integrator program TSIM. A solver is used to solve the equations of motion and the program advances in time with help of a numerical integrator that can be selected. The numerical integrator used in this project is called Heun_c. This method is basically the two step Runge-Kutta method, with step size control and if the tolerance is not met the program makes back steps.

Heun's method (also called modified Euler's method) is a mathematical technique for solving ordinary differential equations with a given initial value, such as the equations of motion for a tram vehicle. Euler's method is used as a basis for this method and can be stated as:

$$\begin{cases} \dot{y}(t) = f(t, y(t)) \\ y(t_0) = y_0 \end{cases} \quad (2.12)$$

The derivatives can be approximated to:

$$\dot{y}(t) \approx \frac{y_{n+1} - y_n}{h} \quad (2.13)$$

Where h is a small time step and n is the current step. Smaller time steps give better results but the calculation time will increase. Using this approximation finally gives the Euler method from the time at step n to the time at step $n+1$ as:

$$y_{n+1} \approx y_n + h f(t_n, y_n) \quad (2.14)$$

Euler's method can then be used on the next time step to calculate the positions of the different components on the tram model. Heun's method uses Euler to first calculate an intermediate value \tilde{y}_{n+1} and after this calculation, the final approximation y_{n+1} can be calculated at the next integration point. The equations used for this method are:

$$\begin{cases} \tilde{y}_{n+1} \approx y_n + hf(t_n, y_n) \\ y_{n+1} \approx y_n + \frac{h}{2}[f(t_n, y_n) + f(t_{n+1}, \tilde{y}_{n+1})] \end{cases} \quad (2.15)$$

Euler's and Heun's method can be seen in figure 2.8 below. As can be seen by using Heun's method it is possible to get closer to the real value compared to Euler's method.

Even if the Euler's method is a quite accurate and easy method it can be less successful when using it on more challenging problems. The Euler's methods can over or even underestimate the change in the time stepping. Getting good results using Euler's method can require very small time steps and this is time consuming for the solver.

Heun's method is a second order method, and this means that the size of the error is decreasing much faster compared to Euler's method which is a first order method. As a result, by halving the time step Euler's method reduces the error by half. However reducing the time step the same amount, Heun's method reduces the error by a factor of four. This means that the results reach four times the accuracy by only doubling the number of steps, i.e. fewer time steps are needed for Heun's method to obtain the same accuracy as with Euler's method [13], [14].

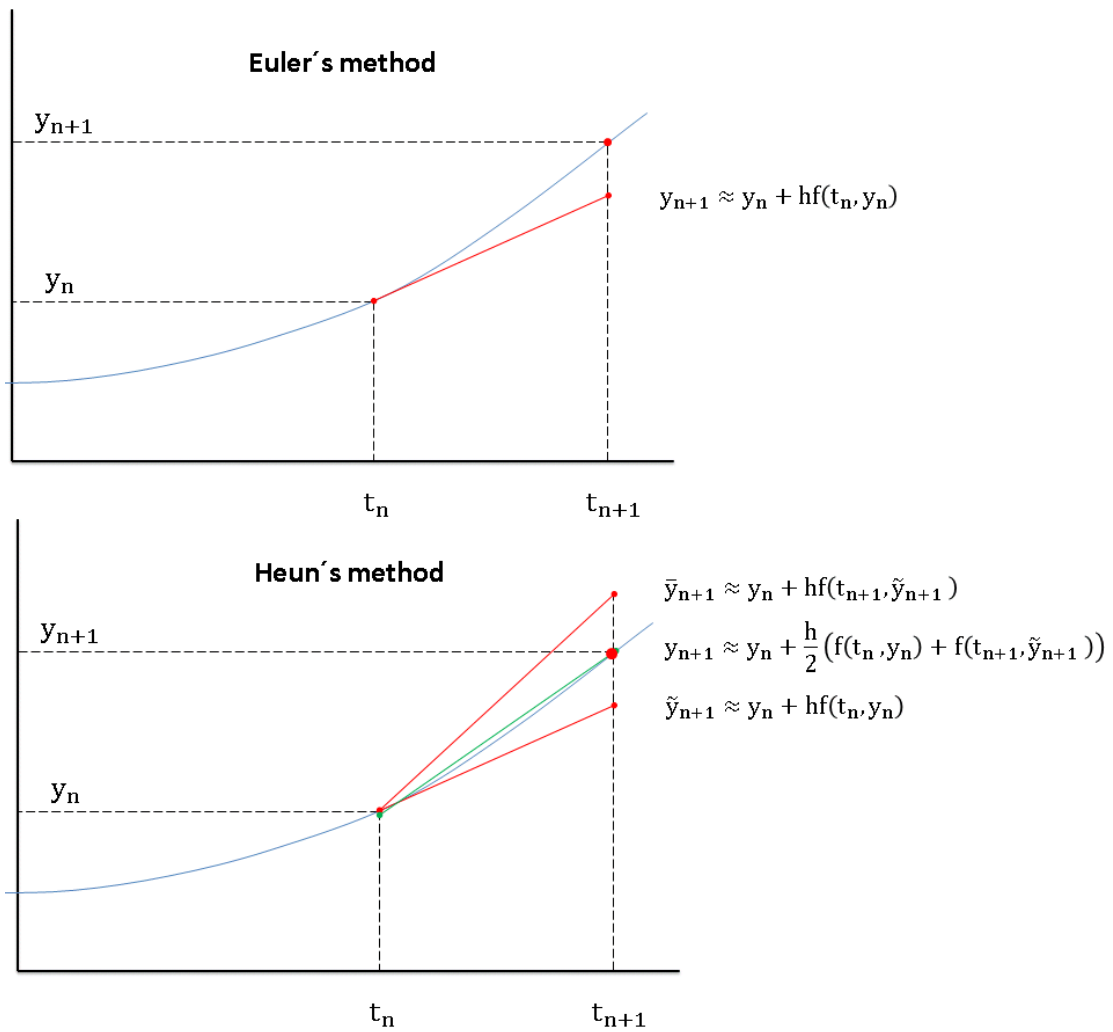


Figure 2.8 – Explanation of Euler's and Heun's methods. The top figure shows Euler's method and the bottom figure shows Heun's method.

2.3.3 Wheel and rail contact model

In GENSYS a contact point function (KPF) is used to simulate the contact between wheels and rail. The program creates the wheel and rail geometries from designed or measured wheel and rail profiles. This means that both nominal and worn profiles can be studied and simulated.

The wheel and rail profiles are imported from two column vectors. The vectors contain lateral and vertical coordinates used to describe the shapes of the profiles. In the beginning of the calculation in the pre-processor KPF, the wheel sets will fall on the rail and between the rail and wheels a distributed layer of springs is attached, as can be seen in figure 2.9. These contact springs will give rise to a force that will act on the wheel set when they make contact with the rail. Hertzian theory for the contact pressure is used. When equilibrium has been obtained, an elliptical contact region between the wheel and rail has formed. The shape of this contact region is defined entirely by the wheel and rail profiles [3], [8].

The program will then move the wheel sets as much as possible to the left and right in the lateral position. At each new lateral position of the wheel set, equilibrium calculations are done. The results are then used as lookup tables in the wheel/track interaction simulations.

In figure 2.9 a model of how the wheel sets are connected to the rails and also how the rails are connected to the ground is shown. The rails are modelled as massless elements, and the stiffness between the wheel and rail contact is defined with the stiffness variable knwr. In the model used, three different contact surfaces between the rail and wheel can be in contact simultaneously [11], [15].

The couplings between the rail and ground can be modelled as a vertical spring and damper and a lateral spring and damper. The values used here are predefined as default in GENSYS and have not been changed. The values used are presented below.

$$\left\{ \begin{array}{l} k_{zrt} = 42e6 \text{ N/m} \\ c_{zrt} = 400e3 \text{ Ns/m} \\ k_{yrt} = 100e6 \text{ N/m} \\ c_{yrt} = 1600e3 \text{ Ns/m} \end{array} \right. \quad (2.16)$$

A more detailed theory of the wheel/rail interaction will not be presented in this thesis, as this is not within the scope of the study. The theory and modelling is predefined in the GENSYS software and is not needed to be defined by the user [3].

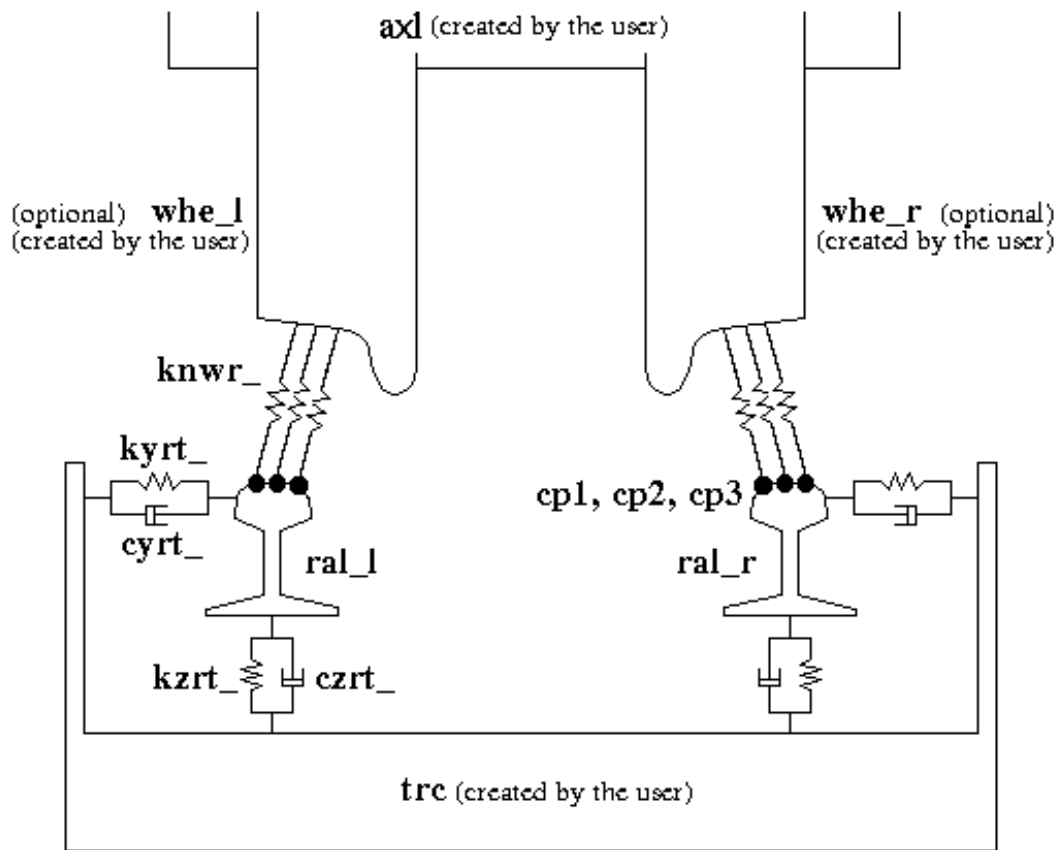


Figure 2.9 – Model of how the wheels are coupled to the rails and how the rails are connected to the track [3].

3. Methods

An explanation of how the thesis work has been carried out will be presented in this chapter. The tram vehicle modelling in GENSYS is an important subject and is presented and discussed. Furthermore, the methods used to validate the models will be described.

3.1 Modelling description

At a first glance, the input data file used to model a vehicle in GENSYS appears quite complicated but is in fact very efficient due to a clever substructure hierarchy. As mentioned earlier, tram vehicle models consist of different masses as car bodies, bogies, wheel axles and wheels. In GENSYS the position of the centre of mass is defined relative to a local coordinate system. The mass of the component (for example a wheel or a car body) is then defined, and the shape is mathematically defined by its moment of inertia in different directions. The tram models are represented by a multibody system model. The bodies are assumed rigid and connected by massless coupling elements such as springs, viscous dampers and friction based couplings. The concept of substructures has been used when modelling the different tram vehicles. The same models of wheel, axle and bogie are used several times. Instead of repeating the same input data numerous times with none or minor differences in the script data, a substructure is used with input arguments.

Before presenting the method used to build the tram models in GENSYS, a definition of the different coordinate systems and their directions is suitable. For the modelling, three-dimensional Cartesian coordinate systems are used and the definitions of the different coordinates are presented in table 3.1. These coordinate systems are connected to each other in a certain way, which can be seen in figure 3.1.

Table 3.1 – Definition of coordinates and their directions.

Name:	Direction:	Positive:
X	Longitudinal	Forward
Y	Lateral	Right
Z	Vertical	Downwards
φ	Roll (X-rot)	Right-hand rule
χ	Pitch (Y-rot)	Right-hand rule
ψ	Yaw (Z-rot)	Right-hand rule

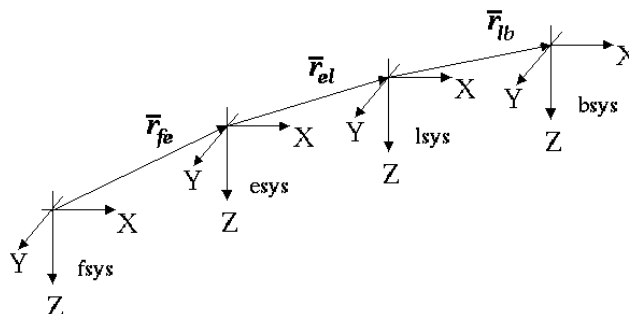


Figure 3.1 – Definition of different coordinate systems used in GENSYS and how they are linked to each other.

The first system called fsys is a fixed coordinate system located in the origin. This system serves as a main reference system and will not change during the simulation. The esys coordinate system is a moving system, which considers large angles. How this system will move has to be defined before the simulation starts. The lsys system is also a moving coordinate system but it only considers linear rotations. The last system bsys is a body fixed coordinate system, which describes the position of a mass body relative to its local system lsys.

For the tram modelling, an esys system is defined for each car body. For example, the M31 tram with three car bodies has three esys systems. Then for each mass (car body, bogie, axles and wheels) an lsys system is defined relative to the esys system [3].

3.1.1 Types of couplings used in the GENSYS modelling

The masses (car bodies, bogies, axles and wheels) are coupled to each other with primary and secondary springs and dampers as was explained earlier. There are also couplings between the different car bodies and between car bodies and bogies that are not physical springs or dampers. However, these couplings are also defined as mathematical springs and/or dampers, for example a solid rod can be seen as a mathematical spring with high stiffness and damping. The value of the axial stiffness and damping can be calculated as:

$$k = \frac{EA}{L} \quad \text{and} \quad c = \frac{\zeta k}{\pi f_0} \quad (3.1)$$

where E is Young's modulus, A is cross section area of the rod, L is length of the rod, ζ is the ratio of critical damping, k is the stiffness of the rod and f_0 the frequency. The different couplings and joints are all modelled as massless springs and/or dampers in GENSYS. The couplings used for the GENSYS models will be presented below.

3.1.1.1. One dimensional couplings with zero length

Couplings having only one working direction equal to one of the coordinates in table 3.1, have in general zero length. A coupling with zero length means that the two ends of the coupling are located at the same position as when it is undeformed [3], [8].

Coupling command: k

The coupling k defines a stiffness coupling between two masses. This coupling does not have a length and only one stiffness property. The direction (x , y or z) of the coupling is defined by the user. The forces generated by the coupling can be seen as:

$$F_k = k_x \Delta x \quad \text{or} \quad F_k = k_y \Delta y \quad \text{or} \quad F_k = k_z \Delta z \quad (3.2)$$

Coupling command: c

The coupling c defines a damping coupling between two masses. This coupling may not have a length and only one damping property. The (x , y or z) direction is defined by the user. The force generated by the coupling can be seen as:

$$F_c = c_x \Delta \dot{x} \quad \text{or} \quad F_c = c_y \Delta \dot{y} \quad \text{or} \quad F_c = c_z \Delta \dot{z} \quad (3.3)$$

Coupling command: `p_nlin_s`

The coupling command `p_nlin_s` defines an symmetric non-linear coupling property. The property of the coupling is considered as piecewise linear and the properties force vs deformation/velocity are described in vector pairs, see figure 3.2 below for the coupling property behaviour.

3.1.1.2 One dimensional couplings with length

If the forces on the coupling should be considered in the coupling's working direction, the coupling must have a defined length or else the direction of the coupling cannot be defined. A typical example of when this type of coupling is used is for dampers, which often have a working direction that is not aligned with the lateral, longitudinal or vertical one. The dampers can only take up forces in its working direction and due to this they need to be modelled as couplings with length [3], [8].

Coupling command: `k`

The coupling `k` defines a stiffness coupling between two masses. This coupling has a defined length with its stiffness property in the working direction. This means that the force is acting in the direction of the element. The coupling direction is defined by the user by its end coordinates. The force generated by the coupling can be seen as:

$$F_k = k \Delta m \tag{3.4}$$

where Δm is the deformation in the working direction.

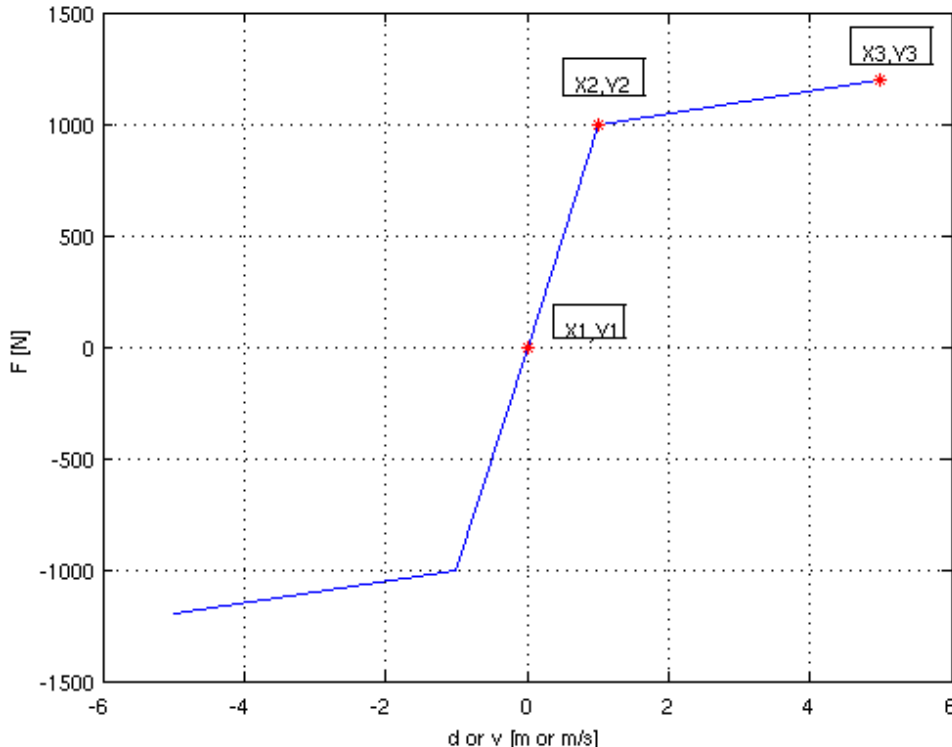


Figure 3.2 – Example of how the coupling `p_nlin_s` is defined. More vector pairs than three is possible.

Coupling command: c

The coupling c defines a damping coupling between two masses. This coupling may also have a defined length with its damping property in the working direction. This means that the force acts in the direction of the element. This coupling direction is defined by the user by its end coordinates. The forces generated by the coupling can be seen as:

$$F_k = c \Delta \dot{m} \quad (3.5)$$

where $\Delta \dot{m}$ defines the used working direction.

3.1.1.3 Matrix couplings

Matrix couplings are usually used when the modelled coupling has spring/damping coefficients in more than one direction. Normally, these couplings have zero length. Examples of when this type of coupling is used is the joint coupling between car bodies and chevron springs between bogies and car bodies [3].

Coupling command: p_lin36

The sub coupling command p_lin36 defines a linear 6x6 matrix property and a vector with preload forces that acts on zero deformation. This coupling type is used for both stiffness and viscous damping. The forces and moments acting on the coupling can be written in components as:

$$\begin{bmatrix} F_x \\ F_y \\ F_z \\ M_\varphi \\ M_\chi \\ M_\psi \end{bmatrix} = \begin{bmatrix} k_{xx} & k_{xy} & k_{xz} & k_{x\varphi} & k_{x\chi} & k_{x\psi} \\ k_{yx} & k_{yy} & k_{yz} & k_{y\varphi} & k_{y\chi} & k_{y\psi} \\ k_{zx} & k_{zy} & k_{zz} & k_{z\varphi} & k_{z\chi} & k_{z\psi} \\ k_{\varphi x} & k_{\varphi y} & k_{\varphi z} & k_{\varphi\varphi} & k_{\varphi\chi} & k_{\varphi\psi} \\ k_{\chi x} & k_{\chi y} & k_{\chi z} & k_{\chi\varphi} & k_{\chi\chi} & k_{\chi\psi} \\ k_{\psi x} & k_{\psi y} & k_{\psi z} & k_{\psi\varphi} & k_{\psi\chi} & k_{\psi\psi} \end{bmatrix} \begin{bmatrix} \Delta x \\ \Delta y \\ \Delta z \\ \Delta \varphi \\ \Delta \chi \\ \Delta \psi \end{bmatrix} + \begin{bmatrix} F0_x \\ F0_y \\ F0_z \\ M0_\varphi \\ M0_\chi \\ M0_\psi \end{bmatrix} \quad (3.6)$$

Coupling command: $k3_l$

This coupling type defines a stiffness coupling between two masses. The coupling is mainly developed for modelling of vertical coil springs with pre stresses acting on these. The coupling can also rotate relative to its esys coordinate system. The couplings pre stress force and its stiffness matrix will follow the rotation. The forces acting on the coupling can be written as:

$$F_k = \begin{bmatrix} k_x & 0 & 0 \\ 0 & k_y & 0 \\ 0 & 0 & k_z \end{bmatrix} \begin{bmatrix} \Delta x \\ \Delta y \\ \Delta z \end{bmatrix} + \begin{bmatrix} F0_x \\ F0_y \\ F0_z \end{bmatrix} \quad (3.7)$$

3.1.2 Tram model M31

An illustration of the modelled tram vehicle M31 can be seen in figure 3.3 below. The model is visualized by boxes and circles. Each component is defined by a mass and its moment of inertia. The masses are attached to each other with different couplings consisting of mathematical springs and dampers. The visualization of the model has been generated with the 3-D visualization and animation postprocessor program GPLOT [3], which is a module of GENSYs.

A detailed description and discussion of how M31 is modelled is presented in *Appendix 6*.

3.1.3 Tram model M32

A GENSYS model of the tram vehicle M32 can be seen in figure 3.4 below. This model has five car bodies compared to M31, which only has three. Also here the components of the tram are presented as boxes and circles. The components are attached to each other with springs and dampers.

A detailed description and discussion of how M32 is modelled is presented in *Appendix 6*.

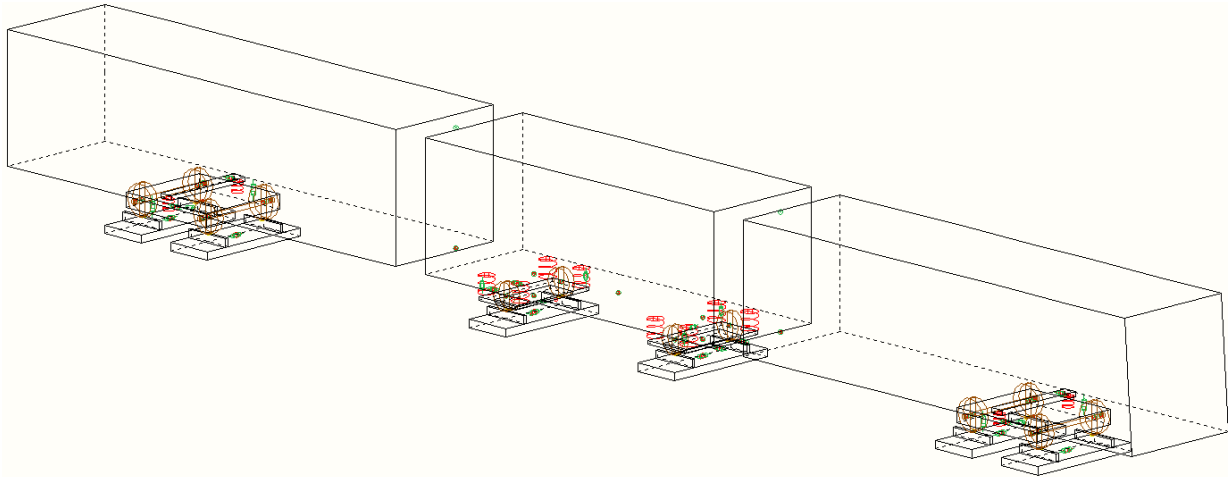


Figure 3.3 – A visualization of a GENSYS model of tram vehicle M31 generated by the post processor program GPLOT. The figure shows the three car bodies, two motor bogies and two trailer bogies with their primary and secondary suspensions.

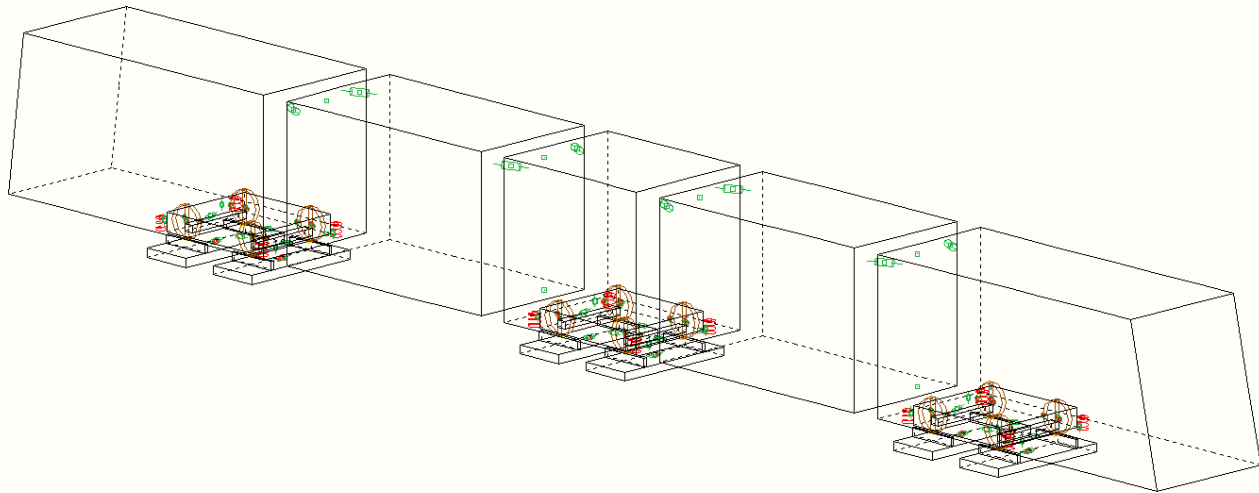


Figure 3.4 – A visualization of a GENSYS model of tram vehicle M32 generated by the post processor program GPLOT. The figure shows the five car bodies, two motor bogies and one trailer bogies with their primary and secondary suspensions.

3.2 Debugging of the vehicle models

A debugging of the vehicle models has been done before starting the analysis to check the models for errors. The debugging has been done by following a recommended check list presented on the GENSYs home page [3].

3.2.1 Graphical check

The models have been generated by the postprocessor program GPLOT. All the couplings have been checked to detect if their positions and directions are correct.

3.2.2 Check of abnormal data

The program runf_info has been used to check abnormal data. This program will print warnings for very long couplings and also for very stiff and soft couplings. Furthermore information on how the different masses are connected to each other is generated by the program.

3.2.3 Time-domain integration check

A time domain simulation for both tram models has been made on a tangent track without any track irregularities. The deformation scale was set to 400 times and the simulation was animated. The purpose of this was to check for unexpected motions. Also a time domain simulation on a curve has been done. Forces between the masses and motions of the components were plotted for checking of abnormal behaviour.

3.2.4 Stability check

Both models have been simulated with a constant speed of 60 km/h on a tangent track without any track irregularities. This speed is the maximum allowed for both tram vehicles M31 and M32 in Gothenburg. The stability check has been done for both nominal and worn wheel/rail profiles. The purpose of this simulation is to check that the bogies run stable on ideal tangent tracks at this speed. The exact critical speed has not been determined, but it is not lower than 60 km/h.

4. Field measurements and validation

During the project work, field measurements have been performed both to provide input to the models and for validation of the calculations. In this chapter measurement on wheel and rail profiles and also measurements on curving behaviour will be presented.

4.1 MiniProf wear measurements on tram wheels and rails

Wheel profiles have been measured with an instrument called MiniProf wheel, and rail profiles have been measured with a MiniProf rail. The instruments are attached magnetically to the backside of the wheel flange or to the top of the rail. The measuring head consists of a magnetic wheel that manually rolls along the wheel/rail profile in its lateral direction. The shape of the profile can then be transmitted to a computer by a two-part linkage between the head and the part attached to the wheel [19]. True worn wheel/rail profiles can then be used for the GENSYS simulations.

In figure 4.1 all the measured wheel profiles can be seen. The figure consists of 13 wheel profiles where the solid black one represents the nominal wheel profile. The purpose of this figure is to show the wear spread for the GS profile. The 12 wheel profiles have been measured on different wheels with different rolling distances since previous reprofiling. The measured profiles have been modified at the left and right end to resemble the nominal one.

In figure 4.2 all the measured rail profiles can be seen. The upper figure represents the outer rail profiles and the lower figure the inner rail profiles at five measured curves at Vagnhallen Majorna and at Rantorget. The top solid black line represents the nominal rail profile, the solid red line is a measured profile at Majorna with low wear and the solid turquoise line represents a curve at Rantorget. The dashed black line is also a measured profile at Rantorget, some weld repairs can be noticed on the outer rail profile. The dashed red line is a measured profile at Majorna. As can be seen there is high wear on this profile and also some plastic deformation, especially on the inner rail.

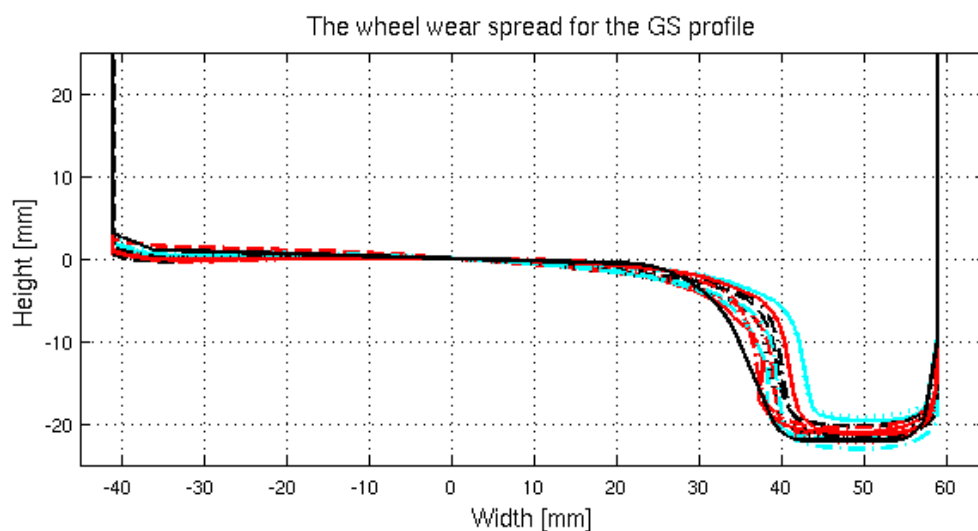


Figure 4.1 – The wheel wear spread for the GS profiles. The solid black profile represents the nominal profile.

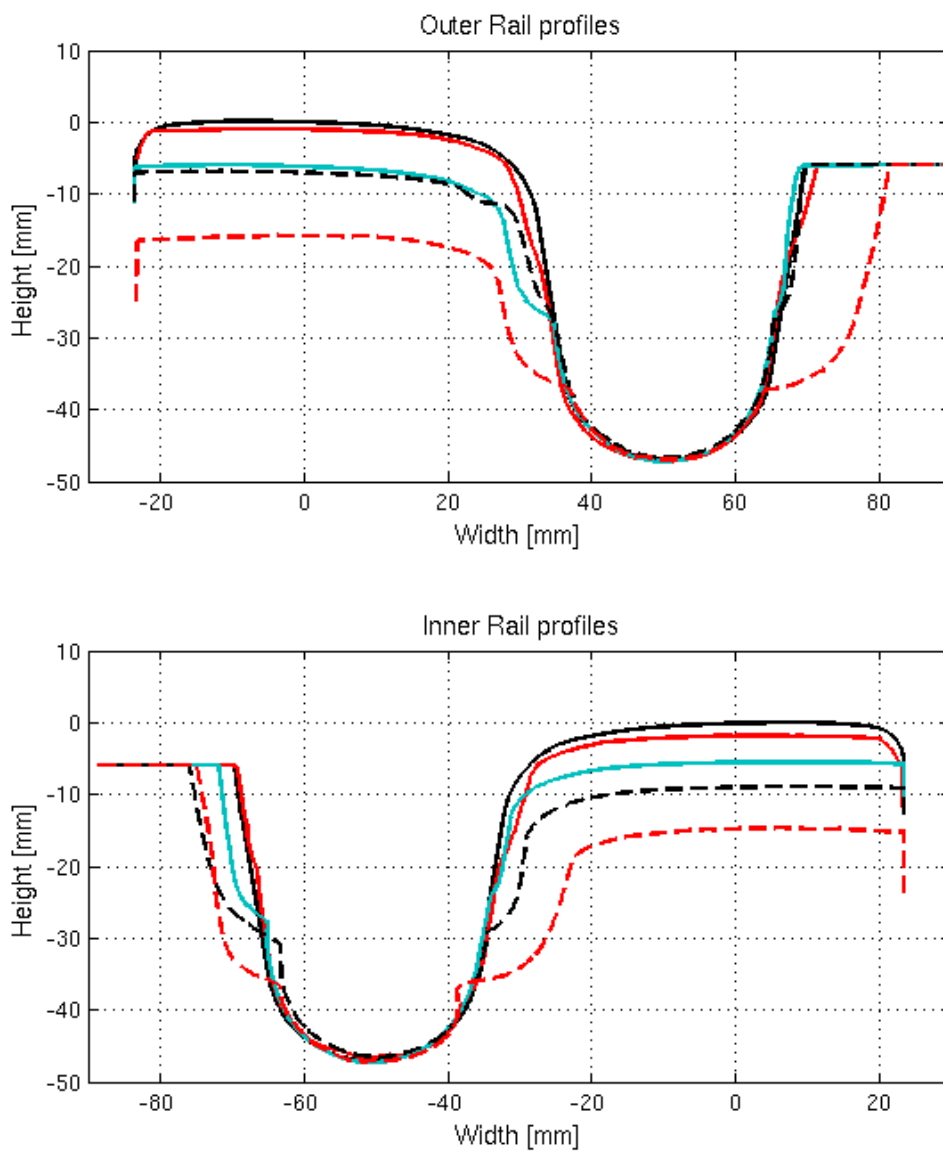


Figure 4.2 – Nominal and measured rail profiles. The top figure shows the outer rails and the bottom figure the inner rails at different curves measured at Vagnhallen Majorna and Rantorget.

4.2 Validation of tram models

Triaxial accelerometers were mounted on the leading car body, bogie and wheel set of an M31 and an M32 tram. For M31 the accelerometers were placed at nine different positions. One on the floor of car body A, directly above the leading bogie, and one on each axle box. Also, one accelerometer was placed on the centre of the bogie frame on each side. The position of the accelerometers can be seen in figure 4.3.

For tram vehicle M32, seven accelerometers were placed at seven different positions. One accelerometer was placed on the beams close to the wheels. One was placed on top of the floor of the leading bogie of car body A. Lastly, one was placed on the centre of the front side of the bogie frame and one at the back of the bogie frame. The position of the accelerometers can be seen in figure 4.4.

The tram vehicles were empty and operated with approximately constant speeds of 15 km/h and 20 km/h. The test track used at Rantorget can be seen in figure 4.5 below. The route consists of four different curve radii of 23, 50, 100 and 50 m. The route is a right handed curve with transition curves of 8 m at the start and 10 m at the end. At the end of the curve there are railway switches.

These driving conditions and curves will also be used in GENSYS for comparison with the field measurements and will be presented below.

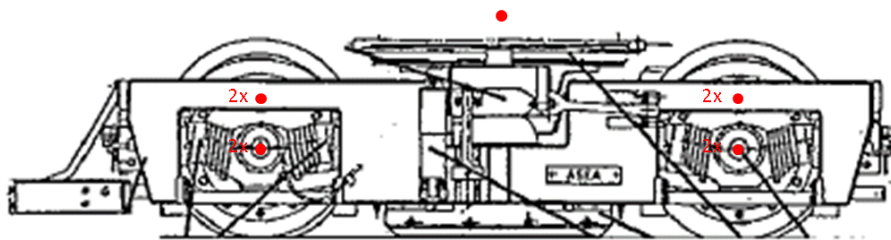


Figure 4.3 – Accelerometer positions on the leading bogie of vehicle M31.

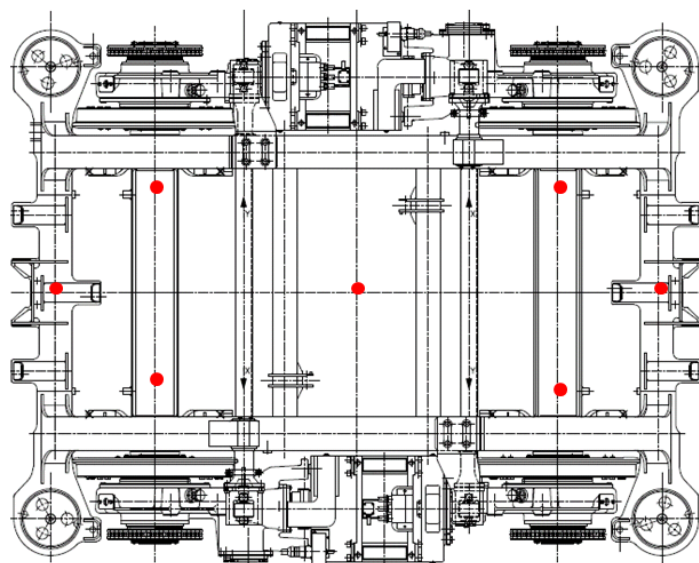


Figure 4.4 – Accelerometer positions on the leading bogie of vehicle M32.

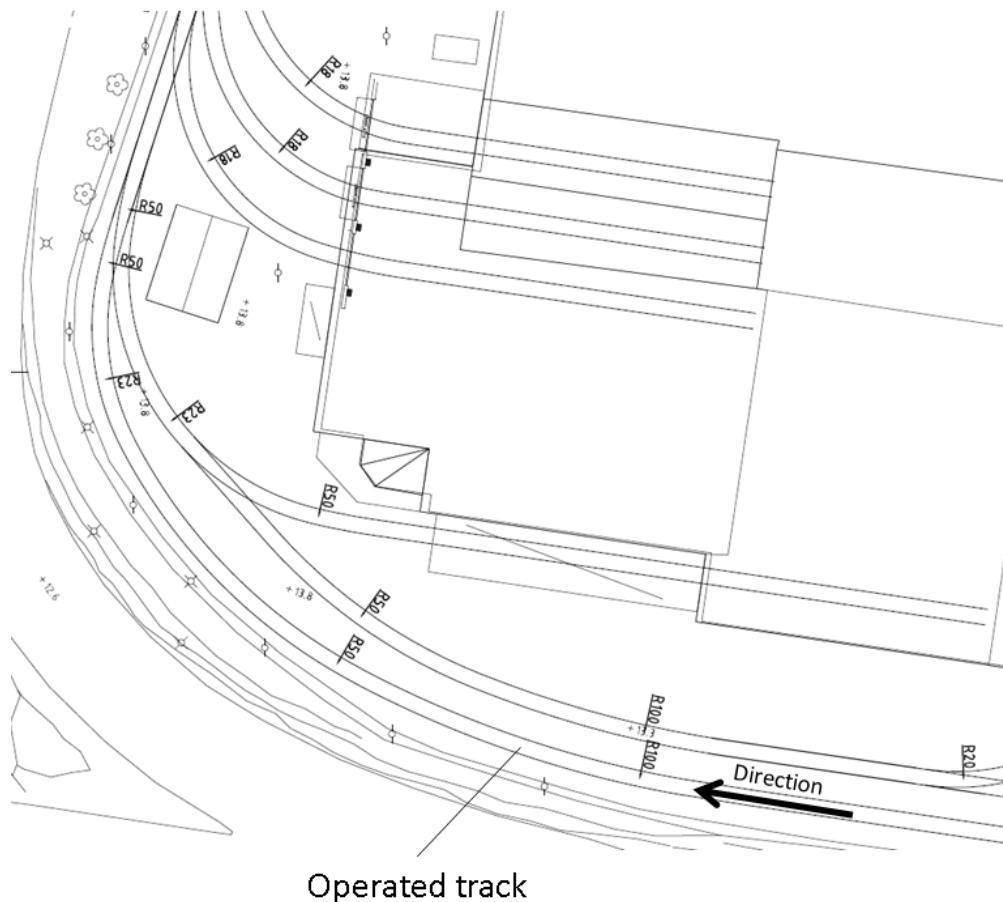


Figure 3.5 – The operated track during the measurements at Rantorget.

The measurements were carried out by ÅF Sound & Vibration on May 13 for tram vehicle M32 in wet conditions and on May 15 for tram vehicle M31 in dry conditions. The wet conditions have some influence on the friction between the wheel and rail. This has been accounted for by using different friction coefficients in the GENSYS simulations. For the dry conditions, the friction between wheel and rail is set to 0.4, while for the wet conditions it is set to 0.25 according to the GENSYS manual. As mentioned, the measurements were performed at two constant speeds, 15 km/h and 20 km/h. Five measurements were performed at each speed. The repeatability was good and in the following only one of these will be presented.

The lateral accelerations of the car bodies can be seen in figure 4.6. The red curve represents the measured acceleration and the black the simulated acceleration. The first plot row represents vehicle M31. The second plot row represents vehicle M32. The left figures are for 15 km/h and right figures at 20 km/h. The accelerometers used in the measurements have a lower frequency limit of 1-2 Hz. This means that frequencies in the signals lower than this (including the quasistatic lateral accelerations) cannot be detected. At the same time GENSYS has an upper frequency limit of, typically, 20 Hz. In order to make the results comparable the calculated accelerations were high pass filtered at 2 Hz in GENSYS to facilitate comparison, a low pas filter was applied to the measured signal to remove contribution from the frequencies above the GENSYS frequency range.

As can be seen there are some differences between the measured and simulated results. Starting by comparing the accelerations between model M31 and M32 it can be seen that the accelerations are generally higher for vehicle M32 compared to M31.

The measurements and simulations starts on a tangent track. In GENSYS the tangent track is modelled as ideal with no track irregularities but in reality irregularities and rail joints will cause accelerations as seen in the measurements.

When entering the curve it can be noticed that also the GENSYS simulations will give rise to accelerations. The magnitudes of the accelerations from the simulations are in acceptable agreement with the measurements when the vehicles enter the curve. This is true for all four plots. At the end of the results of measurements and simulations, the vehicle is leaving the curve. This gives once again rise to lateral accelerations in the opposite direction for the GENSYS simulations. Here the agreement is almost as good but it is harder to compare the results due to the existing track irregularities, disturbances and for the real case there is a railroad switch giving rise to large accelerations.

The high degree of irregularities and the presence of switches and joints directly after the curve make it hard to compare accelerations between simulations and measurements. An overall conclusion is that the agreement between the GENSYS simulations and real measurements are best when the vehicle enters the curve. Here it can be seen that the acceleration values match well.

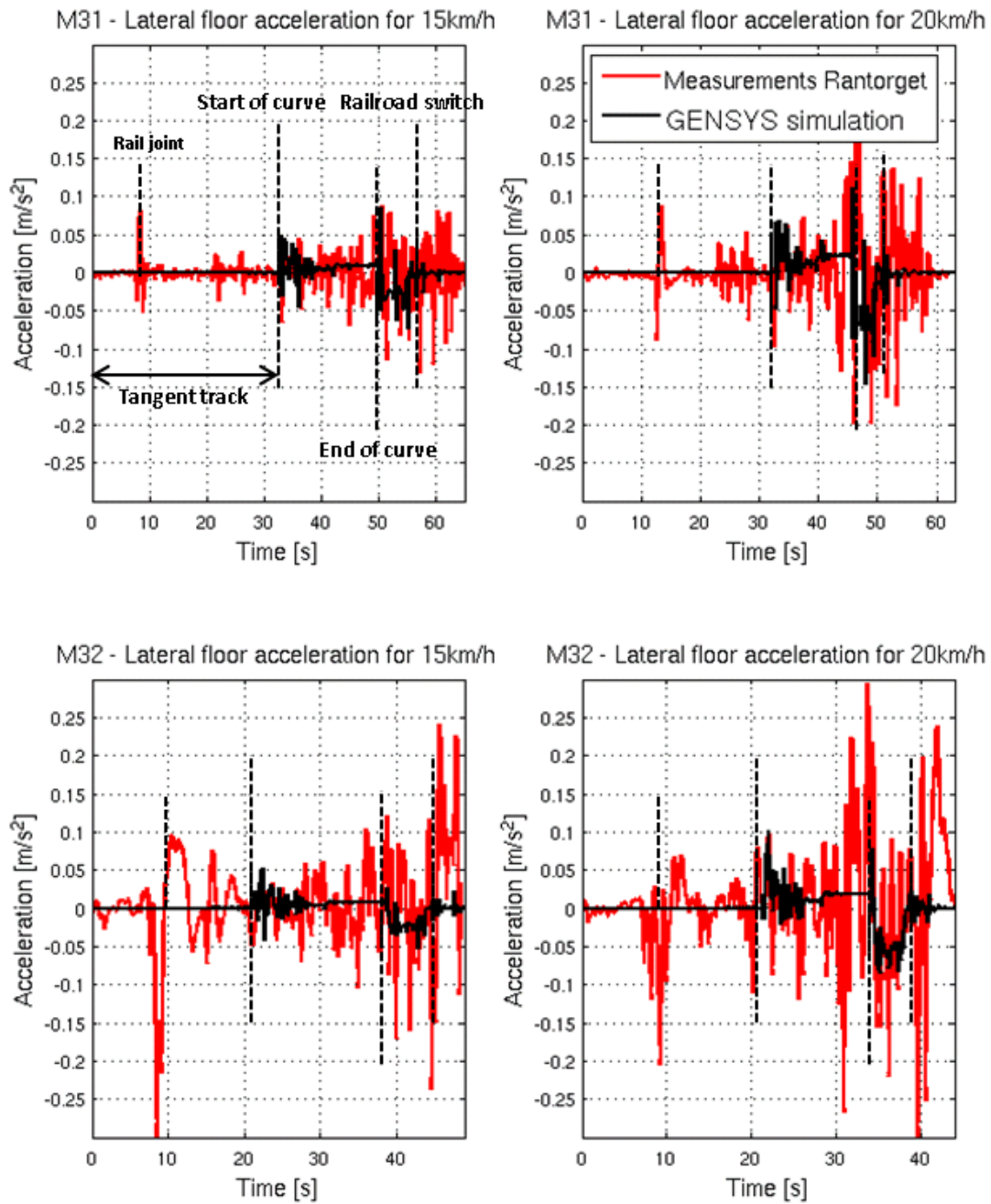


Figure 4.6 – Measured and simulated lateral accelerations on car bodies. Accelerations to the left are defined positive. The top left figure compares the lateral accelerations for the first car body on vehicle M31 at constant speed 15 km/h. The top right figure compares the lateral accelerations for the first car body on vehicle M31 at constant speed 20 km/h. The bottom left figure compares the lateral accelerations for the first car body on vehicle M32 at constant speed 15 km/h. The bottom right figure compares the lateral accelerations for the first car body on vehicle M32 at constant speed 20 km/h.

Measurements of accelerations on bogies, axle boxes (on M31) and wheel beams (on M32) were also performed as mentioned in the method chapter. A comparison between the measurements and simulation for the lateral bogie acceleration can be seen in figure 4.7.

Due to constraints used for axle boxes and wheel beams in the GENSYS models, the same method as used for the car bodies to calculate the simulated accelerations could not be used. For the car bodies the accelerations were calculated by using the total force acting on the mass. For the other components the accelerations were calculated by differentiating the speed of the masses. This calculation method will result in high acceleration levels at the break-points between the transition curves and the circular curves. The high acceleration is due to that the modelling gives a perfect ideal designed geometry for the transition curves. This behaviour can clearly be seen in figure 4.7. A comparison of the lateral acceleration at the right axle box on M31 and wheel beam on M32 can be seen in figure 4.8. Also here the large acceleration peaks are evident at the transition curves.

A conclusion is that the method used for calculating the acceleration on these components cannot be used to verify the measured accelerations. As mentioned earlier it is assumed that all components can be modelled as rigid bodies. To obtain better simulated acceleration values flexible mode shapes can be supplied for the mass bodies. This was considered as out of the scope for this project.

Considering the agreement between models and measurements in acceleration of the car bodies when entering the curve, it is believed that the GENSYS models represent the dynamic curving behaviour of real tram vehicles relatively well.

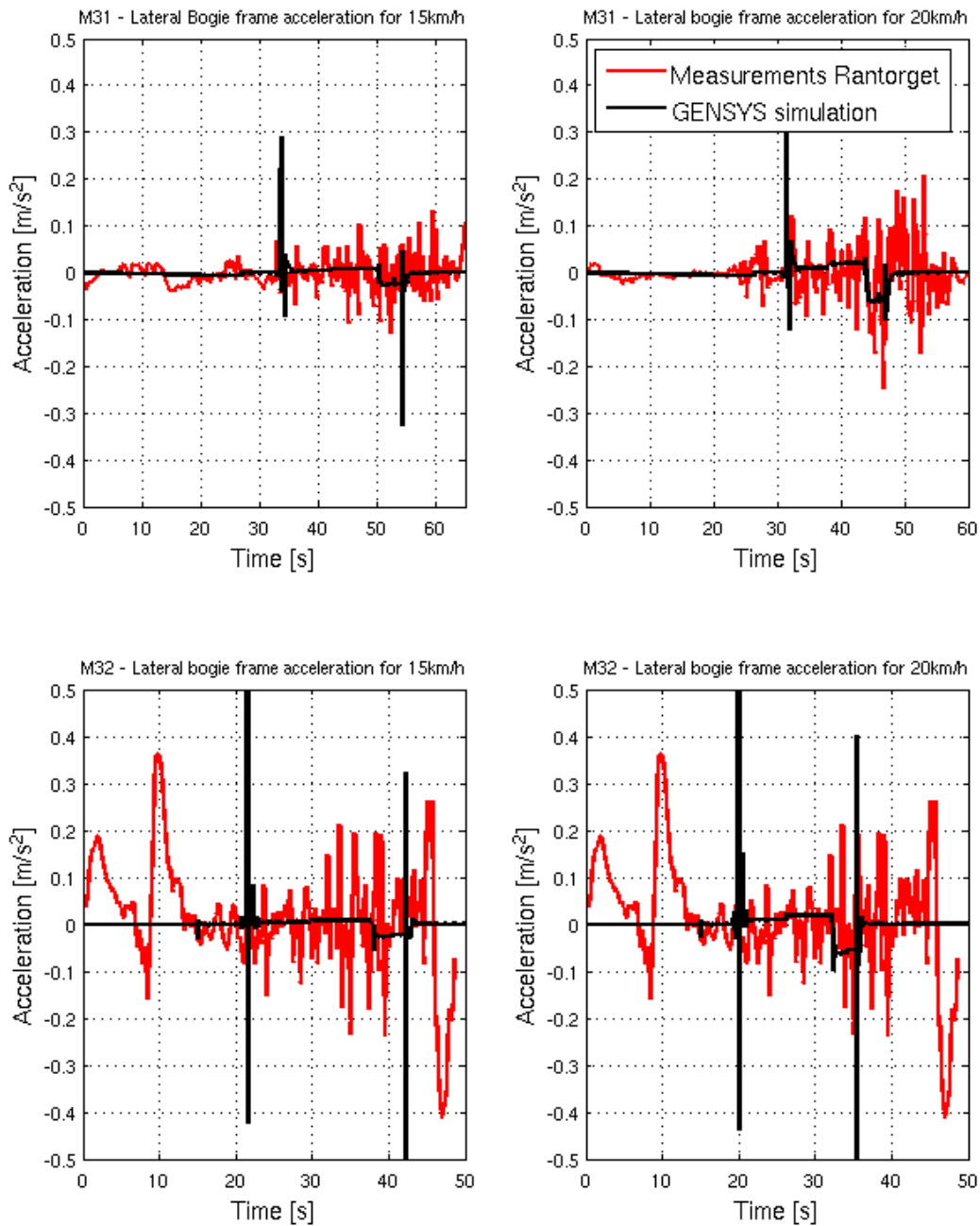


Figure 4.7 – Measured and simulated lateral accelerations on bogie frame. Accelerations to the left are defined positive. The top left figure compares the lateral accelerations for the first bogie frame on vehicle M31 at constant speed 15 km/h. The top right figure compares the lateral accelerations for the first bogie frame on vehicle M31 at constant speed 20 km/h. The bottom left figure compares the lateral accelerations for the first bogie frame on vehicle M32 at constant speed 15 km/h. The bottom right figure compares the lateral accelerations for the first bogie frame on vehicle M32 at constant speed 20 km/h.

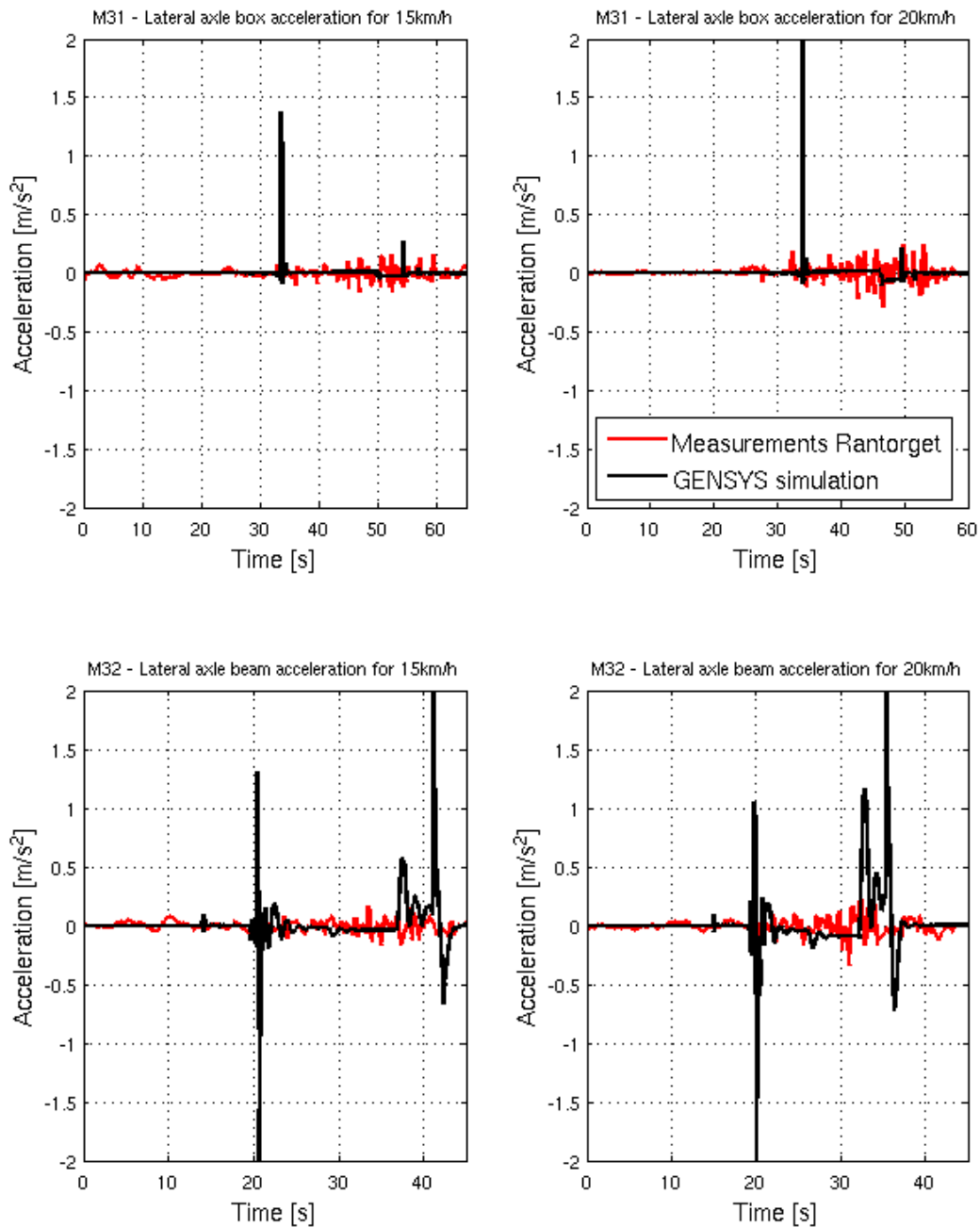


Figure 4.8 – Measured and simulated lateral accelerations on axle box and wheel beam. Accelerations to the left are defined positive. The top left figure compares the lateral accelerations for the axle box on vehicle M31 at constant speed 15 km/h. The top right figure compares the lateral accelerations for the first axle box on vehicle M31 at constant speed 20 km/h. The bottom left figure compares the lateral accelerations for the first wheel beam on vehicle M32 at constant speed 15 km/h. The bottom right figure compares the lateral accelerations for the first wheel beam on vehicle M32 at constant speed 20 km/h.

5. Results

In this chapter the results of the parameter studies of this thesis work will be presented and discussed.

5.1 Parameter study

One purpose of these studies is to show how the different tram vehicles behave compared to each other and also to investigate the influence of different design parameters on track forces during curving. The studies are limited to curves with small curve radii and low speeds. Friction coefficients are assumed to be 0.4 on tangent tracks and 0.25 in the curves due to lubrication.

5.1.1 Nominal dynamic track forces

The nominal dynamic track forces for the simulations are presented in this subchapter. The track forces are divided into two parts called Y - and Q -forces. The first force acts in parallel to the track plane in the lateral direction while the second is normal to the track plane. In this part of the study the wheel and rail profiles are new (nominal). A right-handed circular curve with radius 20 m is entered with a constant speed of 15 km/h. In the simulations the vehicle starts on a tangent track and enters the circular curve after a transition curve with length 2.35 m. The radius of the curve and length of the transition curve used for this study are the smallest allowed values for a curve in Gothenburg [17] and the speed is the highest allowed in such a curve.

The result of the Y -forces acting on the M31 wheels can be seen in figure 5.1. A positive Y -force on the wheel is defined in the direction towards the centre of the right-handed curve i.e. the track pushes the wheels inwards due to wheel friction, conicity and flanges. The left column shows the forces on the outer wheels of tram vehicle M31 and the right column shows the forces on the inner wheels. In some cases, there is more than one contact point between a specific wheel and the rail, one example is when flange steering occurs. The Y -force showed in Figure 5.1 is then the total sum of the all the lateral contact forces. In general, in a curve the Y -forces are higher on the outer wheels compared to the inner ones as can be seen in figure 5.1.

The Q -forces acting on the M31 wheels can be seen in figure 5.2. Observe that these are the dynamic Q -forces, which means that the static forces from the vehicle weight are not included. For the first seconds of the simulation the vehicle is travelling on an ideal tangent track with no track irregularities. This means that the dynamic Q -forces will be zero. The vehicle is then entering the curve and the forces are increased for the outer wheels and decreased for the inner wheels.

Negative values of the dynamic track forces on the inner wheels do not mean that the total force between these wheels and track are negative. The plots show only the dynamic track forces, the static force has to be added to get the total force.

The Y - and Q -forces for tram model M32 are shown in figures 5.3 and 5.4. As was explained earlier this model has a stiffer bogie design and this will give rise to larger lateral forces (Y -

forces), especially on the outer wheel of the leading axle. As seen in figure 5.3, the GENSYS calculations confirms this. Also the oscillating and hammering behaviour in the lateral force discussed earlier can be observed in the simulations.

A plot of the dynamic Q -forces for M32 can be seen in figure 5.4. The same kind of oscillation as for the lateral forces is also visible for the vertical.

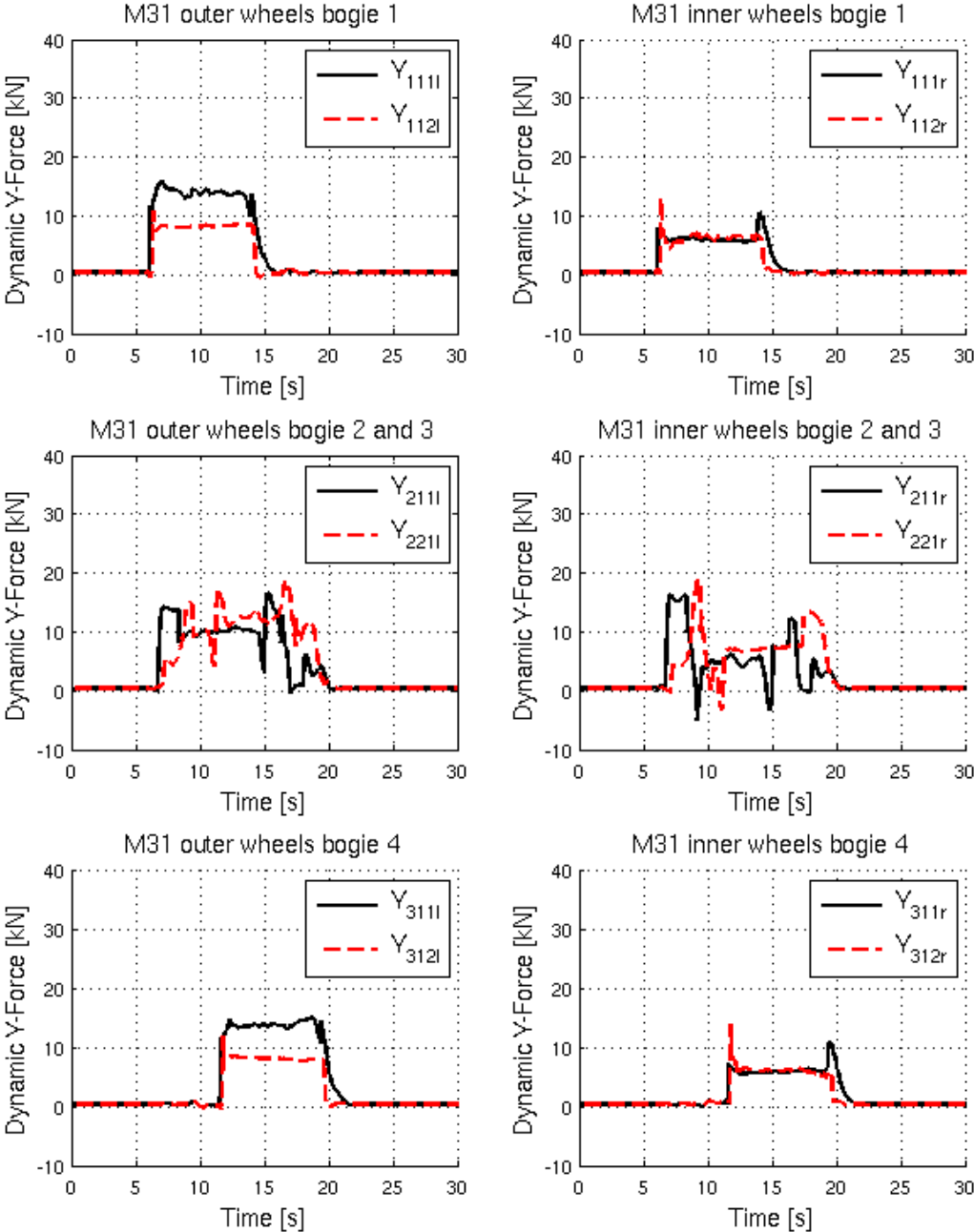


Figure 5.1 – Dynamic Y -forces acting on the wheels during simulation for all twelve wheels on tram model M31. Positive Y -forces on the wheels are acting towards the centre of the curve.

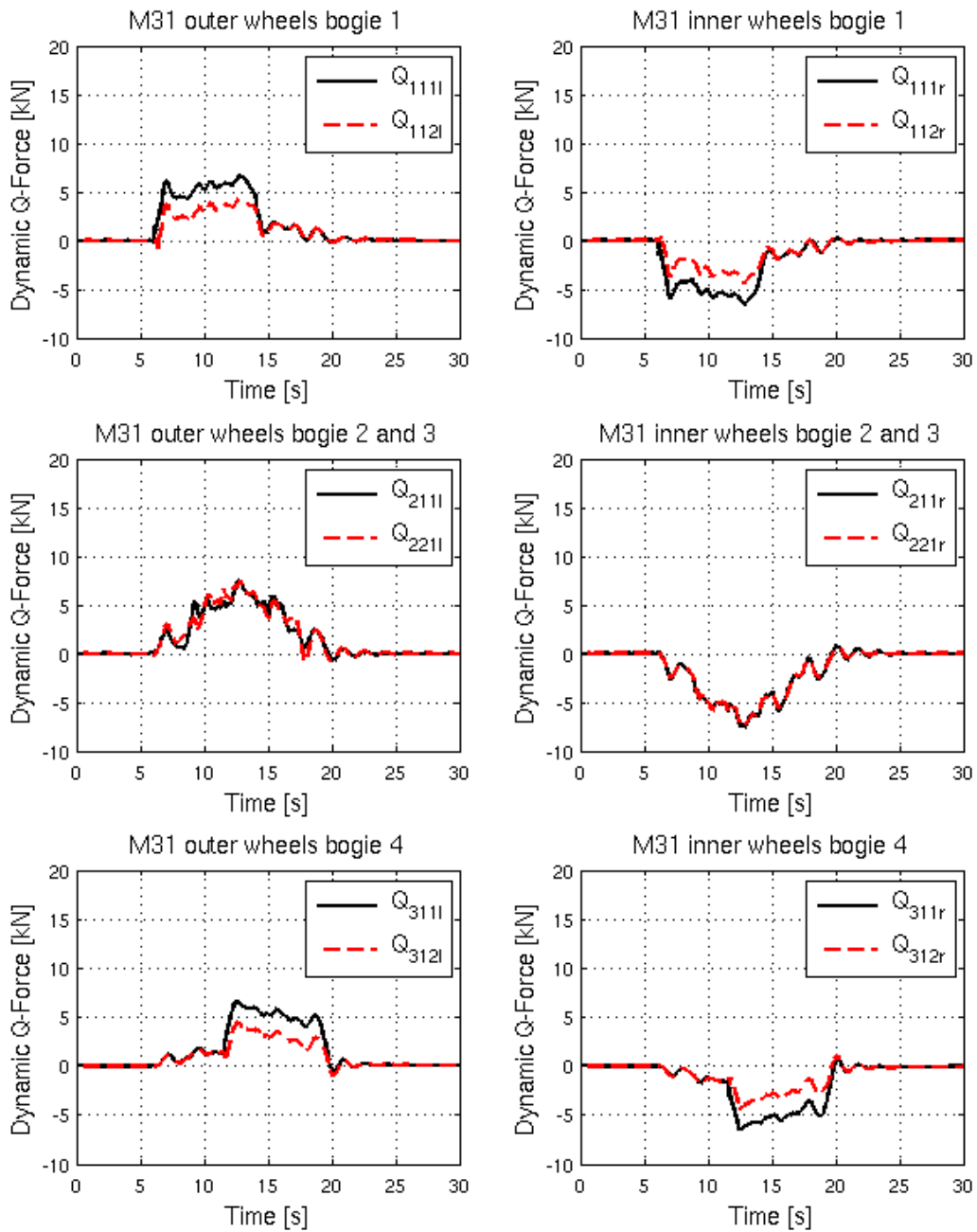


Figure 5.2 – Dynamic Q -forces during simulation for all twelve wheels on tram model M31.

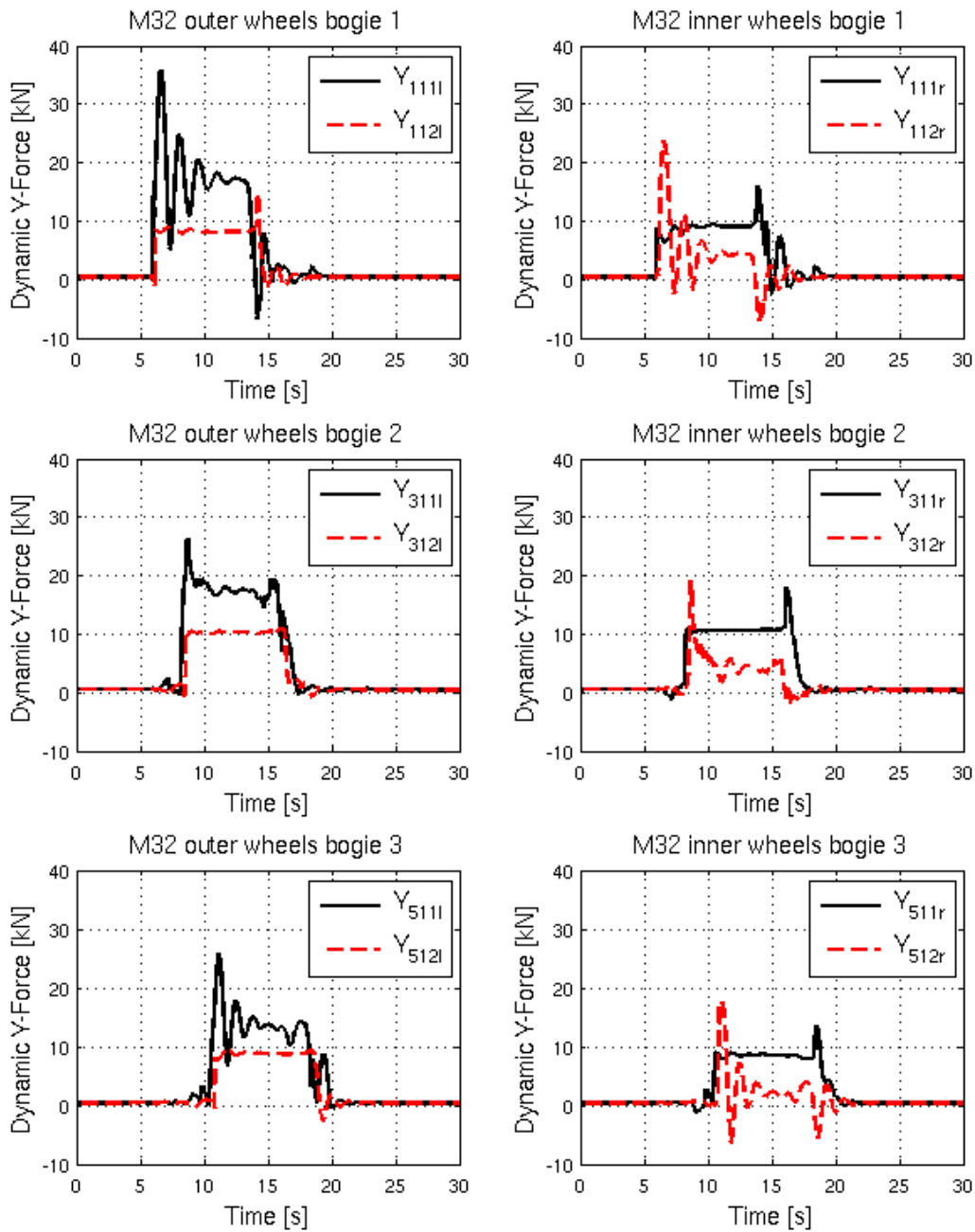


Figure 5.3 – Dynamic Y-forces acting on the wheels during simulation for all twelve wheels on tram model M32. Positive Y-forces on the wheels are acting towards the centre of the curve.

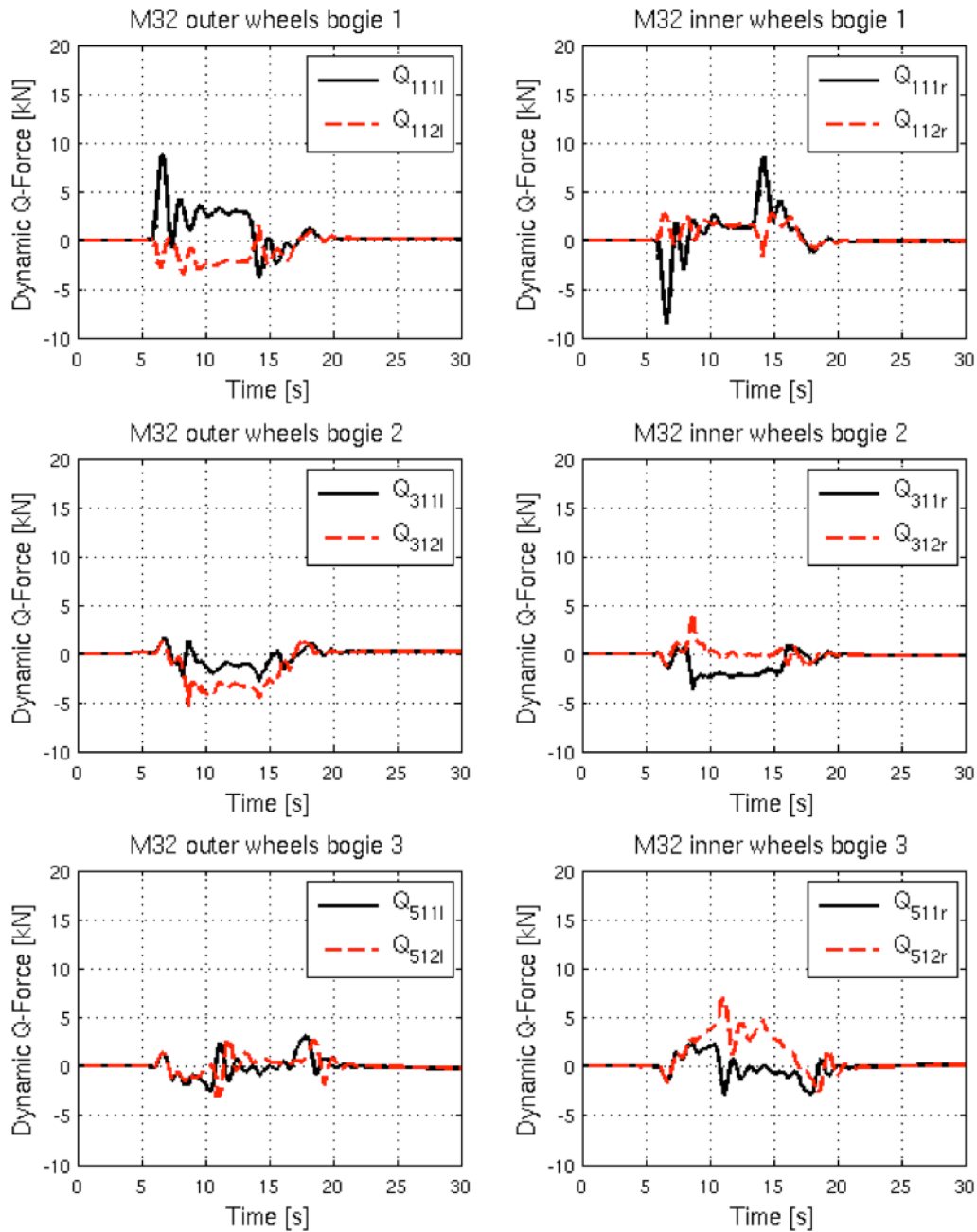


Figure 5.4 – Dynamic Q -forces during simulation for all twelve wheels on tram model M32. The first column of the plots represents the outer wheels and the second column of the plots represents the inner wheels.

According to [10] and also based on observations by GS, the hunting motion of vehicle M32 can occur due to the vehicle design and the conicity of the wheel profiles. High conicity allows the wheels to negotiate curves with smaller radius without flange contact. However, a high conicity may also lead to lateral instability of the wheel sets on tangent track.

An overall conclusion of this study is that the two tram models behave differently when negotiating curves. As expected and discussed in the theory chapter, the dynamic forces are higher on model M32 compared to M31. As can be seen in the figures in this subchapter the forces during the simulations are highest for the outer wheel on the leading axle.

Thus, further studies and results will be limited to the wheels on the leading axle, apart from a parameter study on the influence of misalignment of the lower frame angle on the steering mechanism for axle three on vehicle M31.

In figure 5.5 the Q - and Y -forces for the leading axles of M31 and M32 previously shown in figures 5.1-5.4 are combined to facilitate comparison. Observe that now the total (static + dynamic) Q -forces are shown in the figure, i.e. not only the dynamic ones.

Due to the small radius of the curve there will be flange steering on the outer wheels. In figure 5.6, it can be observed that large Y -forces are obtained between the wheel flange and the rail. When leaving the curve (time 14 s), it is observed in the Y -plots for vehicle M32 (figure 5.3) that the total Y -force on the leading axle is lower than zero. This is because the stiff bogie design generates a hammering motion. Due to the M32 design there will be flange contact on the inner wheels. An illustration of the wheel/rail contact when leaving the curve can be seen in figure 5.7.

For model M31, there is two-point contact between the outer wheel and rail. On M32 the inner wheel instead has flange contact. After some time of running on tangent track the track forces will return to the static level. Model M32 has a tendency of a hunting motion (lateral instability) on tangent track, even at lower speeds. This behaviour is also confirmed by [18].

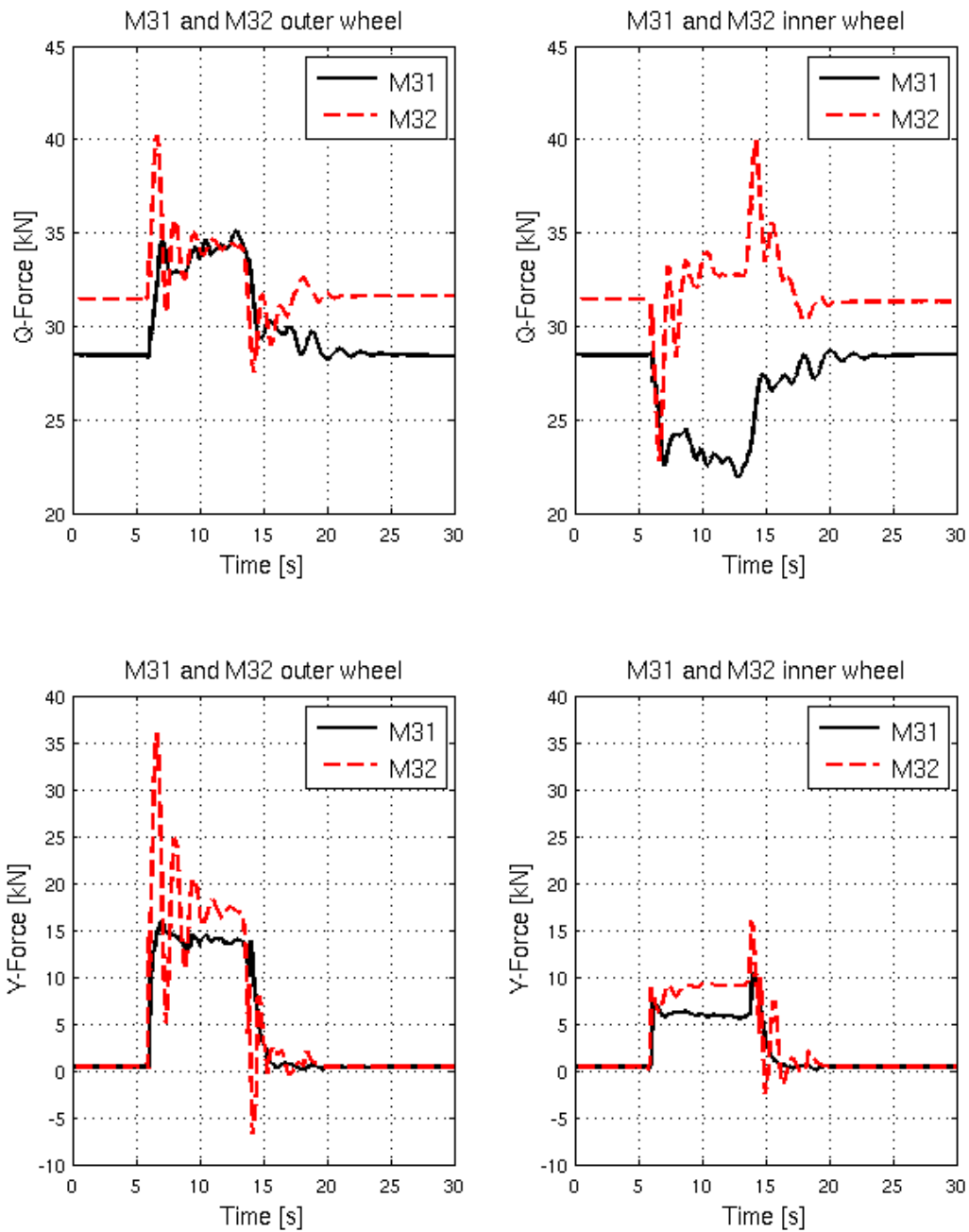


Figure 5.5 – Total Q - and Y -forces for the wheels on the leading axle. The forces are plotted for both tram models. The top left and right figure show the inner and outer Q -forces. The bottom left and right figures show the inner and outer Y -forces. Positive Y -forces on the wheels are acting towards the centre of the curve.

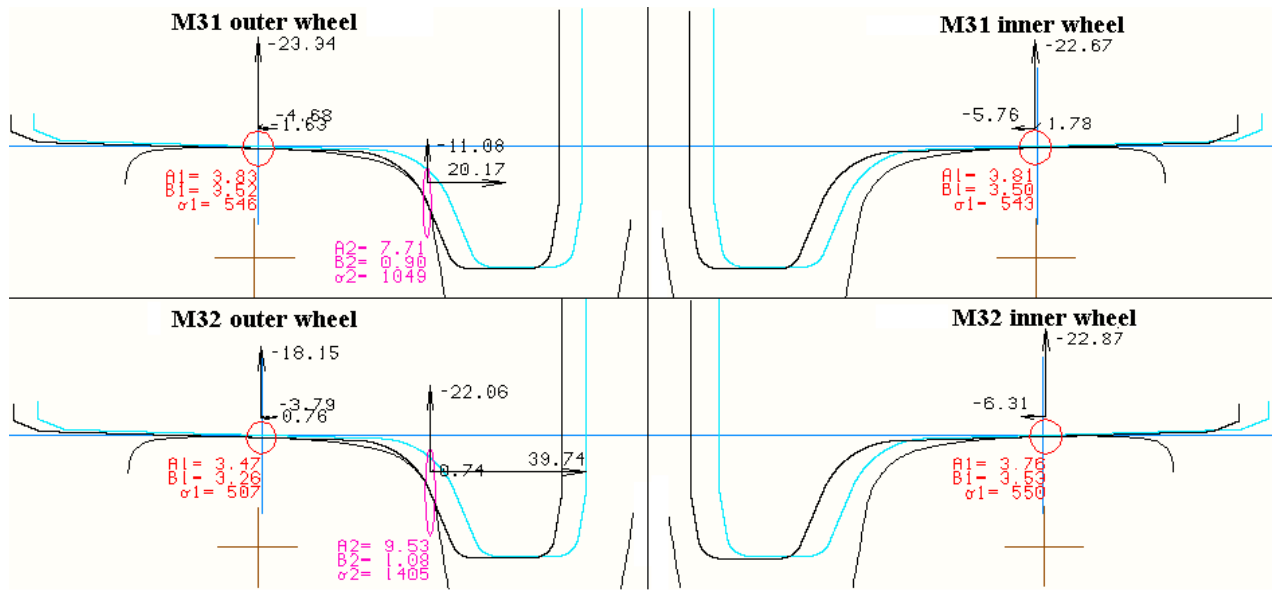


Figure 5.6 – Contact between wheels and rail on the leading axle when entering the right-handed curve (time 6 s). The top figures show the outer and inner wheels on model M31. The bottom figures show the outer and inner wheels on model M32.

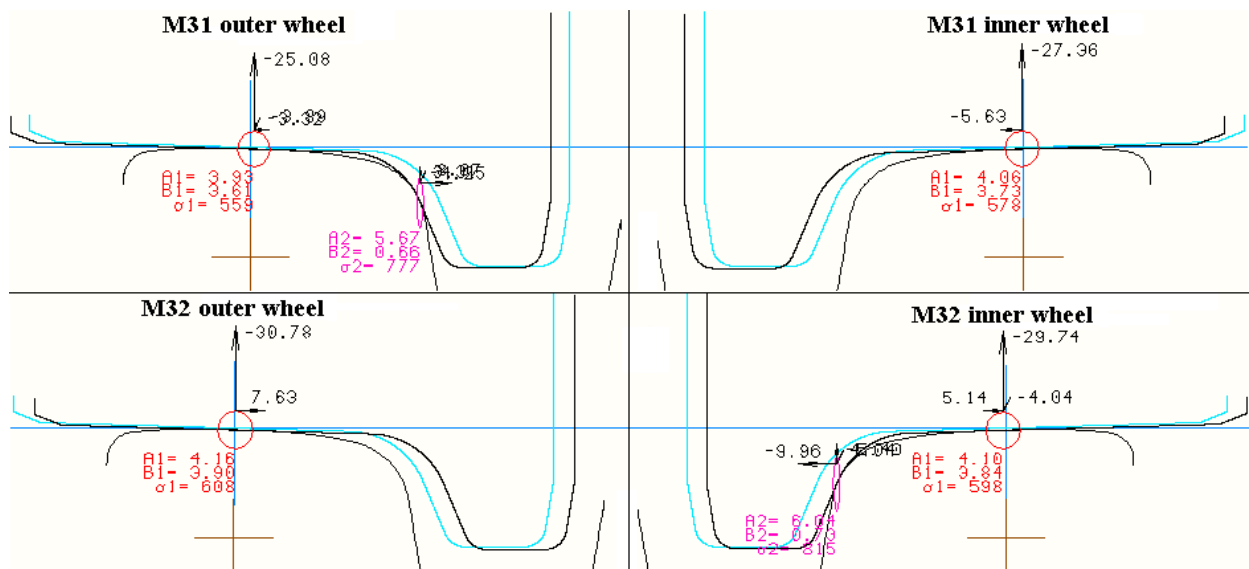


Figure 5.7 – Contact between wheels and rail on the leading axle when leaving the right-handed curve (time 14 s). The top figures show the outer and inner wheels on model M31. The bottom figures show the outer and inner wheels on model M32.

5.1.2 Comparison of track forces for worn and nominal profiles

In this subchapter the effects of different combinations of worn wheel and rail profiles will be presented. The worn wheel and rail profiles have been measured with a MiniProf [19] instrument and the nominal ones have been obtained from drawings. Three wheel profiles and three rail profiles have been used for this study, ending up with a total of 3x3 profile combinations for each tram model. The profiles can be seen in figure 5.8.

The Miniprof measurements will be presented for two worn wheel and rail profiles, here called intermediate and full wear profiles. The full wear profiles have been edited by taking the worst case wear scenario into account. These scenarios were given by GS and TK. The edges of the measured profiles have been adjusted to better fit with the nominal profiles. These edges will not be in contact and a change will not affect the results. The change is only made to make it easier to see the difference between the profiles.

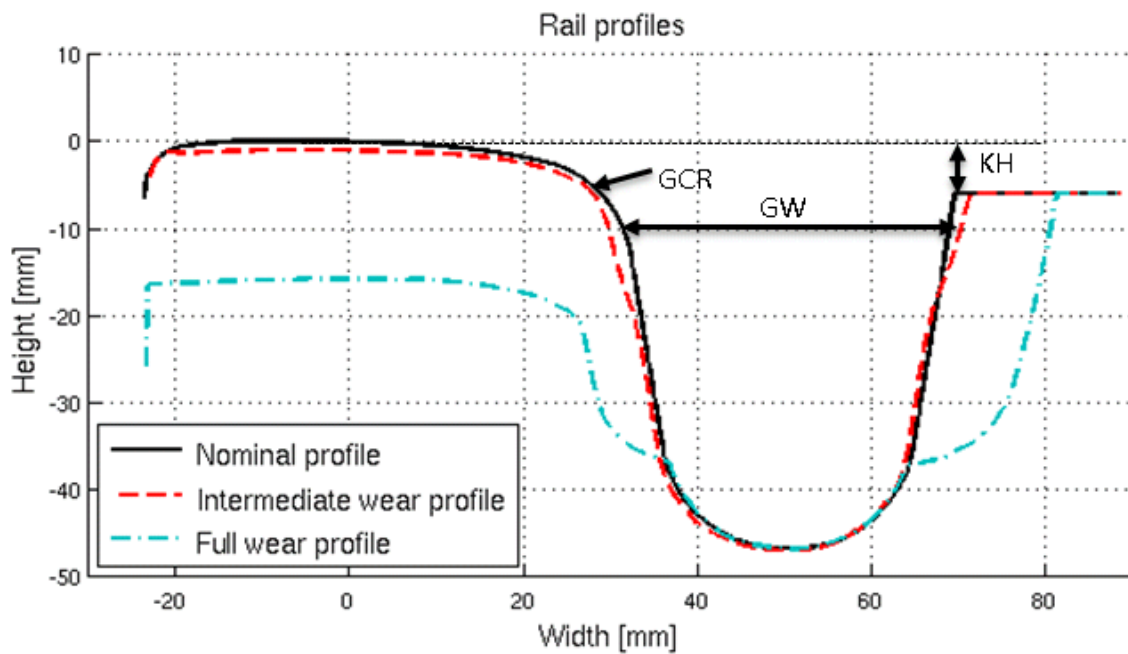
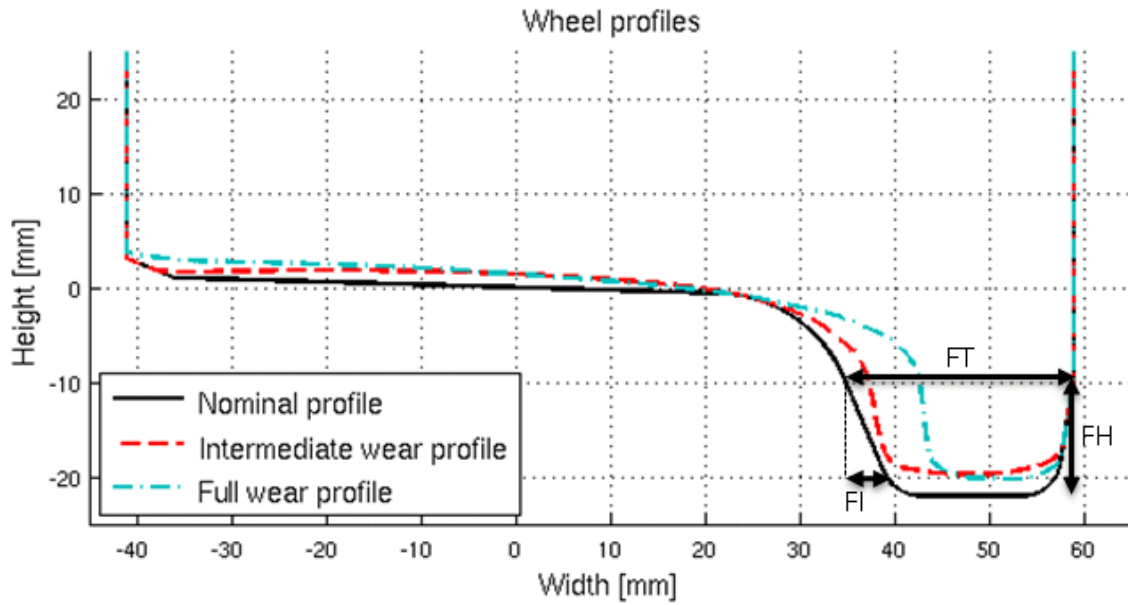


Figure 5.8 – Comparison of different stages of wear on wheel and rail profiles. The top figure shows the used wheel profiles. The black profile represents the nominal profile, the dashed red profile represents the intermediate wear profile and the dash-dotted turquoise profile represents the full wear profile. The bottom figure shows the used rail profiles. The black profile represents the nominal profile, the dashed red profile represents the intermediate wear profile and the dash-dotted turquoise profile represents the full wear profile.

In table 5.1 below a summary of the difference between the characteristics of the wheel profiles can be seen.

Table 5.1 – Summary of the differences between the wheel characteristics.

Wheel Profile	Flange Thickness (FT) [mm]	Flange Height (FH) [mm]	Flange Inclination (FI) [mm]
Nominal	24.08	22.00	4.27
Intermediate	22.40	21.14	2.86
Full	20.66	22.01	1.81

The wear on the wheel profiles affects mostly the flange (thickness and inclination). As can be seen in table 5.1 and also in figure 5.8, the flange inclination is decreased for increased wear on the wheel. This will lead to a sharper and almost vertical wheel flange. This area is of high importance for the wheel/rail contact especially when the vehicle is negotiating a curve. The decrease of flange inclination will result in higher track forces. This can clearly be seen in figure 5.9, where the forces are increased for worn wheel profiles. A table of the difference between the characteristics of the rail profiles can be seen in table 5.2 below.

Table 5.2 – Summary of the differences between the rail characteristics.

Rail Profile	Groove Width (GW) [mm]	Gauge Corner Radius (GCR) [mm]	Keeper height rel. to rail head (KH) [mm]
Nominal	36.35	13.00	-6.00
Intermediate	40.20	6.05	-5.04
Full	48.58	7.02	9.73

As can be noted in figure 5.8 there is a significant difference between the rail profiles, especially for the full wear rail profile. The inner rail profiles were measured on a curve and a tendency of not only vertical but also lateral wear can be noticed on the intermediate profile. The lateral wear can be better observed on the full wear profile, see figure 5.8. One interesting observation is the lateral wear on the keeper (the flange to the right of the groove, which is caused by the vehicle M32. Its design with stiffer bogies will make the wheels get in contact with the keeper even in curves. This behaviour has also been shown and discussed in the curving behaviour chapter. For the three rail profiles the groove width varies from 36.35 mm to 48.58 mm. The horizontal wear on the rail profiles will eventually make the keeper higher than the railhead. This in combination with the increase in groove width can result in a potential safety hazard for cars, cyclists and pedestrians.

The simulations for this study are performed with the same speed and curve radius as in the study for the nominal conditions presented earlier. A bar plot of the mean track forces during the simulation for model M31 can be seen in figure 5.9 and for M32 in figure 5.10. The figures shows the *Y*- and *Q*-forces for both the inner and outer wheel and rail contacts. The bar plots show three groups (1, 2 and 3) and in each group three bars (black, red and turquoise). Each group represents one of the rail profiles and each bar colour represents one of

the wheel profiles. There is a total of nine wheel/rail combinations. An explanation of the colour/group scheme is given in table 5.3.

Table 5.3 – Explanation of the group and colour scheme for wheel/rail combinations used in figure 5.9-5.10.

Group/Colour	Black	Red	Turquoise
1	Nominal rail Nominal wheel	Nominal rail Intermediate wheel	Nominal rail Full wheel
2	Intermediate rail Nominal wheel	Intermediate rail Intermediate wheel	Intermediate rail Full wheel
3	Full rail Nominal wheel	Full rail Intermediate wheel	Full rail Full wheel

It can be noticed that for vehicle M31 the mean lateral forces between the wheels and rails are in general larger when the amount of wear is increased on the wheel profiles. It can also be noticed that the wheel profiles have a larger influence on the track forces compared to the rail profiles. The increase is largest on the lateral forces compared to the vertical ones as can be seen in figure 5.9. The simulation is done on a right-handed curve and this is the reason why the vertical forces on the left wheels are larger than the ones on the right wheels. Also for M32 there is an increase of the lateral forces obtained for wheel profiles with wear compared to nominal ones.

It should be noticed that the number of profile combinations in this study is quite small. The span between the intermediate and full wear profiles is quite large and it cannot be ruled out that there are other combinations between these states that could lead to higher forces. Conclusions from this study are that wear on wheels gives rise to larger track forces compared to nominal profiles, and that rail wear does not have as large influence on the track forces as wheel wear. More about this will be discussed later in this report.

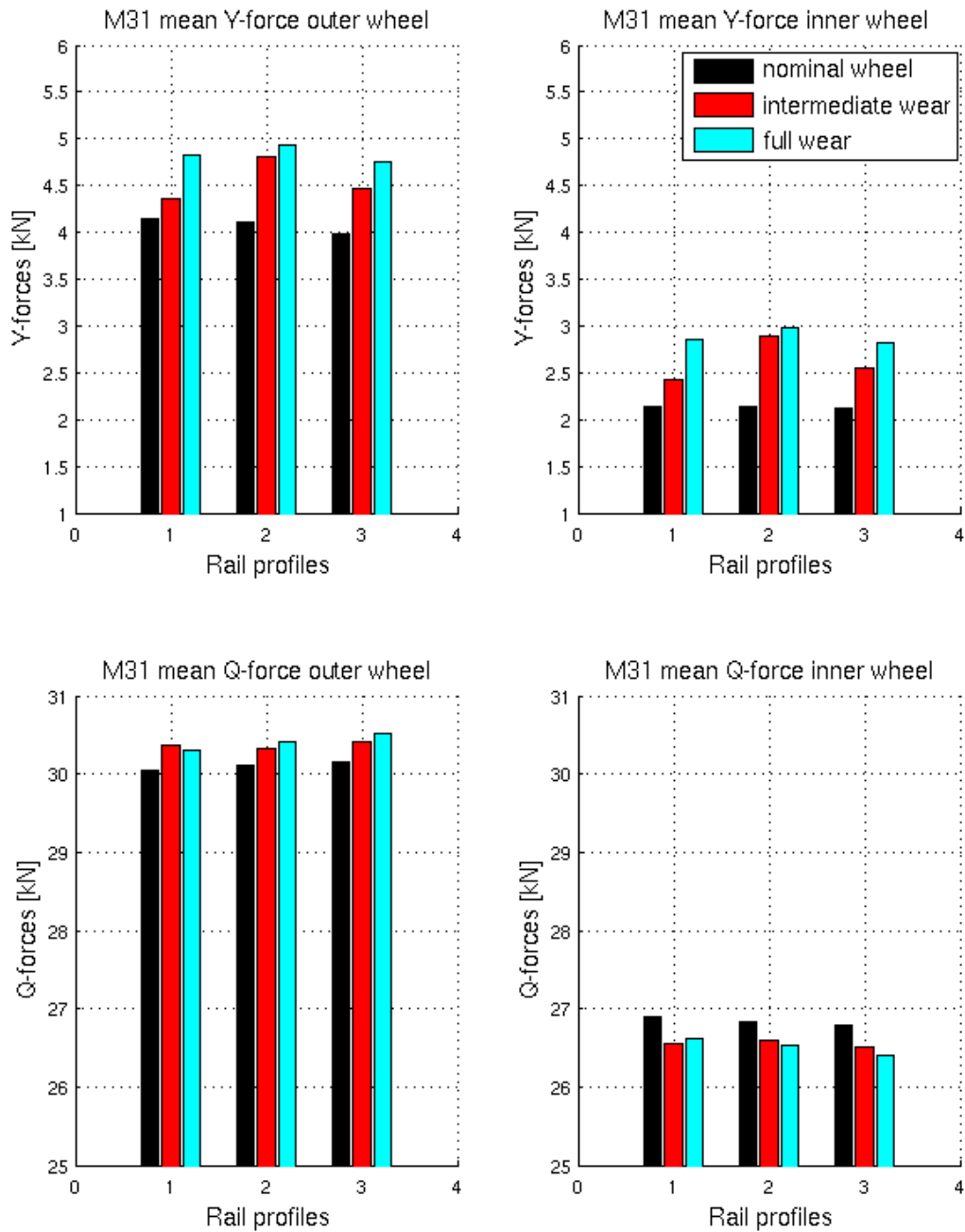


Figure 5.9 – Mean track forces on model M31 for different combinations of wheel and rail profiles. The bar plots are divided into three groups. Each group represents one rail profile. In one group there are three bars, each bar represents one wheel profile.

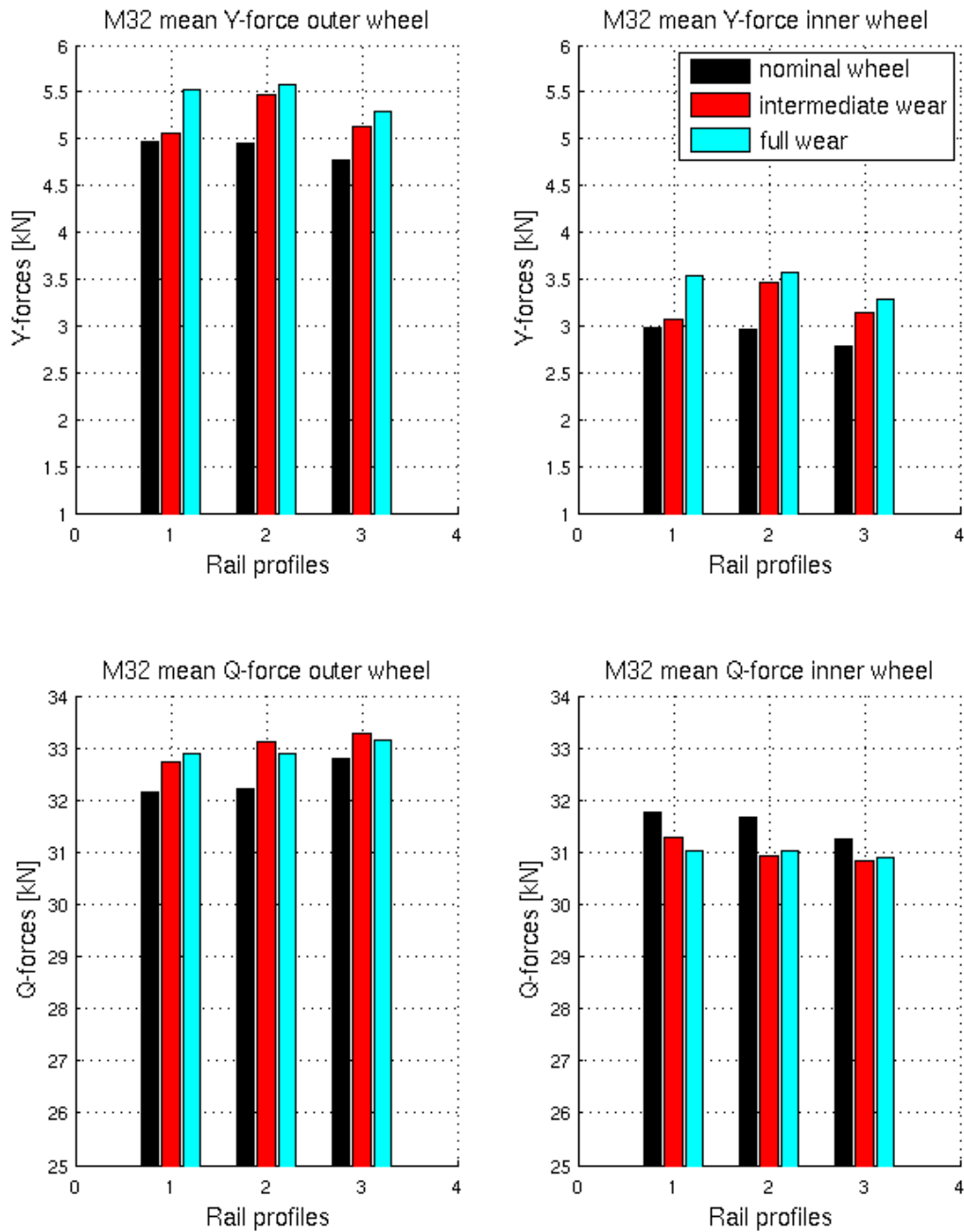


Figure 5.10 – Mean track forces on model M32 for different combinations of wheel and rail profiles. The bar plots are divided into three groups. Each group represents one rail profile. In one group there are three bars, each bar represents one wheel profile.

5.1.3 Influence of M31 car body on wheel set misalignment angle

The wheel sets of car body C of M31 are connected to car bodies A and B through the mechanical coupling described in section 1.5.1 and are aligned manually. According to GS it is difficult to align the wheel sets and a poor alignment result in high wear on the wheels. This has motivated a study of how a setting of wrong angles of the leading wheel set in car body C of M31 influences the track forces. Two cases are investigated and compared to a reference case. The wheel set is set to an initial misalignment angle of ± 2 degrees, which is the worst case. An illustration of the angles can be seen in figure 5.11.

The simulations are performed with nominal wheel and rail profiles. The tram vehicle is travelling on a tangent track and negotiates a right handed circular curve with curve radius 20 m at constant speed 15 km/h. The resulting lateral track forces on the outer and inner rail can be seen in figure 5.12.

An error of -2 degrees (red dashed curve) leads to larger lateral track forces compared to the reference case (solid black curve) with zero misalignment angle in the curve. The figure also shows that the curving behaviour of the wheel set has changed. An error of 2 degrees (turquoise dash-dotted curve) does not result in any significant changes in the curve, but it should be observed that a misalignment will lead to much larger lateral track forces on tangent tracks compared to the reference case. An increase from approximately 1 kN to 14 kN is obtained. A positive misalignment angle gives rise to an extensive increase of force on the inner rail at the end of the curve compared to the reference case. A misalignment does not affect the vertical track forces significantly.

An important conclusion of this study is that a small error of angle set up leads to a large increase of lateral track forces on tangent track. It is recommended that the alignment of the wheel sets is checked regularly.

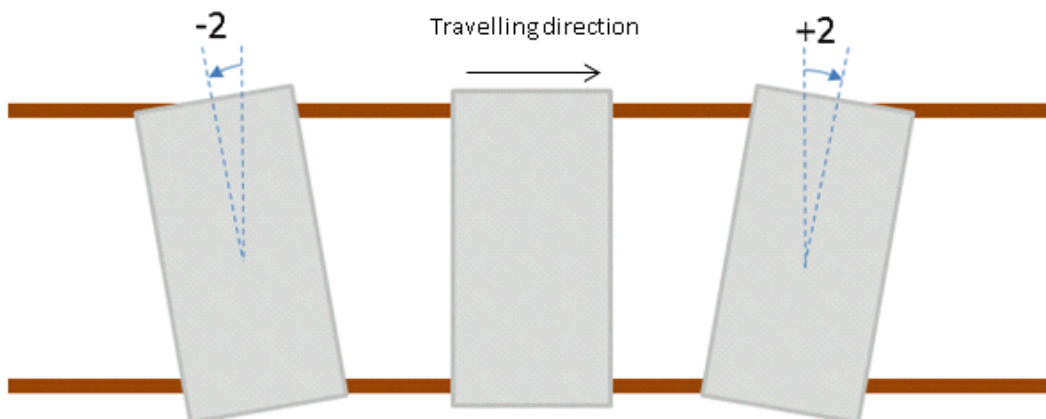


Figure 5.11 – Illustration of the misalignment angle for the leading wheel set in car body C.

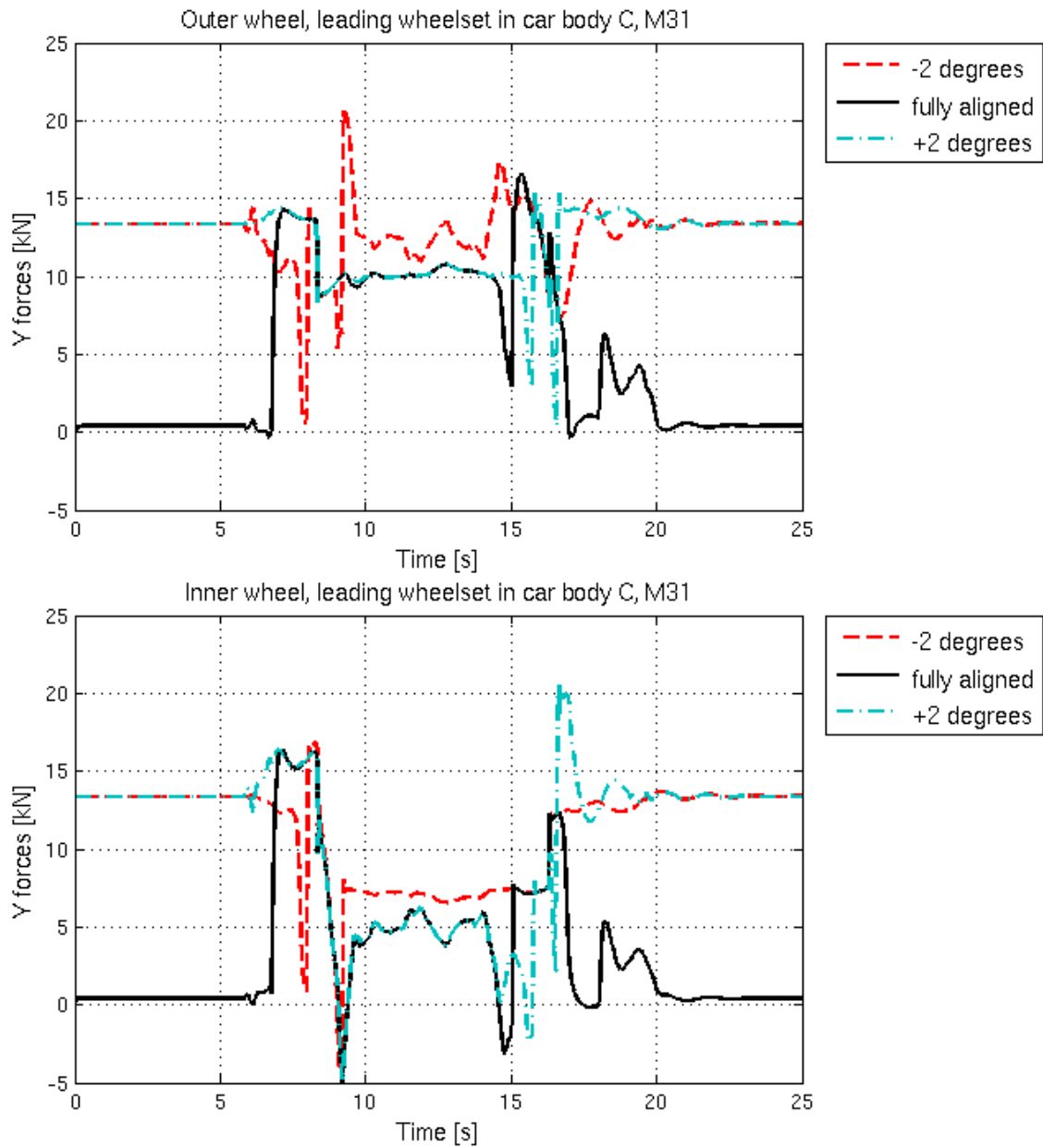


Figure 5.12 – Misalignment angle. Lateral track forces on the outer (top figure) and inner (bottom figure) wheels of the leading wheel set in car body C of M31. Positive Y -forces on the wheels are acting towards the centre of the curve.

5.1.4 Empty and fully loaded tram vehicle

The dynamic track forces have been studied and compared for the case when the trams are full with passengers. As before a curve of radius 20 m is negotiated with a constant speed of 15 km/h. The passenger capacity for tram models M31 and M32 can be seen in [2]. Here it is assumed that an average person weighs 70 kg. The weight of the car bodies, empty and full can be seen in table 5.4 below. Calculations of the car body weights are presented in *Appendix 4*.

Observe here that this is the total weight of the car bodies and not the whole tram vehicle. When comparing empty and full vehicles, the weight of the car bodies on M31 is increased with a factor of 1.57 and on M32 with a factor of 1.51. Thus, the weight of the car bodies are increased a significant amount and this will affect both the static and dynamic track forces.

Table 5.4 – Weight of the car bodies, empty and full.

M31			M32		
	Sitting	Standing	-	Sitting	Standing
Number of passengers	81	109	Number of passengers	87	104
	Empty [kg]	Full [kg]	-	Empty [kg]	Full [kg]
Car body A	7850	12190	Car body A	5000	7660
Car body B	8030	12370	Car body B	6000	8380
Car body C	7650	12270	Car body C	4100	6620
-	-	-	Car body D	6000	8800
-	-	-	Car body E	5000	8010
Total weight	23530	36830	Total weight	26100	39470

A plot of the dynamic *Y*-forces for a full and empty tram model M31 can be seen in figure 5.13. The top figure shows the outer wheel on the leading axle and the bottom figure shows the inner wheel on the same axle. As expected the dynamic forces are increased for the fully loaded vehicle. The *Q*-forces are shown in figure 5.14. Also here the dynamic force is increased for the full tram. Another interesting observation is that there is larger dynamic motion when the vehicle is full. This is particularly evident in the *Q*-force plot.

A plot of the dynamic *Y*-forces for tram model M32 can be seen in figure 5.15 below. A full vehicle behaves in the same way for this model as discussed above for M31. The *Q*-forces for M32 are plotted in figure 5.16. The dynamic motions are increased somewhat but not as much as for M31. The reason for this is that the primary suspension is much stiffer for M32 compared to M31.

A conclusion of this study is that the static and dynamic forces between rails and wheels are increased when a full tram is operated compared to an empty. This will increase the wear on both wheels and rail. These results are somewhat obvious but the study shows one more important thing, which is that the GENSYS models behave as expected.

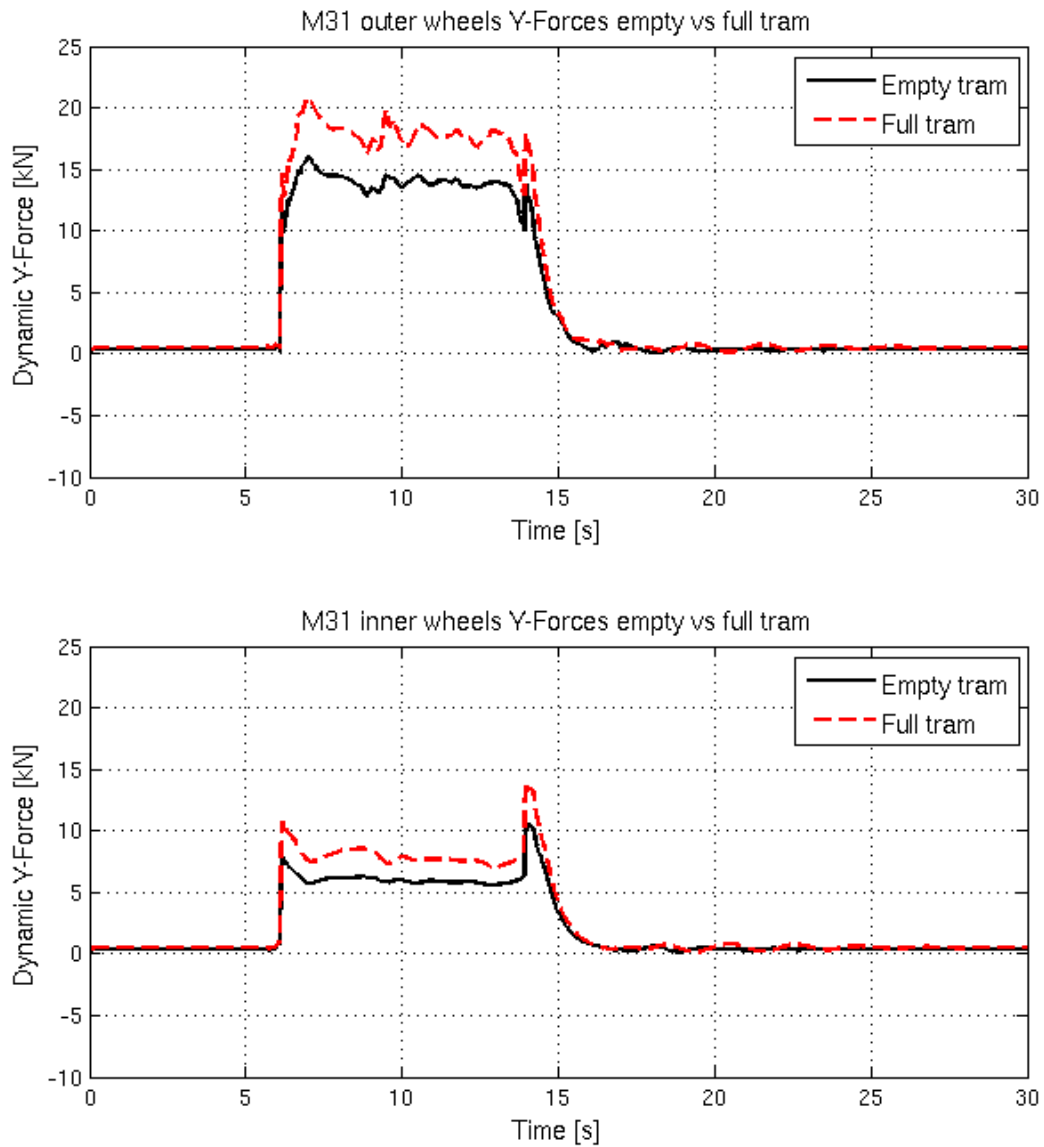


Figure 5.13 – Comparison between Y-forces obtained during simulations with M31 model. The black lines represent an empty tram and the dashed red lines a fully loaded tram. Top figure shows the Y-forces on the outer wheels and bottom figure shows the Y-forces on the inner wheels. Positive Y-forces on the wheels are acting towards the centre of the curve.

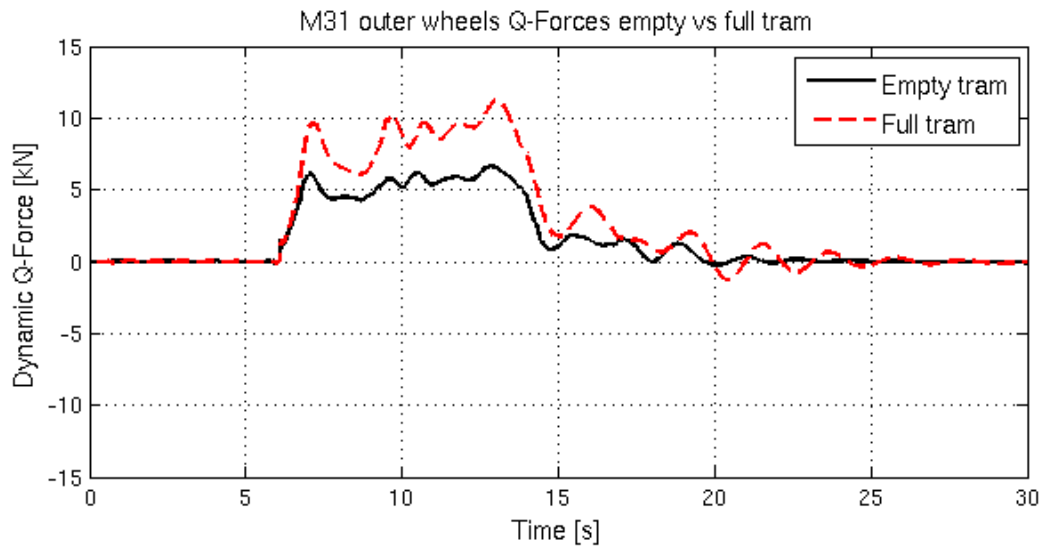


Figure 5.14 – Comparison between Q -forces obtained during simulations with M31 model. The black lines represent an empty tram and the dashed red lines a fully loaded tram. Top figure shows the Q -forces on the outer wheels and bottom figure shows the Q -forces on the inner wheels.

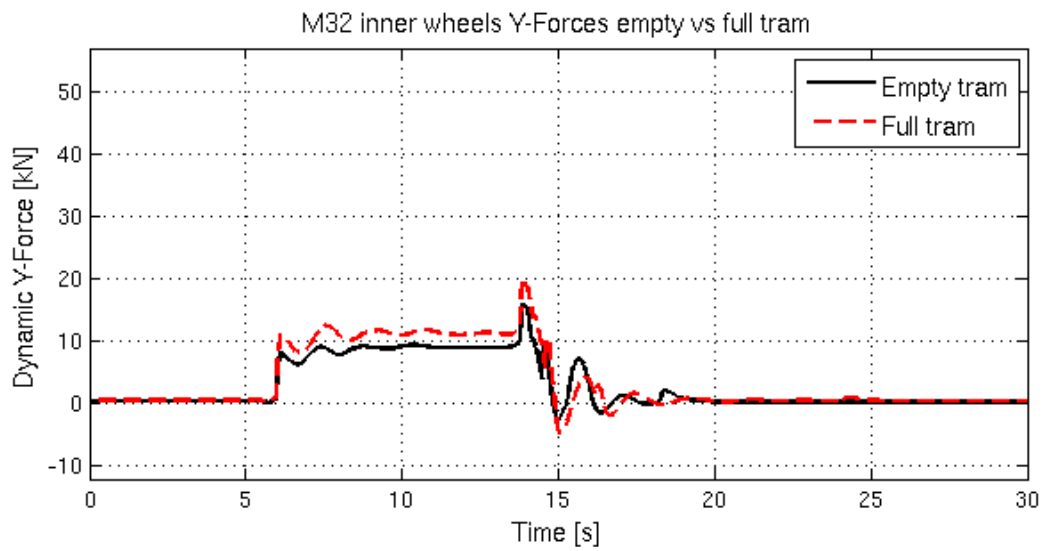
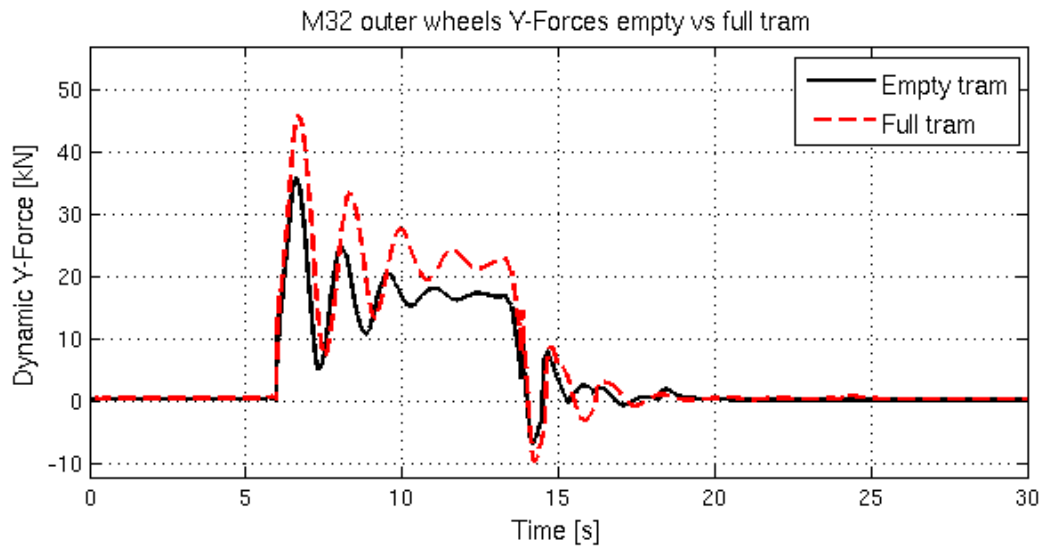


Figure 5.15 – Comparison between *Y*-forces obtained during simulations with M32 model. The black lines represent an empty tram and the dashed red lines a fully loaded tram. Top figure shows the *Y*-forces on the outer wheels and bottom figure shows the *Y*-forces on the inner wheels. Positive *Y*-forces on the wheels are acting towards the centre of the curve.

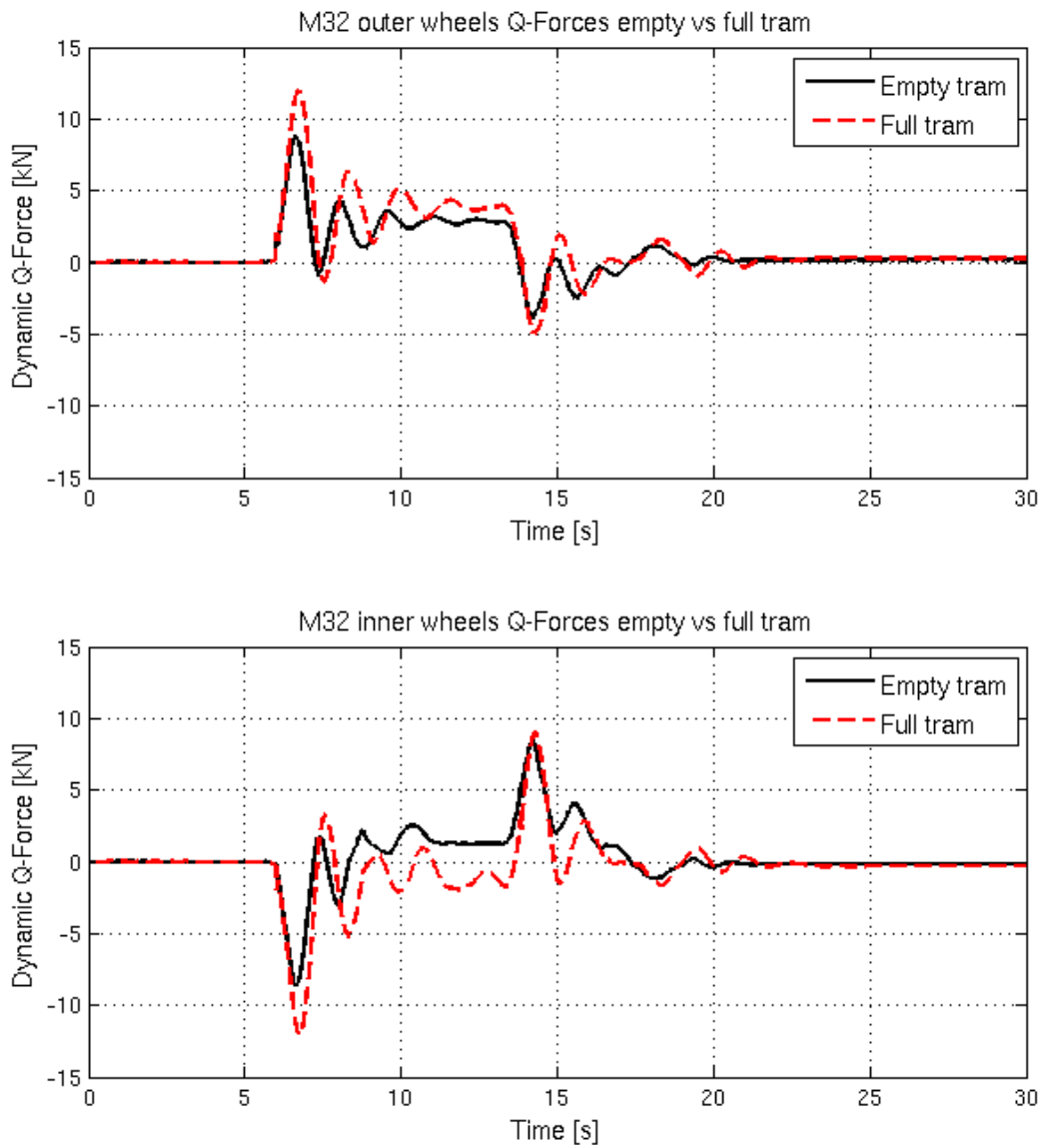


Figure 5.16 – Comparison between Q -forces obtained during simulations with M32 model. The black lines represent the empty tram and the red lines full tram. Top figure shows the Q -forces on the outer wheels and bottom figure shows the Q -forces on the inner wheels.

5.1.5 Primary springs stiffnesses

In this subchapter an investigation of the influence of primary suspension stiffness on the track forces is presented.

As before, the simulations are performed with nominal wheel and rail profiles, and the tram models are negotiating a right handed curve with curve radius 20 m at constant speed 15 km/h. Two cases have been studied, where the primary spring stiffnesses (longitudinal, lateral and vertical stiffnesses) have been increased and reduced with 50%. The calculated track forces have been compared to the nominal case. To change the stiffness in all three directions simultaneously is considered a simplified way of simulating ageing of rubber elements that becomes stiffer with time and hence increases track forces [11]. Values of ageing factors are needed to predict the change of stiffness with time. This is out of scope for this project.

The results of the total (static + dynamic) vertical track forces for tram model M31 and M32, due to change of stiffnesses of the primary springs, can be seen in figure 5.17. The maximal vertical track forces are obtained at the outer wheel of the leading axle and is the only response quantity that will be presented.

As can be seen in figure 5.17, increasing the stiffnesses will slightly increase the vertical track forces relative to when nominal primary springs are used. Notice that the change in absolute stiffness M32 is not as large compared to M31 because this model has stiffer nominal springs.

The lateral track forces are not influenced noticeably and are not presented graphically. In principle, reducing the stiffnesses will reduce the lateral track forces but the changes here were too small to have an effect. A softer primary spring results in a better wheel guidance, which is mainly controlled by the longitudinal and lateral stiffnesses. It should be noted that a reduction will increase the lateral movement of the car body and hence will give a worse riding comfort for the passengers.

A further study can be made by studying longitudinal, lateral and vertical stiffnesses individually to optimize the properties of springs to reduce track forces and maintain a good riding comfort. This is an interesting example of future work.

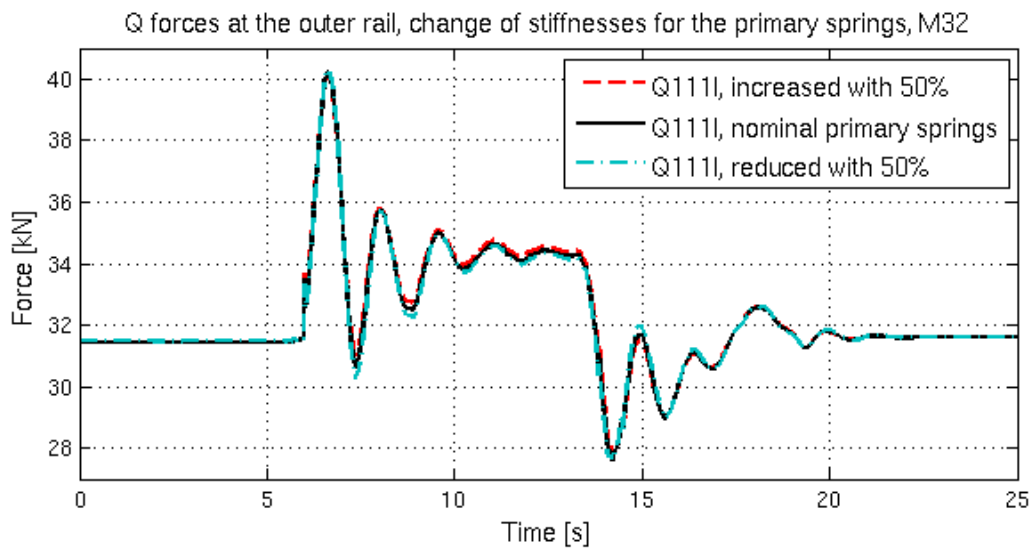
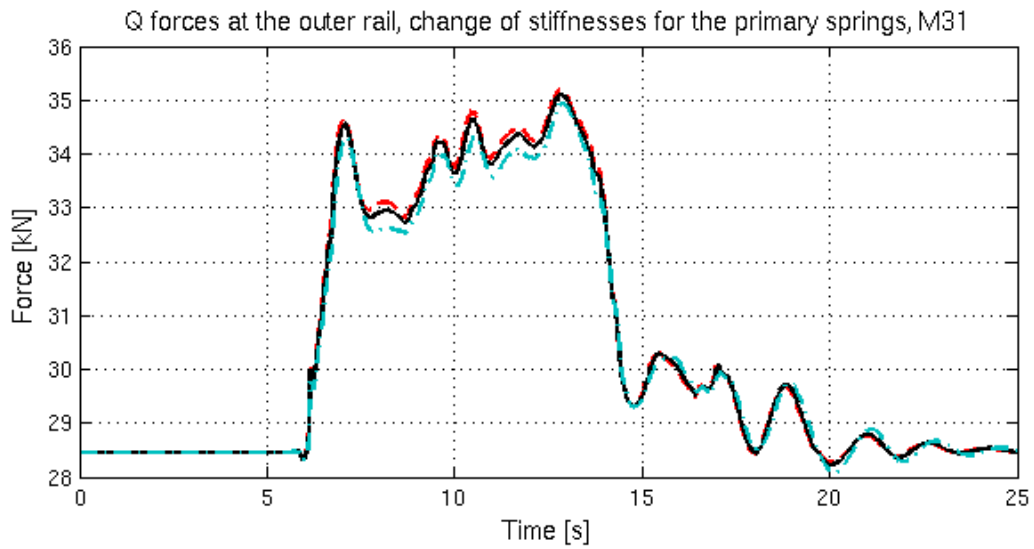


Figure 5.17 – Q forces on the outer rail for leading axle. Change of stiffnesses for the primary springs for the tram vehicles M31 (top figure) and M32 (bottom figure).

5.1.6 Secondary suspension stiffnesses

In this subchapter an investigation of varying the stiffnesses of the secondary springs and the damping constants of the shock absorbers for the tram vehicles is presented. The purpose of the study is to see how these changes affect the track forces.

The simulations are performed with the same conditions as before. Four cases have been studied: the secondary springs and shock absorbers have been increased and reduced with 50% and been compared to a case with nominal springs and shock absorbers.

The results of the total (static + dynamic) vertical track forces for tram vehicles M31 and M32, due to a change of stiffnesses of the secondary springs, can be seen in figure 5.18. Reducing the stiffnesses will increase the vertical track forces relative to when nominal springs are used. The reason for this is that with weaker secondary springs an increase of the roll motion for the car body is obtained. The lateral track forces are not shown in these cases because the deviations relative to the nominal secondary springs were not significant.

Changing the shock absorber damping constants resulted in insignificant changes in the track forces. Increasing the constants of the shock absorbers with 50% will give slightly less oscillation movements and a minor decrease of vertical track forces. Decreasing the damping constants of the shock absorbers with 50% will result in a minor increase of vertical track forces with slightly more oscillating movements.

With these studies it can be concluded that the springs are the controlling factor that affects the track forces. Generally, the primary suspension has a higher impact than the secondary suspension but it is interesting to notice that a change in stiffness for the suspensions tend to have opposite influence on the track forces. Track forces are decreased by softer primary springs and stiffer secondary springs. How the changes affect the ride comfort is an interesting investigation but will not be studied in this project. This is another example of future work.

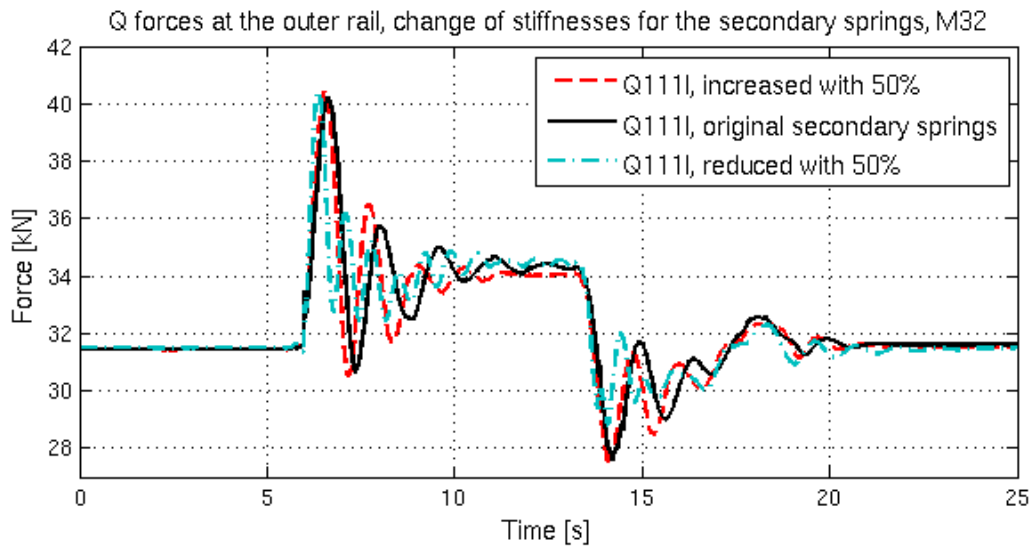
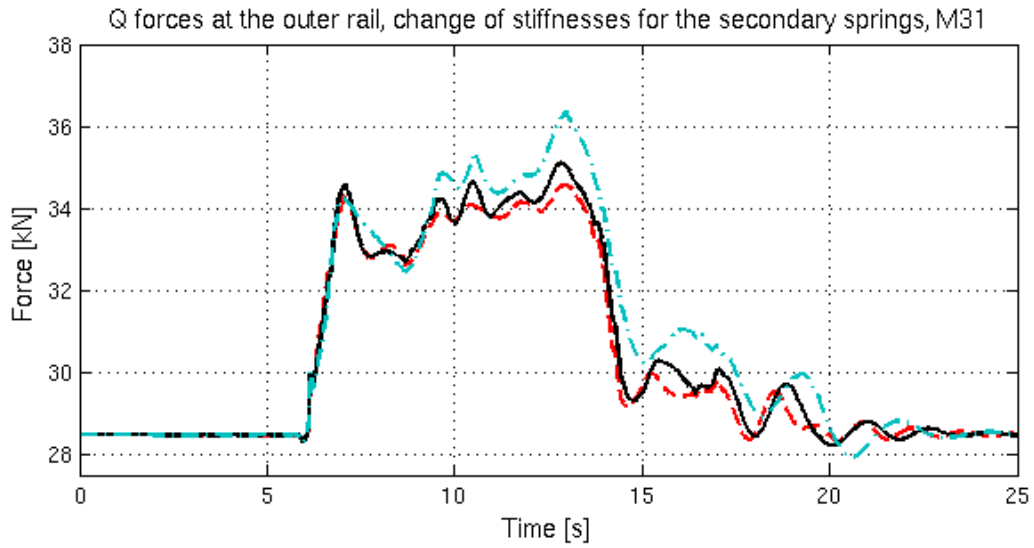


Figure 5.18 – Q forces on the outer rail for leading axle. Change of stiffnesses for the secondary springs for tram vehicle M31 (top figure) and M32 (bottom figure).

5.1.7 Derailment study

The ability to handle different curves at different speeds has been studied for both tram models. The simulations are performed with nominal wheel and rail profiles and friction coefficient 0.25. The tram vehicles are negotiating right handed circular curves with radii of 20-60 m and speeds of 10-50 km/h. The results of the study for tram vehicles M31 and M32 can be seen in table 5.5 below. The green fillings represent a good handling of the curves, while the yellow fillings mean that the trams are able to handle the curves but experience flange climbing. The red fillings represent a case of derailment.

The start of a flange climbing can be predicted and calculated using Nadal’s equation [4]:

$$\left(\frac{Y}{Q}\right)_{lim} = \frac{\tan \beta - \mu}{1 + \mu \tan \beta} = \frac{\tan 64.1673 - 0.25}{1 + 0.25 \tan 64.1673} = 1.20 \tag{5.1}$$

Here β is flange angle and μ friction coefficient in the curve. This means that flange climbing will occur if the ratio between lateral and vertical forces exceeds 1.20.

Table 5.5 – Ability of handling different curves at different speeds for the tram vehicle M31 and M32

M31		Curve radius [m]									
		20	25	30	35	40	45	50	55	60	
Speed [km/h]	10	Green	Green	Green	Green	Green	Green	Green	Green	Green	Green
	15	Green	Green	Green	Green	Green	Green	Green	Green	Green	Green
	20	Green	Green	Green	Green	Green	Green	Green	Green	Green	Green
	25	Yellow	Green								
	30	Yellow	Yellow	Green							
	35	Red	Yellow	Yellow	Yellow	Yellow	Green	Green	Green	Green	Green
	40	Red	Red	Red	Yellow						
	45	Red	Red	Red	Red	Yellow	Yellow	Yellow	Yellow	Yellow	Yellow
	50	Red	Red	Red	Red	Red	Yellow	Yellow	Yellow	Yellow	Yellow

M32		Curve radius [m]									
		20	25	30	35	40	45	50	55	60	
Speed [km/h]	10	Green	Green	Green	Green	Green	Green	Green	Green	Green	Green
	15	Green	Green	Green	Green	Green	Green	Green	Green	Green	Green
	20	Green	Green	Green	Green	Green	Green	Green	Green	Green	Green
	25	Yellow	Green								
	30	Red	Yellow	Green							
	35	Red	Yellow	Yellow	Green						
	40	Red	Red	Yellow	Yellow	Yellow	Yellow	Green	Green	Green	Green
	45	Red	Red	Red	Red	Red	Yellow	Yellow	Yellow	Yellow	Green
	50	Red	Red	Red	Red	Red	Red	Red	Red	Red	Yellow

An interesting conclusion can be made from these studies. It can be noticed that there are fewer cases of flange climbing (yellow and red fillings) for tram model M32 compared to M31. This is due to the stiffer bogie design of M32. Consequently, there is high risk of derailment if the tram model M32 experiences flange climbing. This conclusion is confirmed by [4] and was also discussed in the theory chapter. For safety, a recommendation is that the trams should not be operated at the conditions with yellow fillings.

The risk for flange climbing for a tram vehicle is not only related to the speed in the curve. Flange climbing may also be related to a combination of poor wheel and rail profile conditions. Furthermore, flange climbing is also related to track irregularities such as track twist, poor bogie setup, high wheel-rail friction, poor wheel finish and ageing according to [10].

5.1.8 Track forces as function of vehicle speeds and curve radii

In this subchapter an evaluation of the maximal track forces at different speeds and curve radii is made and will be presented for the two tram vehicles. The simulations are performed with the same conditions as before. The maximal total (static + dynamic) Q forces for different speeds and curve radii are shown in figure 5.19 for both tram vehicles.

It can be seen that with higher speed and smaller curve radius, there will be larger vertical track forces. The black stars in the figures indicate when derailment occurs. It means that according to the simulations, the vehicle cannot handle sharper curves at the specific speeds. For any given combination of curve radius and speed, an interesting observation is that tram vehicle M31 acts on the rails with 5-7 kN lower vertical forces compared to M32.

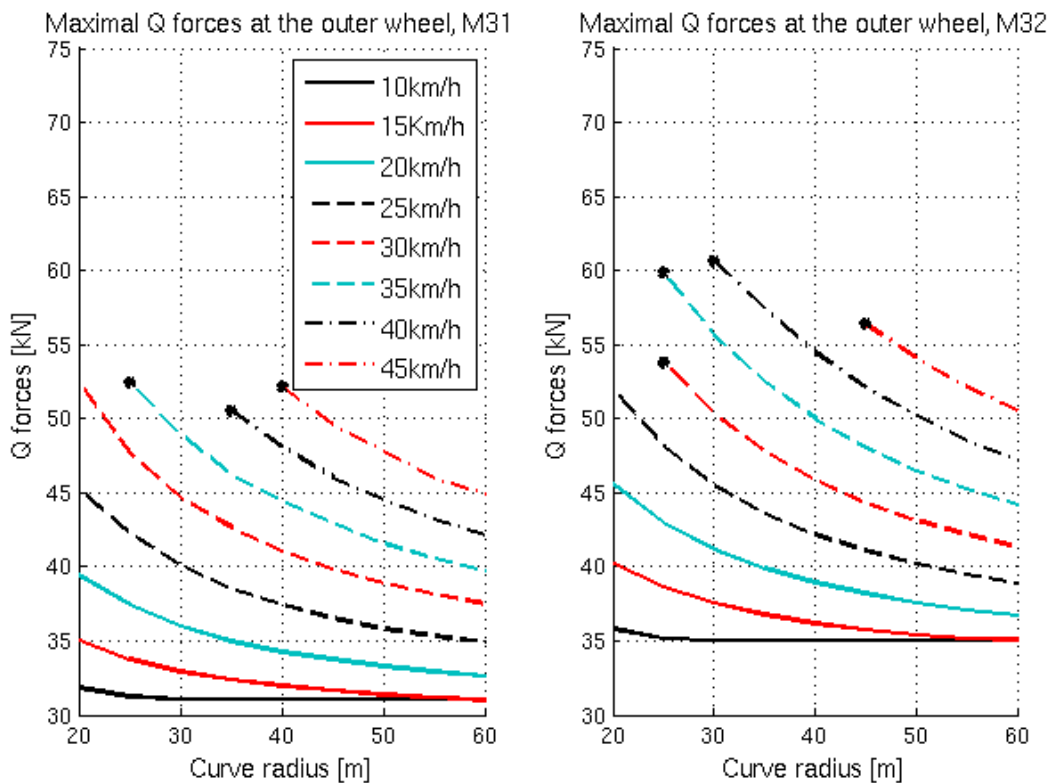


Figure 5.19 – Maximal Q forces on the outer rail for leading axle, M31 (left) and M32 (right).

Similar analyses have been made regarding the *Y*-forces. The maximal *Y*-forces for different speeds and curve radii can be seen in figure 5.20 for both tram vehicles. There are large differences between the tram models (M31 and M32) regarding the lateral track forces. This is due to that the tram vehicle M32 has stiff bogies as was explained earlier in the report.

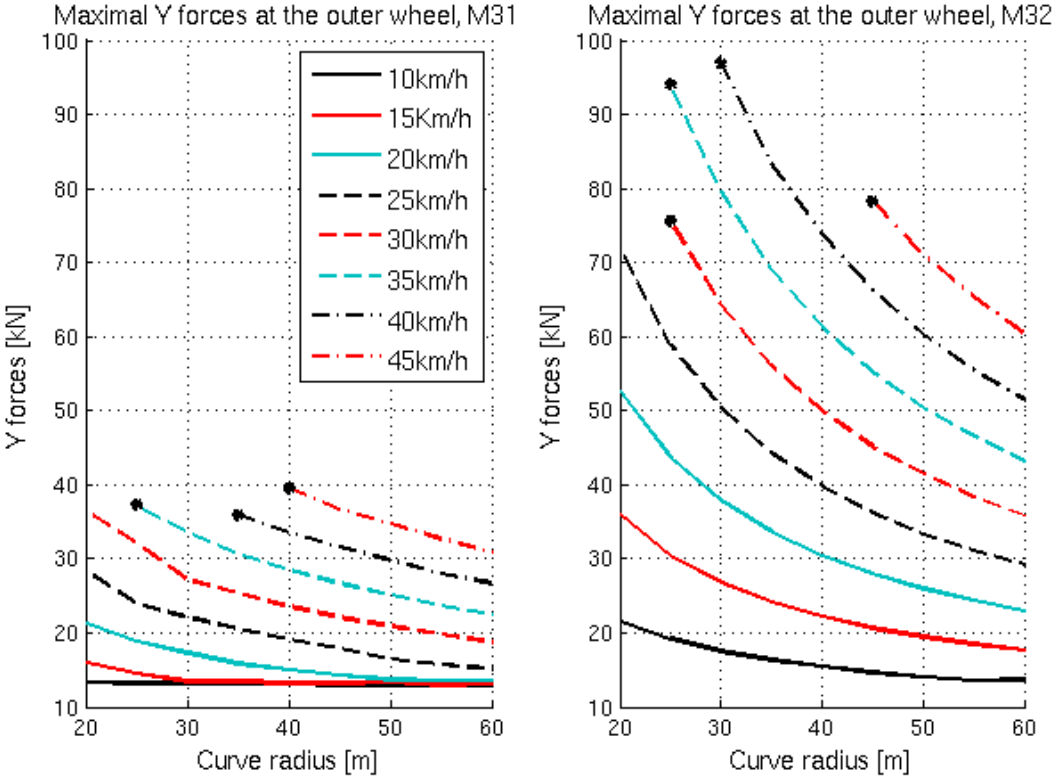


Figure 5.20 – Maximal *Y* forces on the outer rail for leading axle, M31 (left) and M32 (right).

Additionally, the results of the maximal track forces have been presented in contour plots, which can be seen in figure 5.21 below. With these figures the variation in track forces can be easily seen as function of speed and curve radius. The numbers at the contour lines in the figures are forces in kN. For example, if there is a speed restriction of 25km/h in a curve with a given radius, the figures illustrate the magnitude of the maximal track forces.

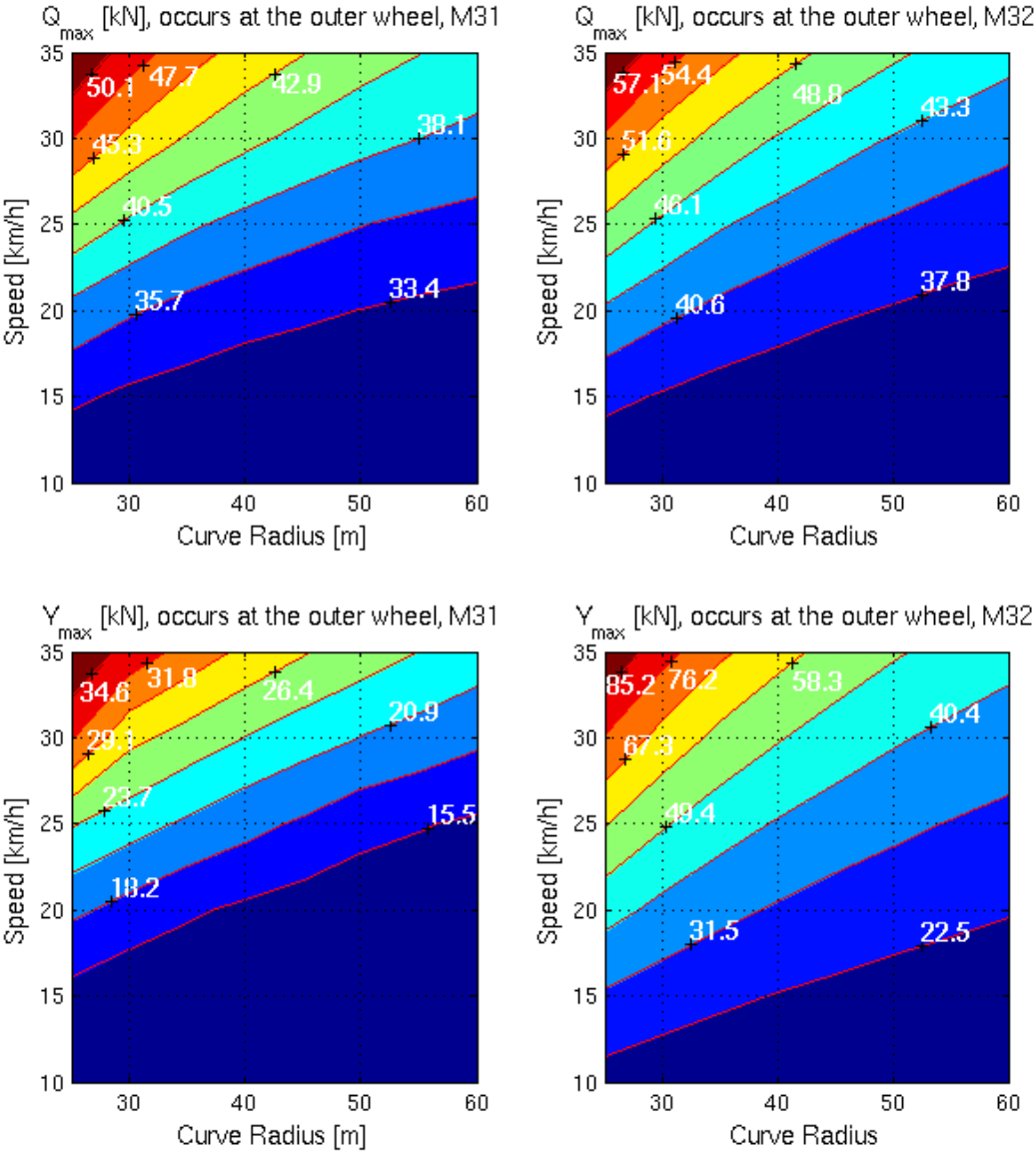


Figure 5.21 – Representation of maximal track forces for different speed and curve radii for M31 and M32. Q forces for M31 (top left) and M32 (top right). Y forces for M31 (bottom left) and M32 (bottom right).

5.1.9 Nominal wheel profiles used on tram vehicle A34 in Stockholm

A comparison has been made between the current nominal wheel profiles on M31 and M32 and the wheel profile (LK600) used on the tram vehicle A34 operating in Stockholm. This study will give a hint of if changing the wheel profiles on the trams in Gothenburg will give rise to higher or lower dynamic forces. The simulation scenario is equivalent to the one explained in subchapter 5.2.1. The wheel profile used today on vehicles M31 and M32 (here called GS) and also the LK600 profile used on vehicle A34 can be seen in *Appendix 1*.

Starting with model M31, the dynamic Y -forces on the wheels attached to the leading axle can be seen in figure 5.22. The figure shows two curves for the Y -force. The black curve is the force when using the current wheel profiles on M31 and the dashed red curve is the same force when using the wheel profile LK600.

As can be seen the lateral forces on the wheels are quite similar to each other when comparing the two wheel profiles. A somewhat higher value is noticed for the LK600 profiles at the outgoing transition curve for vehicle M31. This is true for both the inner and outer wheels. At the transition curve the Y -forces are approximately 1 kN higher for the profile LK600 compared to the profiles used today on the vehicle.

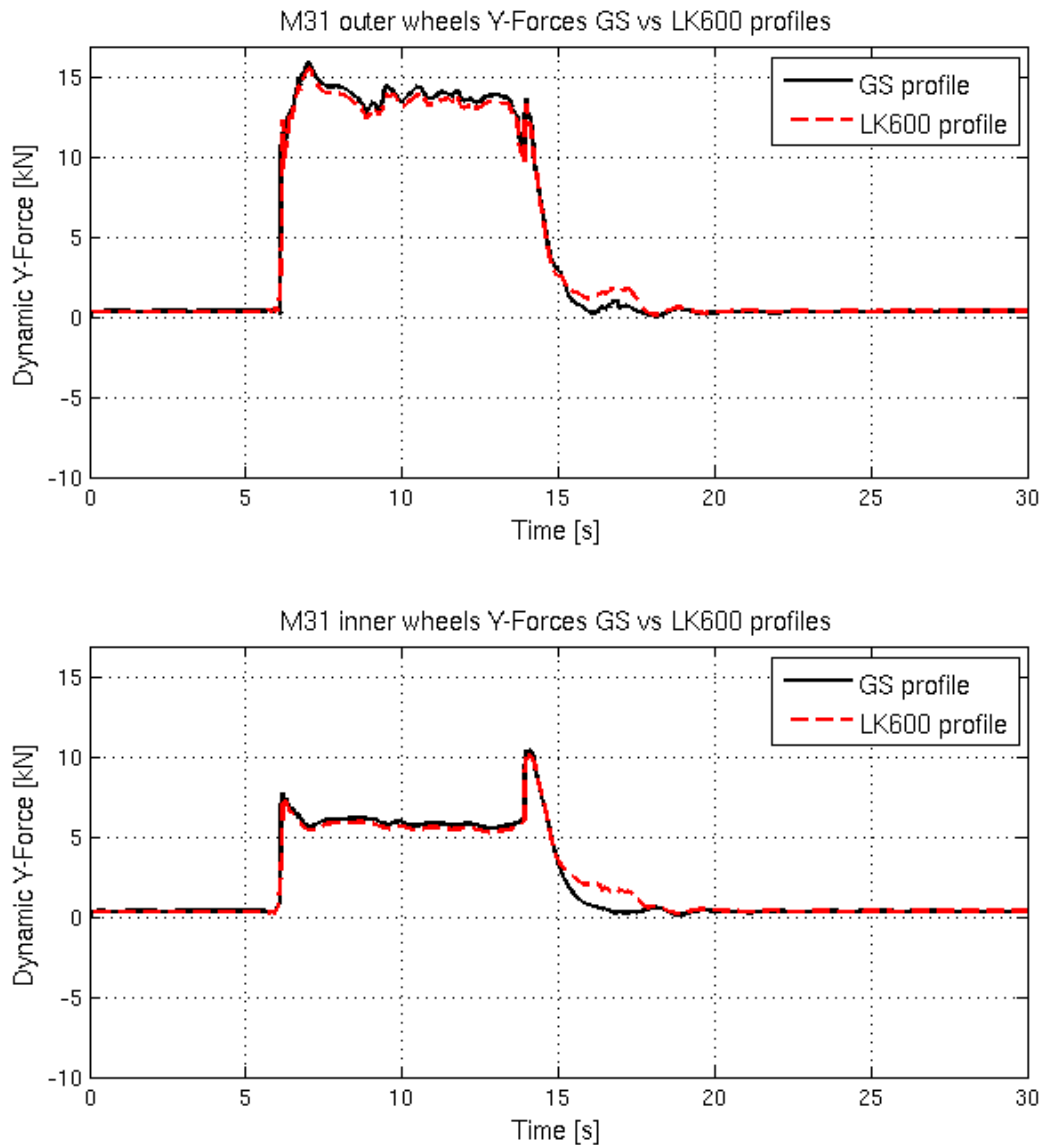


Figure 5.22 – Comparison between *Y*-forces obtained from simulations with M31 model. The black lines represent the current wheel profile used (GS) and the dashed red lines the LK600 wheel profile. Top figure shows the *Y*-forces on the outer wheels and bottom figure shows the *Y*-forces on the inner wheels. Positive *Y*-forces on the wheels are acting towards the centre of the curve.

The vertical forces between the first wheels on tram vehicle M31 are shown in figure 5.23 below. The black curve shows the calculated forces for the GS profile and the dashed red one for the LK600 profile. In this plot it is clear that the forces are higher for the LK600 profile compared to the one used by GS today.

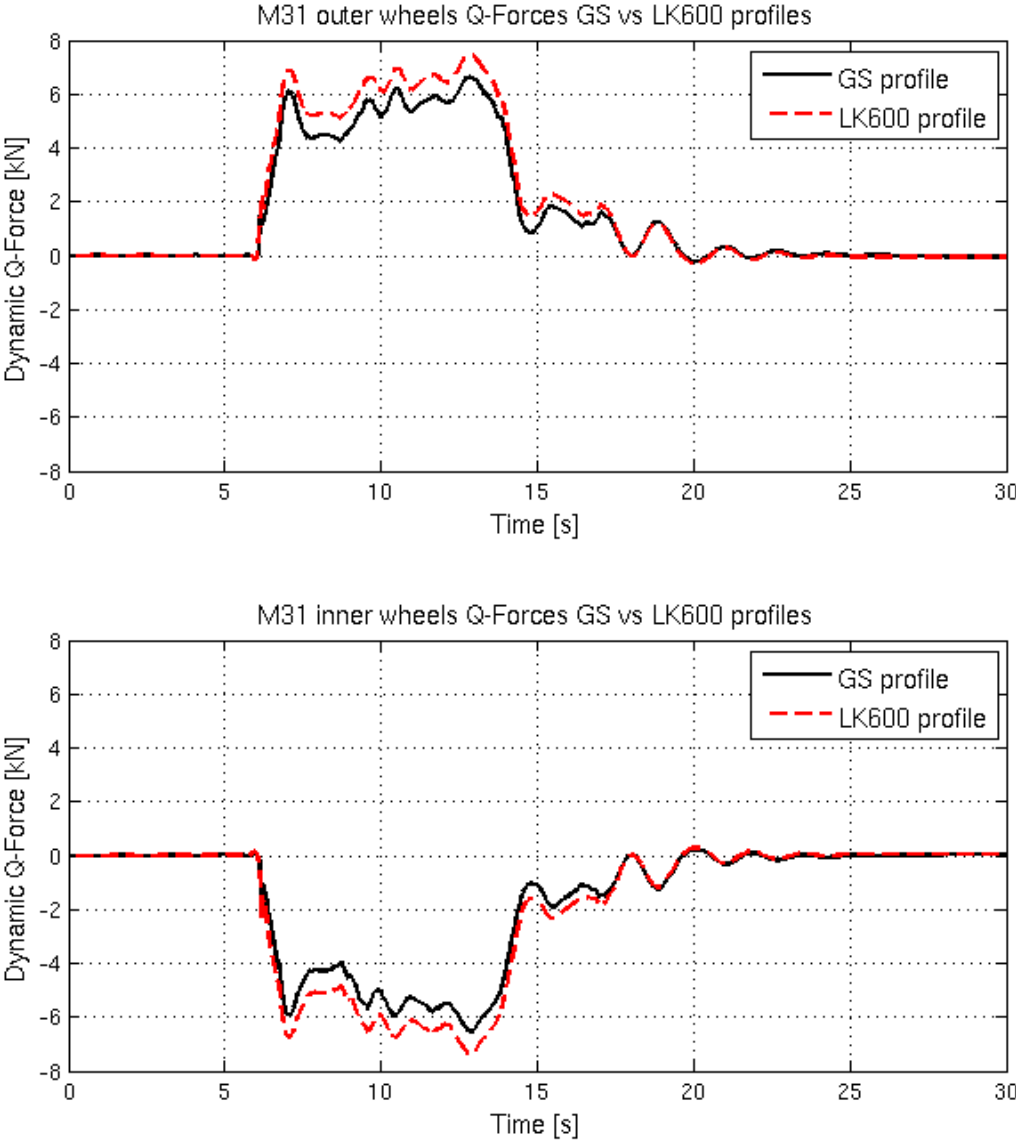


Figure 5.23 – Comparison between Q -forces obtained from simulations with M31 model. The black lines represent the current wheel profile used by GS and the dashed red lines the LK600 wheel profile. Top figure shows the Q -forces on the outer wheels and bottom figure shows the Q -forces on the inner wheels.

The same study has been done for the tram vehicle M32 and the result of the dynamic Y-forces can be seen in figure 5.24 below.

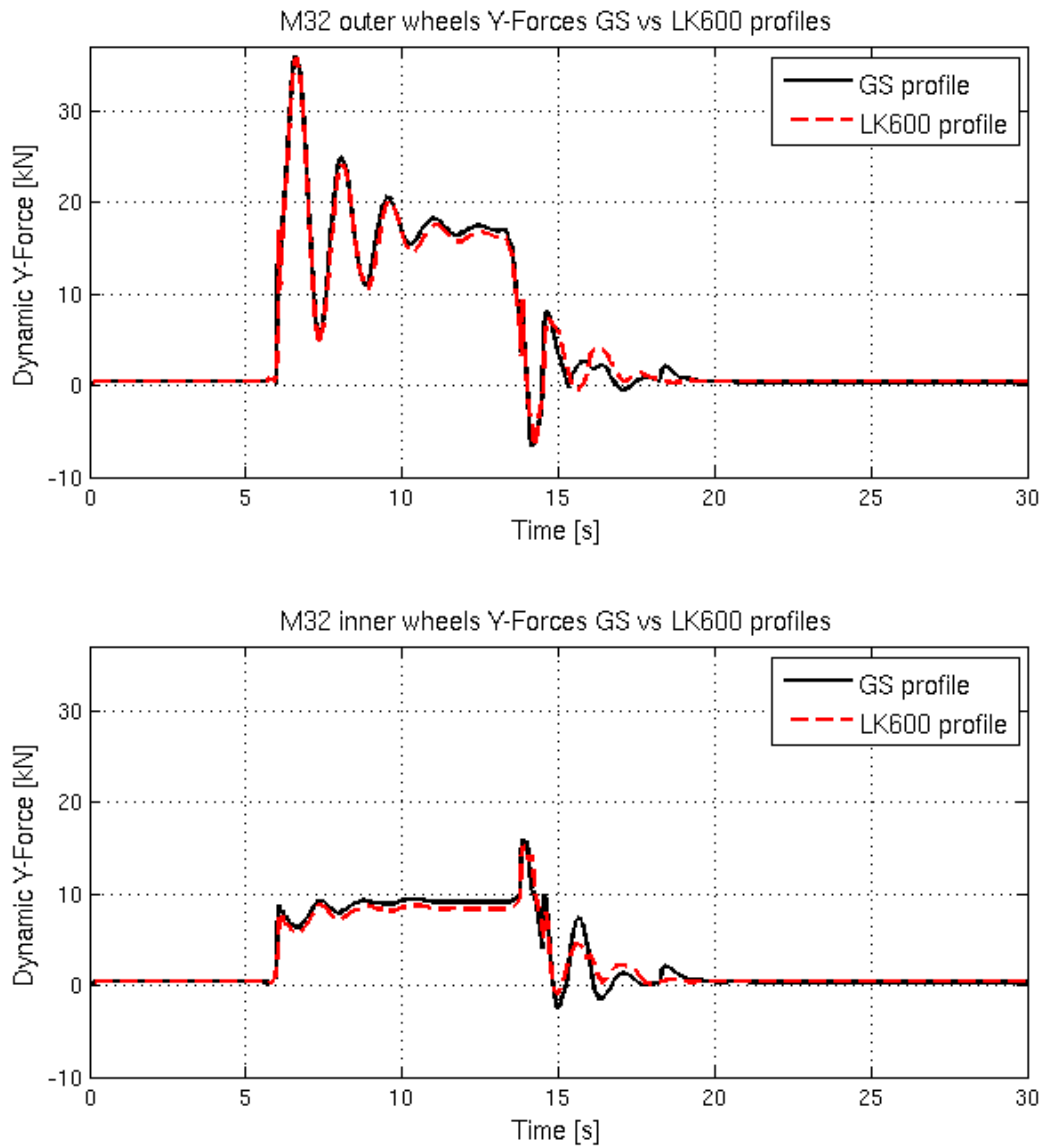


Figure 5.24 – Comparison between Y-forces obtained from simulations with M32 model. The black lines represents the current profile used (GS) and the dashed red lines the new tested one (LK600). Top figure shows the Y-forces on the outer wheels and bottom figure shows the Y-forces on the inner wheels. Positive Y-forces on the wheels are acting towards the centre of the curve.

The Y -forces are relatively similar for the two wheel profiles. The overall mean value during the simulation of the Y -forces for LK600 is slightly smaller compared to the current profiles (GS). However the difference is small and it can be discussed if they can in practice be neglected. There is a large difference on the Q -forces between the two models as can be seen in figure 5.25. The LK600 profile used on tram vehicle A34 in Stockholm will give rise to larger dynamic Q -forces.

The study shows that for an ideal curving case the Q -forces will be higher when using the LK600 wheel profile compared to the GS profile used today. It can also be concluded that the change of wheel profiles has a larger (negative) effect for the vertical dynamic forces on vehicle M32 than on M31.

Prediction of wear is outside the scope of this thesis, but it is reasonable to believe that, due to the higher track forces, a change to the LK600 wheel profile would not lead to reduced wear.

The profile LK600 is currently used on the tram vehicle A34 in Stockholm. From this profile comparison study on M31 and M32 it is difficult to draw any conclusions on how the profiles would behave on the A34 tram without setting up a GENSYS model of it. A34 has some bogies with axles between the wheels which resembles M31 but also some bogies with stiffer primary suspension and free rotating wheels which resembles M32.

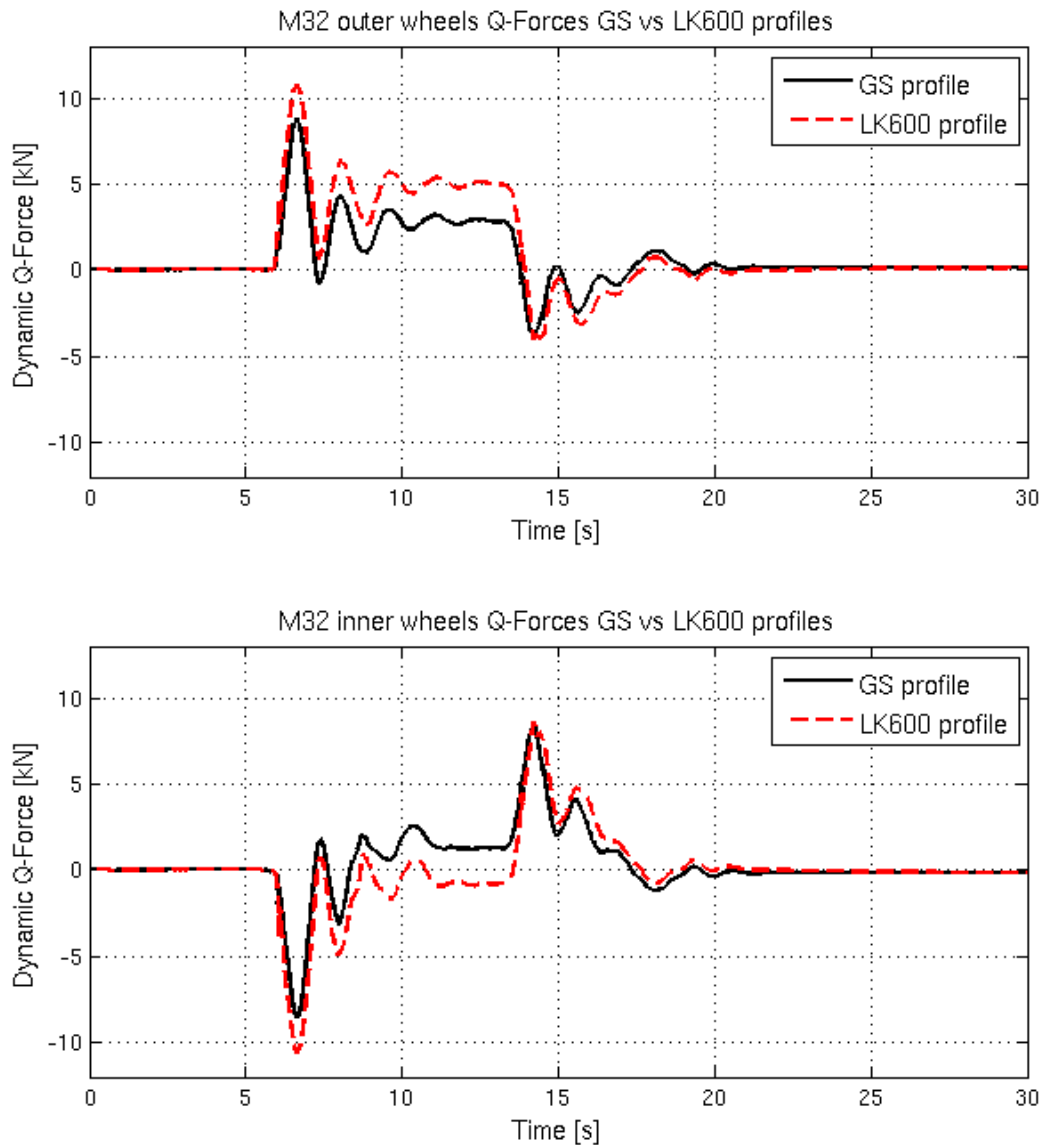


Figure 5.25 – Comparison between Q -forces obtained from simulations with M32 model. The black lines represents the current profile used (GS) and the dashed red lines the new tested one (LK600). Top figure shows the Q -forces on the outer wheels and bottom figure shows the Q -forces on the inner wheels.

6. Discussion

In this chapter an overall reflection and discussion of the report will be presented. Some of the results that were discussed in the result chapter will not be repeated here if not considered necessary.

6.1 Modelling

Even if the GENSYS models have been demonstrated to behave as in reality, it is likely that the input parameters can be further fine-tuned. A few examples will be given below.

The car body masses on the M32 vehicle have been estimated due to lack of information. Only the total weight was known but since M32 consists of five car bodies, there are more unknown masses than equations. This leads to an underdetermined system of equations that could not be solved. It is believed that the weight estimations are good enough and do not differ that much compared to the real weights, and will not give large differences on the results. The correct masses should be able to get from AnsaldoBreda.

Also the stiffnesses of the primary springs on model M32 have been estimated. It is known that these are stiffer than the known primary springs on M31. A compression force spring test can be used here to measure the stiffnesses. The same scenario is true for the secondary springs on model M31. The springs are so called hourglass springs with non-linear characteristics. Based on guidelines in the GENSYS user manual they were modelled as linear springs. It is assumed that this is a good approximation. More detailed descriptions on the modelling assumptions are presented in the appendices.

The centre of gravity of each component in the GENSYS models M31 and M32 has been assumed to be in the geometrical centre. One important example is the car bodies. Due to the seats mounted on the floor and the equipment on the roof, it is difficult to estimate where the centre of gravity is located. No efforts were made to measure/calculate the centre of gravity for the car bodies due to approximations of the mass centre positions are assumed to be good enough.

The shape of most of the real components on the tram vehicles can roughly be approximated as parallelepipeds or cylinders. The moment of inertia is needed for the GENSYS modelling and in the calculations all components are assumed to be either a parallelepiped or a cylinder. Some examples of assumed parallelepiped shapes are car bodies, bogie frames, and bolster beams. A much more accurate inertia representation would of course be to have actual CAD realisations of all these components.

For tram vehicle M32 the rubber blocks between the wheel rings and wheel hubs have not been modelled. Instead the wheel was modelled as a mono block wheel, i.e. the wheel was not divided into a ring and a hub as is the case for model M31. An attempt to include the rubber rings result in numerical instability in the GENSYS calculations. Discussions with the GENSYS developer Ingemar Persson at DEsolver about this problem led to the conclusion that the rubber rings should have a small influence on the M32 GENSYS model in the studied frequency range. The reason for this is that the rubber rings are relatively stiff and also that

the wheels are not linked, but rather rotates freely relative to each other. Another reason that the rubber rings can be neglected is due to that the speeds of tram vehicles are relatively low compared to other railway vehicles such as trains. This will lead to that bogies and wheel axles of M32 will in all probability be stable. It is believed that including the stiff rings would not influence the simulation results much, but it would lead to longer simulation times.

On vehicle M32 the non-linear damping characteristics for the longitudinal, lateral and vertical dampers were known and used in the modelling. However this was not true for model M31. Here it was assumed that the dampers were linear with a damping constant in the same order of magnitude as the ones on M32. Efforts have been made to contact the shock absorber supplier with no result. A parameter study of the influence of the dampers was presented in the results chapter. It was concluded that increasing the constants of the dampers will give reduced oscillating movements and a minor decrease of the vertical track forces. Thus, the dampers have not that large effect on the values of the dynamic track forces but rather on the ride comfort.

6.2 Validation

The GENSYS models of the trams M31 and M32 have been validated against measurements on real tram vehicles. It is important to note that the measurements were only performed on one specific M31 vehicle and one specific M32 vehicle. The exact conditions of these two vehicles are hard to know or estimate. For example the different wheel sets had been operated different distances since their previous reprofiling and this may result in different amounts of wear on the wheels. In the GENSYS models all wheels are assumed to have the same wheel profiles. Also the conditions of the secondary and primary suspensions are not known. The values of the spring and damping constants will vary depending on their age and usage.

An overall conclusion to this is that there can be a significant difference not only between tram models M31 and M32 but also between individuals of each model type. This will give rise to some difference in the results between the real tests and the GENSYS models. Further, track irregularities were not accounted for in the GENSYS models. It is possible to include irregularities in GENSYS but this requires measurement data that were not available in the project. The neglect of track irregularities will also influence the results.

The rails in the curve used for the validation was measured with a MiniProf equipment. The instrument had not been calibrated for a long time and this gave rise to “noisy” rail profiles. The KPF function in GENSYS could not be run for these profiles without first using a spline commando to smoothen the profiles. Due to this the profiles lost some of their original shape but it is believed that this did not result in any large influence on the results.

6.3 Results

One of the main purposes with the parameter studies in the result chapter was to show that the GENSYS modelled tram vehicles behave as observed in reality. This has been done by comparing the vehicle models to each other and also by changing different component values and showing that the results are as expected. Also the fundamental curving behaviour of the dynamic models has been confirmed by the theory presented in chapter 2.

Furthermore, some parameter studies were made to point out problems with the tram vehicles and also show the potential of future work. This will be discussed in the next chapter. The focus for the simulation has been on sharp curves at low operating speed, which was identified as the most critical situation by GS and TK.

The studies of track forces when using nominal or worn profiles deserve a deeper discussion. There are large differences between the potential contact points depending on what combination of wheel and rail profile is used. Due to this it is hard to define a worst case, i.e. a case where the track forces are at their maximum. One example is when using severely worn wheel profiles with thin flanges. This will make the inner part of the wheel (outside of the flange) to make contact with the keeper and the track force characteristics when negotiating the curve will be significantly different, compared to the case with no contact on the inner part of the wheel. Large differences between contact points for the different wheel/rail combinations were observed and the maximum track forces were obtained at different positions in the curve. Due to this, the maximum track forces were not a good measure to use when comparing the profiles. This was solved by taking the mean value of the track forces during the curve negotiation simulations. The mean track force is believed to be a better measure used to compare the wheel/rail combinations compared to the maximum track force. However, the question is if the mean track force is the best measure to compare the wheel/rail combinations. Perhaps calculating the energy dissipation for different combinations of wheel and rail profiles during the simulation is a better approach. This can be investigated further.

7. Conclusions and future work

During the project the collection of input data to build the tram models has been a big challenge. There was lack of data for almost all components. Typically spring stiffnesses, damping coefficients, mass of components and moments of inertia were missing. To fill these gaps a combination of complementary measurements, calculations, estimations from lab reports and data sheets of similar components plus discussions with contact persons experienced in the field have been done. A conclusion is that with these different methods enough data could be gathered to develop the GENSYS models.

Two GENSYS models have been obtained, one for tram vehicle M31 and one for tram vehicle M32. To compare the computer models with real vehicles some validations have been made. A conclusion from these validations is that the models resemble the real cases and are not way off.

Tram model M32 has a stiffer bogie design compared to tram model M31. This leads to larger track forces, especially the lateral track forces. Due to the stiff bogie design the curving behaviour differs. A major difference is the “hammering” behaviour of M32. The wheels will oscillate and hammer on the rail when negotiating a curve and hence affects the riding comfort. Also if the tram model M32 experiences flange climbing then there is a high risk of derailment due to the bogie design. M32 gives rise to larger track forces and worse ride comfort compared to M31. An overall conclusion is that there are significant differences between the dynamic behaviour of vehicles M31 and M32.

Both vehicle models have some problems with their design. On vehicle M32 the low floor construction design with independently rotating wheels leads to stiffer bogies which increase the lateral track forces and also the derailment risk. The model M31 has a conventional bogie design. Due to its reconstruction from M21, mechanical couplings have been introduced on car body C. The mechanical couplings on the wheel sets lead to unnecessary wheel and rail wear and also squeal when negotiating a curve for poorly aligned wheel sets. A conclusion is that using a tram vehicle with conventional axles and ramped floor sections to provide required accessibility seems to be a better option. This will reduce the problems which are associated with the low floor vehicle M32, where the independently rotating wheels give lack of guidance.

Another alternative is to adopt tram models with steered independently rotating wheels. This bogie design will allow the independent wheels to yaw/steer during curve negotiation, reducing the problems obtained with stiff bogies. A recommendation is to investigate if tram models with bogie designs like these can be a better alternative for future investments of new tram models operating in Gothenburg.

Worn profiles result in larger track forces compared to nominal profiles. Some of the results may be somewhat obvious, but the purpose of the studies is to conclude that the GENSYS models behave as expected. The nominal profile used on tram vehicle A34 operating in Stockholm has been tried on models M31 and M32. The results did not show that a change to the Stockholm profile would lead to any significant improvements to the dynamic track

forces. The GENSYS models can be used to investigate and compare other wheel profiles that are used on tram vehicles in other cities or other countries. This gives an opportunity for a future work where the work consists of finding wheel profiles that reduces the track forces.

Using softer primary springs results in lower track forces due to a better wheel guidance. Using stiffer secondary springs results in lower track forces due to less dynamic motions of the car bodies. These analyses were made to investigate how an overall change of stiffnesses affects the track forces. A further study can be made by studying longitudinal, lateral and vertical stiffnesses individually and optimize the springs to reduce track forces and improve ride comfort. This would be an interesting study in future work.

With the dynamic models wear on wheels and rails can be simulated. According to [8] the wear calculations can be divided into four categories, the simulation set design, track-vehicle simulations, wear calculations and updating the rail/wheel profiles. These simulations can be combined with different wheel profiles to investigate which one results in the lowest wear. This would be an interesting study in future work that can be used to determine wheel profiles that result in the lowest wear. According to GS (Florencio Garcia), a life increase of 5000 km for only one wheel can save up to 200 000 kr/year. This statement shows how important it is to understand the wear and hence try to decrease it as much as possible.

The curving noise is a well-known problem in Gothenburg. This could be investigated as a follow-up study in which the curving behaviour obtained from GENSYS is used as input to a separate noise calculation model.

References

- [1]. Göteborgs Spårvägar, Historik, *En del av Göteborgs historia*.
<http://www.goteborgssparvagar.se/kul-tur/historik/> (2015-04-13)
- [2]. Göteborgs Spårvägar, *vår flotta*.
<http://www.goteborgssparvagar.se/om-oss/var-flotta/> (2015-04-10)
- [3]. Persson, I. *GENSYS User's Manual*, AB DEsolver, www.gensys.se
(2015-04-02)
- [4]. Andersson, E, Berg M. and Stichel S. (2014) *Rail Vehicle Dynamics*.
Compendium. Stockholm: KTH printing.
- [5]. ABB TRACTION. (1989) *Teknisk beskrivning på boggierna spårvagn M21*.
Västerås: ABB
- [6]. AnsaldoBreda. (2015) *Technical description of the SIRIO platform vehicle*.
AnsaldoBreda street cars.
http://www.ansaldobredainc.com/images/stories/Sirio_Technical_Specifications.pdf
(2015-04-13)
- [7]. AnsaldoBreda. (2015) More information on Sirio. *AnsaldoBreda street cars*.
http://www.ansaldobredainc.com/images/stories/Sirio_Streetcars.pdf
(2015-04-13)
- [8]. Orvnäs, A. (2005) *Simulation of rail wear on the Swedish light rail line Tvärbanan*.
Stockholm: Royal Institute of Technology (KTH).
(The division of Aeronautical and Vehicle Engineering)
- [9]. Ouyang, Z. (2014) *Investigation of causes for wheel squeal on Roslagsbanan in Stockholm*.
Stockholm: Royal Institute of Technology (KTH), Division of Railway Technology,
Department of Aeronautical and Vehicle Engineering
- [10]. Allen, P and Bevan, A. (2008) *Determination of tramway wheel and rail profiles to minimise derailment*.
Manchester ,UK: Manchester Metropolitan University.
(report no: 90/3/A)
- [11]. Torstensson, P. (2009) *Rail corrugation growth on curves*. PhD thesis, Chalmers
University of Technology, Department of Applied mechanics, Gothenburg.
Sweden: Chalmers Reproservice.
- [12]. Romani, M. (2001) *Simulation of dynamic behavior of the new low floor tram SIRIO for Milan*.
SIMPAC User Meeting 2001.
<http://www.simpack.com/fileadmin/simpack/doc/usermeeting01/um01-ansalfo.pdf>
(2015-04-02)

- [13]. Mayers, D. Süli, E. (2003) *An introduction to numerical analysis*. [Electronic]. Cambridge: Cambridge University Press. (ISBN 0 521 00794).
- [14]. Råde, L. Westergren B.(2012) *Mathematics Handbook for Science and Engineering*. Beijing: Elanders Beijing Printing Co. Ltd, China.
- [15]. Persson, I. (2013) *Kontaktpunktsberäkning för Spårväg City och A34*. Östersund: Ingemar Persson report.
- [16]. Reumann, U. (2012) Göteborgs Spårvägar *Comfort Measurements M31/M32*. Gothenburg Sweden: Bombardier (Identity number: 100182120)
- [17]. Hultgren, S and Olsson N. (2014) *Trafiksäkerhetsinstruktion, utgåva för behöriga: säkerhetsledare, säkerhetsman, fordonsförare och bevakare*. Göteborg: Göteborgs stad trafikkontoret.
- [18]. Johansson, T and Lange, T. (2009) *Spårväg guide för etablering, Internationella erfarenheter för nordiska förhållanden*. Borlänge:Banverket (ISBN 978-91-633-5845-6)
- [19]. Christian, J. Hansen, R. (2008) *MiniProf for Windows Advanced Guide*. Brändby: Greenwood Engineering A/S.
- [20]. Melkersson K. and Mägi M. (2006) *Lärobok i maskinelement*. Compendium. Sweden : EcoDev international AB.
- [21]. Boberg, P. (2006) *A-måttet – En slitageanalys på spårvägsrälsen i Göteborg*. Chalmers University of Technology, Department of Civil and Environmental Engineering
- [22]. Edstrand, J. (2012) *Calculation method for powering a tramway network*. Göteborg. Chalmers university of Technology, Department of Energy and Environment
- [23]. Olsson, S. (2005) *Formelsamling i mekanik*. Gothenburg. Sweden: Chalmers Reproservice,
- [24]. Trelleborg Industrial AVS. *Chevron product data sheet*. [Electronic]. Leicester, UK: Trelleborg Industrial AVS.
<http://www.trelleborg.com/upload/IndAVS/Files/Rail%20PDF/ChevronSprings.pdf> (2015-04-14)
- [25]. Alström, S. (2010) *Compression force of springs*. Borås: SP (Report reference FX011079-1)
- [26]. Granta design limited. CES EDUPACK 2013 (Version 12.2.13) [Computer program]. Available at <http://www.grantadesign.com/education/edupack/index.htm> (Accessed 20 may 2015)

[27]. AnsaldoBreda. (2008) *CAR-AA073ER Revision*. AnsaldoBreda.

APPENDICES

Appendix 1 – Wheel and rail profiles

Appendix 2 – Calculation of steering ratio

Appendix 3 – Calculation of spring stiffness for coil springs

Appendix 4 – Calculation of masses for tram components

Appendix 5 – Calculation of moments of inertias for tram parts

Appendix 6 – Vehicle modelling method of M31 and M32 in GENSYS

Appendix 7 – Coupling commands used in GENSYS

Appendix 8 – Calculation of the secondary springs for M32

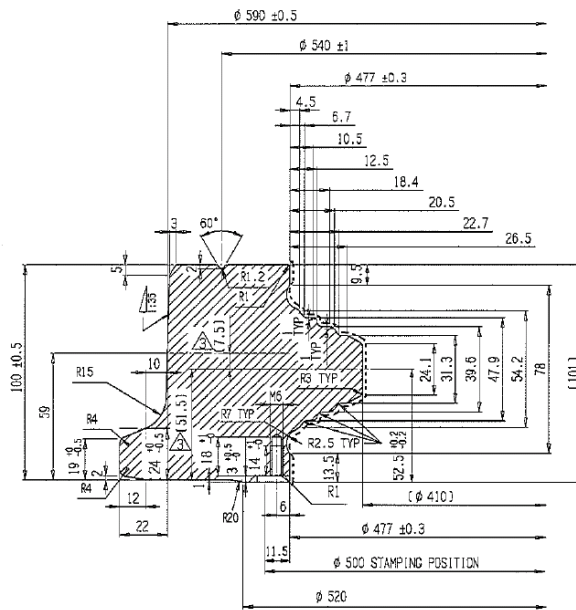


Figure A1.2 – Wheel ring for the wheels under car body C

A more detailed figure of the nominal wheel profiles is shown in figure A1.3 below. This wheel has the same profile as the ones above.

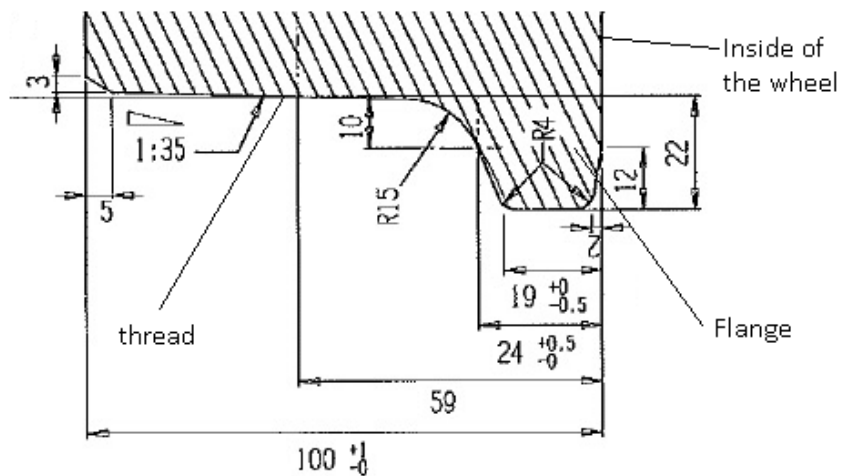


Figure A1.3 – A nominal wheel profile

All the wheels have a width of 100 mm. These have a conical thread with an inclination of 1:35 and a flange. The wheels are in contact with the rail by the threads. The flange has a thickness of 24 mm and a height of 22 mm. The flange improves the lateral guiding and is a further assistance in the steering.

A1.1.2 Wheel profile M32

All the wheels on this tram model have the same nominal wheel diameters of 660 mm. The wheel profiles are the same for both tram models M31 and M32, hence will not be described furthermore. A detailed drawing of the wheel rings can be seen in figure A1.4.

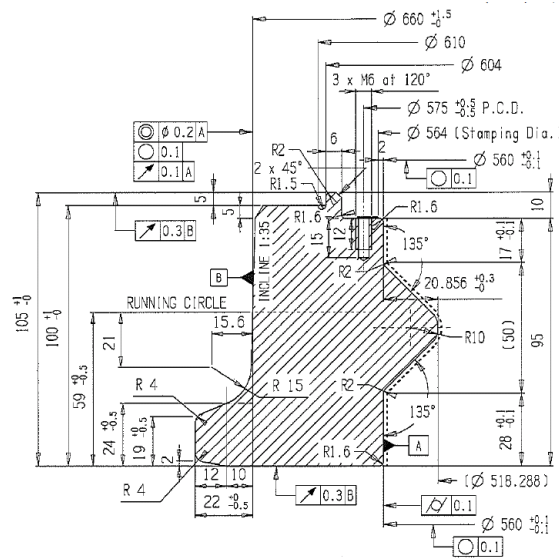


Figure A1.4 – Wheel ring for the wheels for M32

In between the wheel ring and hub, there are 25 pieces of stiff rubber blocks that form a rubber ring. This will give a dampening effect and decreases the wheel squeal.

A1.1.3 Wheel profile A34

One of the operating tram vehicles in Stockholm is the tram A34. The wheel profile of all wheels on this vehicle can be seen in figure A1.5 below.

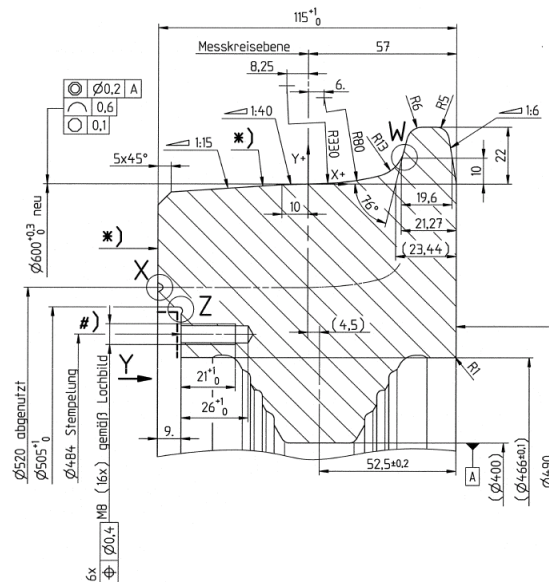


Figure A1.5 – Wheel profile on tram vehicle A34.

As can be seen this profile differs significantly compared to the ones used today on M31 and M32. A study of how this profile will influence the dynamic track forces can be seen in the results chapter.

Appendix 2 – Calculation of steering ratio

The angle difference between car body A (or B) and the frame (under car body C) connecting the wheels is calculated. This is illustrated in figure A2.1 below. The difference can be explained with a steering ratio i.e. how much the frame should steer relative to the car body.

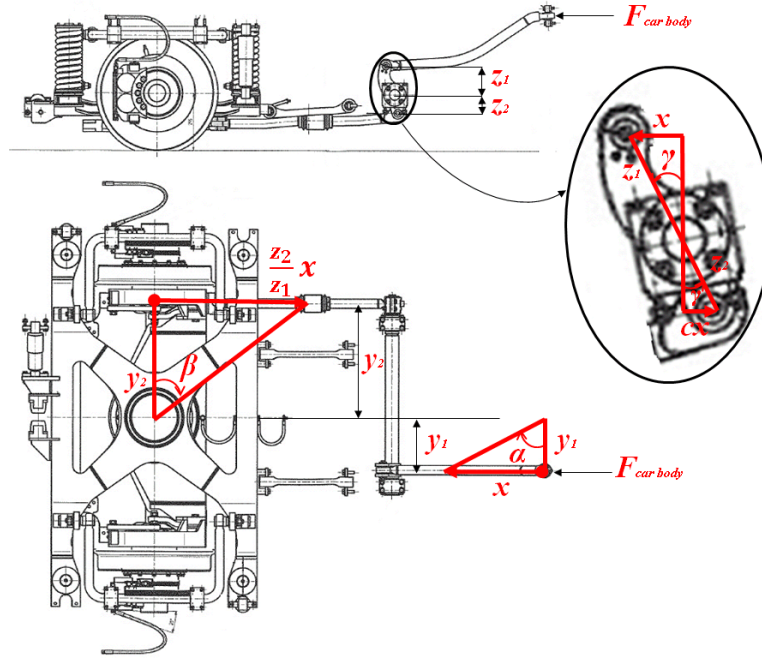


Figure A2.1 – Illustration of angle difference between the frame that connects the wheels and car body A (or B)

Assume that the car body is turning so that an angle α is obtained relative to the initial state with zero angle. Assuming that the couplings are frictionless, an angle β will arise between the frame and the initial state. With this information the angles can be calculated as:

$$\tan(\alpha) = \frac{x}{y_1} \quad \text{and} \quad \tan(\beta) = \frac{cx}{y_2} \quad (\text{A2.1})$$

where:

$$\tan(\gamma) = \frac{x}{z_1} = \frac{cx}{z_2} \quad (\text{A2.2})$$

This will give that:

$$c = \frac{z_2}{z_1} \quad (\text{A2.3})$$

The distances are obtained from drawings and the steering ratio finally reads:

$$S_r = \frac{\tan(\beta)}{\tan(\alpha)} = \frac{\frac{z_2}{z_1} \frac{cx}{y_2}}{\frac{x}{y_1}} = \frac{z_2 y_1}{z_1 y_2} = \frac{0.09422 \cdot 0.2651}{0.14725 \cdot 0.58734} = 0.29 \quad (\text{A2.4})$$

This means that the frame will rotate with 0.29 degrees for every degree that the car body rotates.

Appendix 3 – Calculation of spring stiffness for coil springs

The secondary coil springs used between car body C and the trailer bogie on M31 and M32 have helical structures with circular treads, an illustration of a coil spring can be seen in figure A3.1. The theory for calculating the stiffnesses for a coil spring is obtained from [20] and presented below.

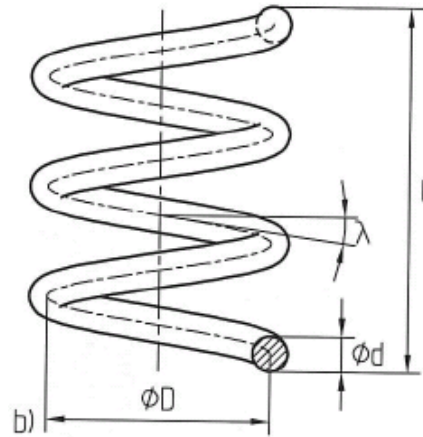


Figure A3.1 – Coil spring

A standard cylindrical coil spring is defined by the following quantities:

- D = Mean diameter
- d = Wire diameter
- n = Number of active coils
- λ = Coil angle
- l = Length of the spring

The stiffness of an ideal coil spring can be calculated by dividing the applied load with the deformation. The spring constant in translation can be calculated as:

$$c = \frac{F}{\Delta} \quad (\text{A3.1})$$

The external work for the linear spring can be calculated by integrating the applied load over a deformation distance and is defined as:

$$W_u = \frac{F\Delta}{2} \quad (\text{A3.2})$$

When the spring is loaded in tension or compression with a force F_a , each wire is influenced by a torque moment and a shear force as shown in figure A3.2.

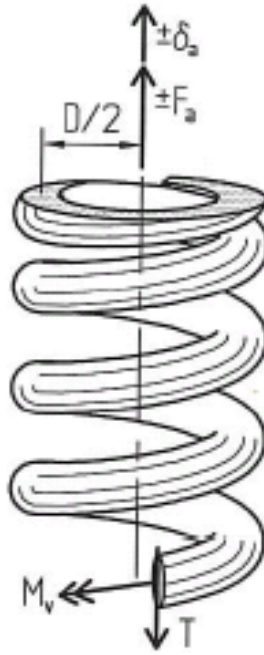


Figure A3.2 – Cut of a coil spring. Internal and external Forces and Moments acting on a spring wire.

The force and moment can be calculated as:

$$\begin{cases} M_T = \frac{F_a D}{2} \\ T = F_a \end{cases} \quad (\text{A3.3})$$

The total stored elastic energy in the spring can be calculated as:

$$W_{el} = \int_0^L \left[\frac{\beta T^2(x)}{2GA} + \frac{M_T^2(x)}{2GK} \right] dx = \frac{F_a^2 \pi D n}{2G} \left(\frac{\beta}{\pi d^2/4} + \frac{D^2}{4\pi d^4/32} \right) \quad (\text{A3.4})$$

where it has been used that:

$$\begin{cases} A = \frac{\pi d^2}{4} \\ K = \frac{\pi d^4}{32} \end{cases} \quad (\text{A3.5})$$

For the spring, the law of energy conservation can be used. This leads to that the elastic energy is equal to the outer work, i.e. $W_u = W_{el}$. Using this will finally give:

$$k_c = \frac{Gd^4}{8D^3n} \left[1 + 0.5\beta \left(\frac{d}{D} \right)^2 \right]^{-1} \quad (\text{A3.6})$$

where:

- G = shear modulus
- β = geometrical constant (1.1 for circular thread cross-sections)

By using the Haringx shear spring theory, the shear stiffness can be calculated when the spring is loaded in axial compression. The Haringx theory will not be presented and discussed in this *appendix*, only the result will be shown. The lateral/longitudinal stiffness can be calculated as:

$$k_{shear} = \frac{F_a}{l} \frac{1}{1 - \Gamma \frac{\tan \kappa}{\kappa}} \quad (\text{A3.7})$$

where:

- $l = l_o + \frac{F_a}{k_c}$ = The actual (deformed) spring length
- l_o = free length of the spring
- $\Gamma = 1 - \frac{F_a}{S_s}$
- $\kappa = p \frac{l}{2}$
- $p^2 = -\Gamma \frac{F_a}{S_b}$

It should be noted that the relation in equation (A3.7) is only valid for springs with compressive loads ($F_a < 0$). Further,

- $S_b = \frac{Eld^4}{32(2+\nu)nD}$ = bending stiffness for one thread loop, also called section stiffness
- $S_s = \frac{Eld^4}{8nD^3}$ = shear stiffness for one thread loop
- E = elastic modulus
- ν = poisson's ratio

The procedure to calculate the stiffnesses for the springs on M31 is straightforward by using the equations A3.6 and A3.7. On M32 there are two parallel coupled springs and the total stiffness is the sum of the two spring stiffnesses. The results of the calculations can be seen in the table A3.1 below.

Table A3.1 – The longitudinal, lateral and compression stiffness for the coil springs used as secondary suspension in tram vehicle M31 and M32.

	Longitudinal stiffness (x) [N/m]	Lateral stiffness (y) [N/m]	Stiffness in compression (z) [N/m]
Secondary springs in car body C for M31	0.052e6	0.052e6	0.220e6
Secondary springs in car body C for M32	0.635e6	0.635e6	0.567e6

Appendix 4 – Calculation of masses for tram components

The masses of the tram vehicles and tram components that are used in the models are presented here. The weights have been calculated with the information that have been provided or found electronically [5], [6], [7], [21], [22]. M31 is a reconstruction of M21. The tram model M21 can be seen in figure A4.1 below.

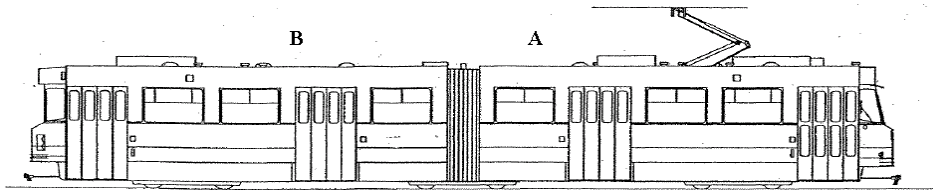


Figure A4.1 – Tram model M21

The total weight of the tram model M21 is 27200 kg. The weight of car body A and B is:

$$\text{Total weight} - \text{bogies} = 27200 - (4200 + 3300 + 4200) = 15500 \text{ kg} \quad (\text{A4.1})$$

It is assumed that car body A is 200 kg heavier than car body B due to driver seat with equipment. The extended M31 vehicle can be seen in figure A4.2.

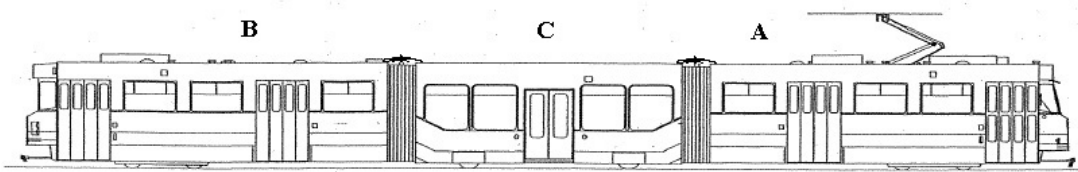


Figure A4.2 – Tram model M31

The total weight of tram model M31 is 35600 kg. The bogies under car bodies A and B are simplified and divided into a bogie frame, bolster beam, two axles and four wheels.

A bogie frame is assumed to have the shape of a parallelepiped. Masses of the traction motors, traction rods and couplings are included in the frame. The mass of a frame is calculated as:

$$m_{\text{frame}} = \rho_{\text{steel}} * a * b * h + m_{\text{extra}} \quad (\text{A4.2})$$

where a = length, b = width, h = height, ρ_{steel} = density of steel and m_{extra} = included components .

A wheel consists of a wheel ring and a hub. The components are of steel. The weights are calculated as two solid rings as:

$$m = \rho_{\text{steel}} * t * \pi (r_{\text{outer}}^2 - r_{\text{inner}}^2) \quad (\text{A4.3})$$

where t = thickness, r_{outer} = outer radius and r_{inner} = inner radius

In the modelling it is assumed that the axles and hubs can be seen as one. Also the components that are mounted on the axle are added to the weight. The components are gear box, disc brake and two axle boxes:

$$m_{axle} = Axle + gear\ box + 2\ axle\ boxes + 2\ hubs + disc\ brake \quad (A4.4)$$

The masses for car bodies A and B in M31 can be seen in table A4.1 below.

Table A4.1 – Masses of tram components for parts A and B in M31

Part A and B	masses [kg]	Procedure
Car body A	7850	Calculation
Car body B	7650	Calculation
Bogie	4200	Catalogue
Bogie frame	2428	Calculation
Bolster beam	350	Estimation
Axle + 2 wheels + disc brake	531	Reference
Wheel	208.5	Calculation
Wheel ring	108.5	Calculation
Hub	100	Estimation
Gear box	170	Catalogue
Axle box	50	Estimation
Axle + gear box + 2 axle boxes + 2 hubs+ disc brake	494	Calculation

The weight of car body C is:

$$m_c = Total\ weight - part\ A\ and\ B - wheel\ sets \quad (A4.5)$$

The wheel sets for part C have two frames that are two solid parallelepipeds. The frame connected to the car body is estimated, while the frame connecting the wheels is calculated with equation (A4.2). An addition of 140 kg has been added to the frame due to extra components.

The masses of the components for car body C can be seen in table A4.2 below.

Table A4.2 - Masses of tram components for part C in M31

Part C	Masses [kg]	Procedure
Car body C	8030	Calculation
Frame connected to car body	700	Estimation
Frame connecting the wheels	467.4 + 140	Calculation + estimation
Wheel	213.8	Calculation
Wheel ring	106.9	Calculation
Hub	189.9	Estimation
Wheel box and disc brake	50	Estimation

Furthermore, the wheel boxes and disc brakes mounted on the wheels have been added to the hubs. For simplicity, the hubs have been calculated as a solid cylinder.

There was not sufficient information to calculate the masses of the car bodies for model M32.

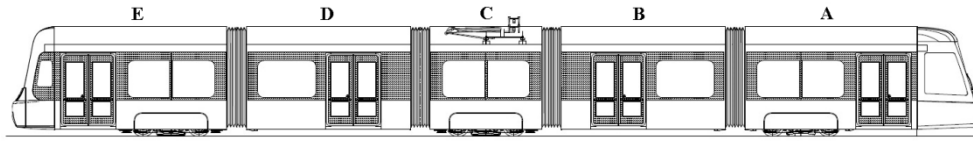


Figure A4.3 – Tram model M32

The total mass of M32 is 42100 kg. Most of the masses have been estimated and can be seen in tables A4.4, A4.5 and A4.6 below.

Table A4.4 – Masses of tram components for part A and E in M32

Part A and E	Masses [kg]	Procedure
Car body A	5000	Estimation
Car body E	5000	Estimation
Bogie	5600	Reference
Bogie frame	3672	Calculation
Frame connecting the wheels	290	Calculation
Wheel + disc brake	337	Calculation

The mass of the bogie frame has been calculated as:

$$Bogie\ frame = Bogie - 2 * Frame\ connecting\ the\ wheels - 4 * (wheel + disc) \quad (A4.7)$$

The wheels in this case have been calculated as a solid cylinder as:

$$m_{wheel,m32} = \rho_{steel} * t * \pi r^2 + disc\ brake \quad (A4.8)$$

The mass of the disc brake has been added to the wheels for simplicity in the modelling. The frame connecting the wheels, also called wheel beam, is calculated as:

$$m_{frame} = \rho_{steel} * a * b * h \quad (A4.9)$$

Table A4.5 – Masses of tram components for part B and D in M32

Part B and D	Masses [kg]	Procedure
Car body B	6000	Estimation
Car body D	6000	Estimation

The bogie frame in part C is calculated with equation A3.7 and can be seen in table A3.6.

Table A4.6 – Masses of tram components for part C in M32

Part C	Masses [kg]	Procedure
Car body C	4100	Estimation
Trailer bogie	4800	Estimation
Bogie frame	2872	Calculation

Appendix 5 – Calculation of moments of inertias for tram parts

The moment of inertia calculations of the tram and tram components that are used in the modelling, are presented here. The formulas are obtained from [23].

The bogie frames, framework and car bodies are assumed to have the form of a solid parallelepiped, which can be seen in figure A5.1 below.

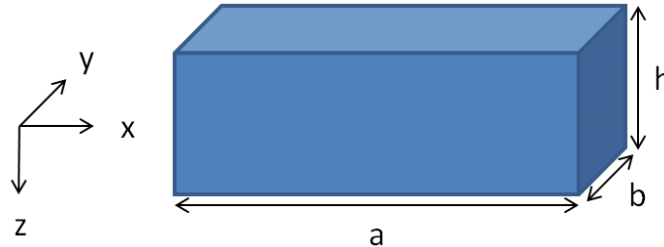


Figure A5.1 – A solid parallelepiped

The calculations of the moments of inertia for the bogie frames, bolster beam and car bodies are as following:

$$J_x = \frac{1}{12} m(b^2 + h^2) \quad (\text{A5.1})$$

$$J_y = \frac{1}{12} m(a^2 + h^2) \quad (\text{A5.2})$$

$$J_z = \frac{1}{12} m(a^2 + b^2) \quad (\text{A5.3})$$

where a = length, b = width, h = height and m = mass

The wheel sets under the motor bogies for the tram model M31 are constructed as an axle, hubs and wheel rings. In the modelling, it is assumed that the axle and the hubs can be seen as one component, this can be seen in figure A5.2.

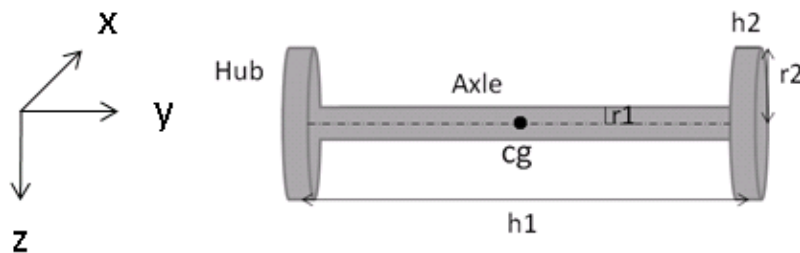


Figure A5.2 – Axle assembled with hubs. (cg = center of gravity)

The calculations of the moment of inertias for an axle assembled with hubs are as following:

$$J_x = \frac{1}{12} m_1(3r_1^2 + h_1^2) + 2 \left[\frac{1}{12} m_2(3r_2^2 + h_2^2) + m_2 \left(\frac{h_1}{2} \right)^2 \right] \quad (\text{A5.4})$$

$$J_y = \frac{1}{2}m_1r_1^2 + 2\frac{1}{2}m_2r_2^2 \quad (\text{A5.5})$$

$$J_z = \frac{1}{12}m_1(3r_1^2 + h_1^2) + 2\left[\frac{1}{12}m_2(3r_2^2 + h_2^2) + m_2\left(\frac{h_1}{2}\right)\right] \quad (\text{A5.6})$$

It should be noticed that Steiner's theorem (parallel axis theorem) is used in equation (A5.4) and (A5.6). This is because of a special case of three parts. In this case, the centres of gravity of the hubs are moved to the centre of the gravity of the whole component. The wheel rings for the tram model M31 has been calculated as:

$$J_x = \frac{1}{12}m_{wh} \left(3(r_{outer}^2 + r_{inner}^2) + t^2 \right) \quad (\text{A5.7})$$

$$J_y = \frac{1}{2}m_{wh} * 3 \left(r_{outer}^2 + r_{inner}^2 \right) \quad (\text{A5.8})$$

$$J_z = \frac{1}{12}m_{wh} \left(3(r_{outer}^2 + r_{inner}^2) + t^2 \right) \quad (\text{A5.9})$$

The hubs for part C is assumed to have a form of a solid cylinder for simplicity and is calculated as:

$$J_{x,hub} = \frac{1}{12}m_h(3r_h^2 + t^2) \quad (\text{A5.10})$$

$$J_{y,hub} = \frac{1}{2}m_h * (3r_h^2) \quad (\text{A5.11})$$

$$J_{z,hub} = \frac{1}{12}m_h(3r_h^2 + t^2) \quad (\text{A5.12})$$

All the moments of inertias for the tram model M31 can be seen in table A5.1 below.

Table A5.1 – Moments of inertias for the tram model M31

M31	Roll [kgm ²]	Pitch [kgm ²]	Yaw [kgm ²]
Part A and B			
Car body A	9.47e3	78.31e3	78.03e3
Car body B	9.23e3	76.31e3	76.04e3
Bogie frame	886.73	1.63e3	2.43e3
Bolster beam	182.53	4.54	186.60
Axle with hubs incl. axle boxes and gear box	240.85	8.20	240.85
Wheel rings	5.35	10.52	5.35
Part C			
Car body C	9.69e3	46.22e3	45.94e3
Frame connecting the wheels	87.60	21.20	108.30
Frame connected to the car bodies	119.77	64.63	183.77
Wheel rings	3.93	7.69	3.93
Hubs	9.45	18.34	9.45

The moments of inertias for tram model M32 that have been used in the modelling can be seen in table A5.2 below.

Table A5.2 – Moment of inertia for the tram model M32

M32	Roll [kgm ²]	Pitch [kgm ²]	Yaw [kgm ²]
Part A and E			
Car body A	6.72e3	25.50e3	24.42e3
Car body E	6.72e3	21.78e3	20.69e3
Bogie frame	1.22e3	2.15e3	3.16e3
Frame connecting the wheels	33.56	1.42	33.81
Wheels	9.45	18.34	9.45
Part B and D			
Car body B	8.06e3	17.18e3	15.88e3
Car body D	8.06e3	17.18e3	15.88e3
Part C			
Car body C	5.51e3	7.15e3	6.26e3
Trailer bogie frame	0.95e3	1.68e3	2.47e3

The wheels in the tram model M32 have been calculated as a solid cylinder with equations (A5.10)-(A5.12).

Appendix 6 – Vehicle modelling method of M31 and M32 in GENSYS

Some masses on the different tram vehicles were not known and could not be found by searching or asking, hence qualified estimations were used to solve this problem. The components with estimated masses are the five car bodies on tram M32. Only the total weight was known and due to more unknowns than equations the problem could not be solved. It is also assumed that the mass centre of the car bodies is located in the middle. The calculations of masses and moments of inertia for all components can be seen in *Appendix 4* and *Appendix 5*. The procedure and information about modelling in GENSYS was found in [3]. Also some guidance and discussions was made with the GENSYS software developer Ingemar Persson. A complete table of the couplings used in the modelling can be seen in *Appendix 7*.

A6.1 – M31 and M32, joint couplings between car bodies

The couplings between car bodies on both tram vehicles are modelled in the same way. The only difference is that the tram M32 has more couplings due to its design compared to M31. Instead of one coupling between each car body, M32 has two. The modelled couplings and the difference between the two trams can be seen in figure A6.1 below.

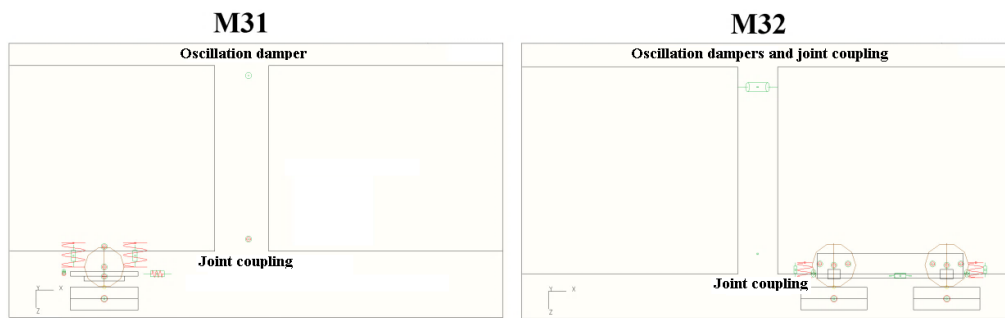


Figure A6.1 – The left figure shows the couplings between the car bodies on M31 and the right figure shows the couplings between the car bodies on M32.

The coupling type used for the joint couplings is called *p_lin36* in the GENSYS algorithm. This sub coupling command defines a linear 6x6 matrix property and a vector with preload forces that acts on zero displacement. This coupling type is used for both the stiffness and viscous damping when modelling the joint couplings. The forces and moments acting on the coupling can be written in components as:

$$\begin{bmatrix} F_x \\ F_y \\ F_z \\ M_\varphi \\ M_\chi \\ M_\psi \end{bmatrix} = \begin{bmatrix} k_{xx} & k_{xy} & k_{xz} & k_{x\varphi} & k_{x\chi} & k_{x\psi} \\ k_{yx} & k_{yy} & k_{yz} & k_{y\varphi} & k_{y\chi} & k_{y\psi} \\ k_{zx} & k_{zy} & k_{zz} & k_{z\varphi} & k_{z\chi} & k_{z\psi} \\ k_{\varphi x} & k_{\varphi y} & k_{\varphi z} & k_{\varphi\varphi} & k_{\varphi\chi} & k_{\varphi\psi} \\ k_{\chi x} & k_{\chi y} & k_{\chi z} & k_{\chi\varphi} & k_{\chi\chi} & k_{\chi\psi} \\ k_{\psi x} & k_{\psi y} & k_{\psi z} & k_{\psi\varphi} & k_{\psi\chi} & k_{\psi\psi} \end{bmatrix} \begin{bmatrix} \Delta x \\ \Delta y \\ \Delta z \\ \Delta\varphi \\ \Delta\chi \\ \Delta\psi \end{bmatrix} + \begin{bmatrix} F0_x \\ F0_y \\ F0_z \\ M0_\varphi \\ M0_\chi \\ M0_\psi \end{bmatrix} \quad (\text{A6.1})$$

The forces in the last column are used to define a preloaded spring. In the modelling there is only a preload force in the vertical direction and the magnitude of this force is the weight from the car body acting on the coupling. For the viscous damper the 6x6 matrix represents

damping coefficients instead of spring stiffness. The values used for the stiffness and damping coefficients are presented in the matrix below.

$$\left\{ \begin{array}{l} \mathbf{F}_k = \begin{bmatrix} 30e6 & 0 & 0 & 0 & 0 & 0 \\ 0 & 30e6 & 0 & 0 & 0 & 0 \\ 0 & 0 & 30e6 & 0 & 0 & 0 \\ 0 & 0 & 0 & 1e6 & 0 & 0 \\ 0 & 0 & 0 & 0 & 1e6 & 0 \\ 0 & 0 & 0 & 0 & 0 & 0 \end{bmatrix} \begin{bmatrix} \Delta x \\ \Delta y \\ \Delta z \\ \Delta \phi \\ \Delta \chi \\ \Delta \psi \end{bmatrix} + \begin{bmatrix} 0 \\ 0 \\ F0_z \\ 0 \\ 0 \\ 0 \end{bmatrix} \\ \mathbf{F}_c = \begin{bmatrix} 30e3 & 0 & 0 & 0 & 0 & 0 \\ 0 & 30e3 & 0 & 0 & 0 & 0 \\ 0 & 0 & 30e3 & 0 & 0 & 0 \\ 0 & 0 & 0 & 0 & 0 & 0 \\ 0 & 0 & 0 & 0 & 0 & 0 \\ 0 & 0 & 0 & 0 & 0 & 0 \end{bmatrix} \begin{bmatrix} \Delta \dot{x} \\ \Delta \dot{y} \\ \Delta \dot{z} \\ \Delta \dot{\phi} \\ \Delta \dot{\chi} \\ \Delta \dot{\psi} \end{bmatrix} + \begin{bmatrix} 0 \\ 0 \\ 0 \\ 0 \\ 0 \\ 0 \end{bmatrix} \end{array} \right. \quad (\text{A6.2})$$

The values of the stiffness and damping coefficients for this coupling was determined by discussions with Ingemar Persson who have good experience in modelling vehicles in GENSY. As can be seen the stiffness are higher in the longitudinal, lateral and vertical direction compared to the roll and pitch stiffnesses. The joint should rotate freely around the z-axis. This leads to that the yaw stiffness is set to zero.

A6.2 – M31, Oscillation dampers

On the top and between the car bodies oscillation dampers are attached. The coupling subcommand “c” is used to model the oscillation dampers. The dampers are modelled as a one dimensional coupling with zero length. The damping coefficient used for the lateral damping between the car bodies can be seen below.

$$F_c = \begin{bmatrix} 0 & 0 & 0 \\ 0 & 30e3 & 0 \\ 0 & 0 & 0 \end{bmatrix} \begin{bmatrix} \Delta \dot{y} \\ \Delta \dot{z} \end{bmatrix} + \begin{bmatrix} 0 \\ 0 \end{bmatrix} \quad (\text{A6.3})$$

A6.3 – M31, motor bogie couplings

A schematic figure of the couplings between the different components can be seen in figure A6.2. The car body is attached to the bolster beam by a slewing ring. The bolster beam and motor bogie are connected together with the secondary suspension, bump stop, traction rods and a lateral damper. The wheels are connected to a wheel axle and this axle is connected to the bogie via the primary suspension.

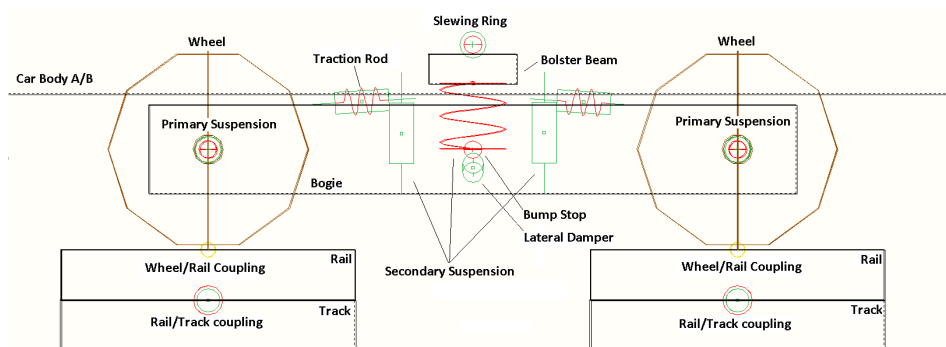


Figure A6.2 - The couplings on the motor bogies. The figure shows how the different components are connected to each other.

Slewing ring

The slewing ring is used so that the bolster beam and bogie can yaw freely relative to the car body. A slewing ring can be modelled as a point spring and damper. The coupling used to model the slewing ring is *p_lin36* with the following values:

$$\left\{ \begin{array}{l} \mathbf{F}_k = \begin{bmatrix} 10e6 & 0 & 0 & 0 & 0 & 0 \\ 0 & 10e6 & 0 & 0 & 0 & 0 \\ 0 & 0 & 10e6 & 0 & 0 & 0 \\ 0 & 0 & 0 & 5e6 & 0 & 0 \\ 0 & 0 & 0 & 0 & 5e6 & 0 \\ 0 & 0 & 0 & 0 & 0 & 0 \end{bmatrix} \begin{bmatrix} \Delta x \\ \Delta y \\ \Delta z \\ \Delta \varphi \\ \Delta \chi \\ \Delta \psi \end{bmatrix} + \begin{bmatrix} 0 \\ 0 \\ F0_z \\ 0 \\ 0 \\ 0 \end{bmatrix} \\ \mathbf{F}_c = \begin{bmatrix} \frac{0.05k_{xx}}{5\pi} & 0 & 0 & 0 & 0 & 0 \\ 0 & \frac{0.05k_{yy}}{5\pi} & 0 & 0 & 0 & 0 \\ 0 & 0 & \frac{0.05k_{zz}}{5\pi} & 0 & 0 & 0 \\ 0 & 0 & 0 & \frac{0.05k_{\varphi\varphi}}{5\pi} & 0 & 0 \\ 0 & 0 & 0 & 0 & \frac{0.05k_{\chi\chi}}{5\pi} & 0 \\ 0 & 0 & 0 & 0 & 0 & 0 \end{bmatrix} \begin{bmatrix} \Delta \dot{x} \\ \Delta \dot{y} \\ \Delta \dot{z} \\ \Delta \dot{\varphi} \\ \Delta \dot{\chi} \\ \Delta \dot{\psi} \end{bmatrix} + \begin{bmatrix} 0 \\ 0 \\ 0 \\ 0 \\ 0 \\ 0 \end{bmatrix} \end{array} \right. \quad (\text{A6.4})$$

The values on the slewing ring stiffnesses and damping coefficients were determined by discussions and consultation with Ingemar Persson. The stiffness in yaw is set to zero so that the bolster beam and bogie can rotate freely relative to the car body.

Secondary suspension

The secondary suspension consists of two hour-glass springs and two vertical dampers, as was explained in the description chapter. The hour-glass springs in GENSYS can be modelled with the coupling command *k3_l*. This command defines stiffness coupling between the bolster beam and the bogie. The input data to the command is the longitudinal, lateral and vertical stiffnesses. The coupling can rotate relative to its predefined esys and when it rotates the stiffness matrix and preload force follows the given rotation. The spring stiffnesses used for this spring can be seen below.

$$\mathbf{F}_k = \begin{bmatrix} 0.15e6 & 0 & 0 \\ 0 & 0.15e6 & 0 \\ 0 & 0 & 0.50e6 \end{bmatrix} \begin{bmatrix} \Delta x \\ \Delta y \\ \Delta z \end{bmatrix} + \begin{bmatrix} 0 \\ 0 \\ F0_z \end{bmatrix} \quad (\text{A6.5})$$

The stiffnesses for the spring were determined by estimation. The values were not known and could not be determined during the project. However the secondary suspension for the other tram vehicle M32 could be calculated. The car bodies of M31 and M32 have similar weight. Due to that, it was determined to use stiffnesses in the same order of magnitude as the ones in M32. The vertical hydraulic dampers can be modelled with the coupling command *c*. This command defines a damper between two masses with a predefined property. The damping coefficient for the damper is presented below.

$$F_c = 30e3\Delta\dot{c} \quad (\text{A6.6})$$

For this coupling, the force acts in the direction of the damper element. That is why $\Delta\dot{c}$ is used in the equation above instead of $\Delta\dot{z}$. In this case the dampers are vertically mounted and this will give that $\Delta\dot{c} = \Delta\dot{z}$. However, depending on how the dampers are attached, this will not

always be true. The value of the damper coefficient could not be calculated or found during the project. The value used here is estimated and the damper is assumed to be linear.

Bump stop

The bump stop is modelled with the coupling p_nlin_s . The command defines an asymmetric non-linear property that is suitable to use for a bump stop. The stiffness characteristic can be seen as piecewise linear. The characteristic can be seen in the figure A6.3 below.

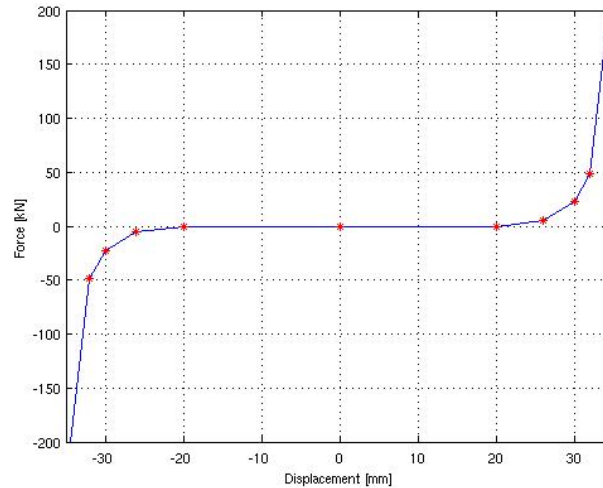


Figure A6.3 – The spring characteristic of the modelled bump stop.

The bump stop is mounted so that the bolster beam can move 20 mm in the lateral direction before it hits the bogie frame. The modelled spring is hence not active before the deformation has reached this value. The stiffness is then increased when the deformation is increased. This behaviour shows that the rubber bump stop is compressed. Finally the bump stop can not be compressed anymore and this is modelled with a very high stiffness.

Traction rods

The traction rods will prevent a yaw motion on the bolster beam. These have been modelled as a spring and damper. Due to that there are rubber rings at the attachment points the stiffness have not been set as high as the axial stiffness for a normal steel rod. The values of the stiffness and damping constant have been set by discussion and consultation with Ingemar Persson. The values are presented below.

$$\begin{cases} F_k = 2.5e6\Delta c \\ F_c = \frac{0.2e6}{4\pi}\Delta\dot{c} \end{cases} \quad (\text{A6.7})$$

Note that the mounting of these rods is not completely horizontal. The force acts in the direction of the spring and damper elements (in direction Δc and $\Delta\dot{c}$, observe that c is a direction not a damping constant in this case).

Lateral damper

The same dampers are used for both the vertical and lateral damping. The lateral dampers are hence modelled in the same way and with the same constants as the vertical dampers.

Wheel rings and wheel hub

A schematic figure of how the coupling in between the wheel and axle is modelled, can be seen in A6.4 below. The wheel hub is press fitted against the axle and this coupling is relatively stiff. When modelling, the wheel hubs and axle were assumed to be as one solid component, as shown in figure A6.4 below.

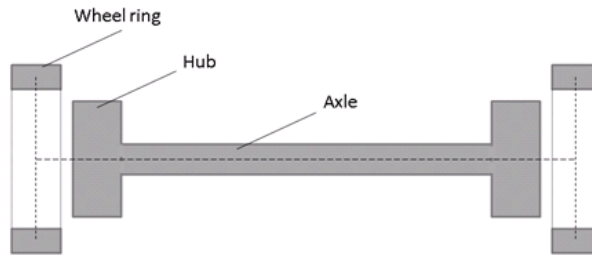


Figure A6.4 – Schematic figure on the axle, hub and wheel ring.

There are rubber rings in between the hubs and wheel rings. These rings are relatively stiff and they are modelled with the coupling subcommand *p_lin36*. The values of the stiffness and damping can be seen below.

$$\left\{ \begin{array}{l} \mathbf{F}_k = \begin{bmatrix} 120e6 & 0 & 0 & 0 & 0 & 0 \\ 0 & 80e6 & 0 & 0 & 0 & 0 \\ 0 & 0 & 120e6 & 0 & 0 & 0 \\ 0 & 0 & 0 & 0 & 0 & 0 \\ 0 & 0 & 0 & 0 & \frac{20e3 \cdot 180}{2\pi} & 0 \\ 0 & 0 & 0 & 0 & 0 & 0 \end{bmatrix} \begin{bmatrix} \Delta x \\ \Delta y \\ \Delta z \\ \Delta \varphi \\ \Delta \chi \\ \Delta \psi \end{bmatrix} \\ \mathbf{F}_c = \begin{bmatrix} \frac{0.2k_{xx}}{4\pi} & 0 & 0 & 0 & 0 & 0 \\ 0 & \frac{0.2k_{yy}}{4\pi} & 0 & 0 & 0 & 0 \\ 0 & 0 & \frac{0.2k_{zz}}{4\pi} & 0 & 0 & 0 \\ 0 & 0 & 0 & 0 & 0 & 0 \\ 0 & 0 & 0 & 0 & \frac{0.2k_{\chi\chi}}{20\pi} & 0 \\ 0 & 0 & 0 & 0 & 0 & 0 \end{bmatrix} \begin{bmatrix} \Delta \dot{x} \\ \Delta \dot{y} \\ \Delta \dot{z} \\ \Delta \dot{\varphi} \\ \Delta \dot{\chi} \\ \Delta \dot{\psi} \end{bmatrix} \end{array} \right. \quad (A6.8)$$

Primary suspension

For the motor bogies in car bodies A and B the primary suspension consists of chevron springs. In GENSYS this type of spring can be modelled as a zero length spring and damper located in the centre of the wheel and axle. The spring and damper connects the wheel axle to the bogie, see the modelled spring in figure A6.5 below.

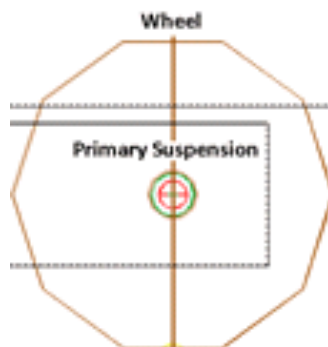


Figure A6.5 – Model of the chevron springs mounted in between the bogie and wheel axle

The coupling type used for the springs is p_lin36 with the following values:

$$\left\{ \begin{array}{l} \mathbf{F}_k = \begin{bmatrix} 10e6 & 0 & 0 & 0 & 0 & 0 \\ 0 & 3e6 & 0 & 0 & 0 & 0 \\ 0 & 0 & 0.8e6 & 0 & 0 & 0 \\ 0 & 0 & 0 & 0 & 0 & 0 \\ 0 & 0 & 0 & 0 & 0 & 0 \\ 0 & 0 & 0 & 0 & 0 & 0 \end{bmatrix} \begin{bmatrix} \Delta x \\ \Delta y \\ \Delta z \\ \Delta \varphi \\ \Delta \chi \\ \Delta \psi \end{bmatrix} + \begin{bmatrix} 0 \\ 0 \\ F0_z \\ 0 \\ 0 \\ 0 \end{bmatrix} \\ \mathbf{F}_c = \begin{bmatrix} \frac{0.2k_{xx}}{4\pi} & 0 & 0 & 0 & 0 & 0 \\ 0 & \frac{0.2k_{yy}}{4\pi} & 0 & 0 & 0 & 0 \\ 0 & 0 & \frac{0.2k_{zz}}{4\pi} & 0 & 0 & 0 \\ 0 & 0 & 0 & 0 & 0 & 0 \\ 0 & 0 & 0 & 0 & 0 & 0 \\ 0 & 0 & 0 & 0 & 0 & 0 \end{bmatrix} \begin{bmatrix} \Delta \dot{x} \\ \Delta \dot{y} \\ \Delta \dot{z} \\ \Delta \dot{\varphi} \\ \Delta \dot{\chi} \\ \Delta \dot{\psi} \end{bmatrix} + \begin{bmatrix} 0 \\ 0 \\ 0 \\ 0 \\ 0 \\ 0 \end{bmatrix} \end{array} \right. \quad (\text{A6.9})$$

The preloaded force is the weight that is applied on the spring from the bodies it supports. The springs in car body B have a lower preload. This is due to that car body B is lighter than car body A. The chevron springs used as a primary suspension on tram vehicle M31 are from the manufacturer Trelleborg. The spring model is 17-1371 and the stiffness values for this spring were given in a product sheet from Trelleborg [24].

A6.4 – M31, wheel set couplings on car body C

There are two wheel sets mounted under car body C. The wheels are attached to a lower frame via the primary suspension. The lower frame can yaw freely relative to the upper frame due to the slewing ring. The upper frame is attached to car body C by the secondary suspension, anti-pitch bar, lateral damper, traction rods and bump stop, see this in figure A6.6 below.

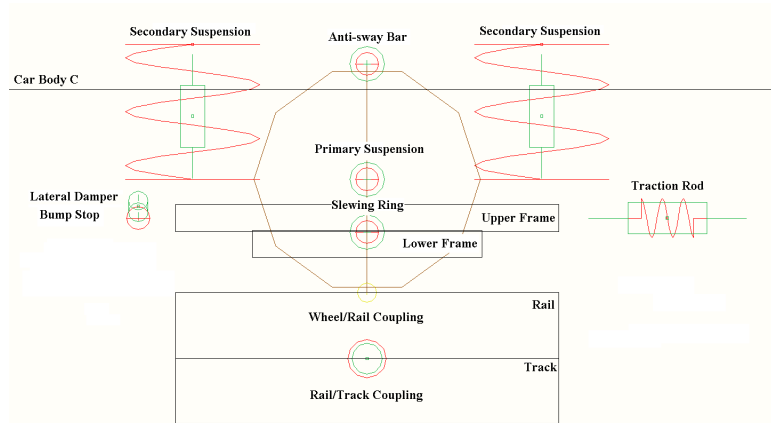


Figure A6.6 – The couplings on the wheel sets. The figure shows how the different components are connected to each other.

Secondary suspension

The secondary suspension consists of four coil springs and two dampers. The coupling used for modelling the coil springs is $k3_l$. This coupling was discussed earlier in this report and will not be explained once more. The values for the compression and shear stiffness are shown below.

$$\mathbf{F}_k = \begin{bmatrix} 0.81e5 & 0 & 0 \\ 0 & 0.81e5 & 0 \\ 0 & 0 & 0.22e6 \end{bmatrix} \begin{bmatrix} \Delta x \\ \Delta y \\ \Delta z \end{bmatrix} + \begin{bmatrix} 0 \\ 0 \\ F0_z \end{bmatrix} \quad (\text{A6.10})$$

Due to that the secondary suspension consists of standard coil springs, a theoretical equation has been used for calculating the stiffnesses. The theory and calculations are presented in *Appendix 3*. Information about damping characteristics could not be found for the vertical dampers. The vertical dampers are the same as the ones used on the motor bogie and hence the same damping coefficient is used.

Anti-pitch bar

A point spring and damper is used for modelling the anti-pitch bar. Stiffness and damping are applied to prevent pitch rotation of the upper frame relative to the car body. The values used can be seen below.

$$\begin{cases} F_k = 300e3\Delta\chi \\ F_c = \frac{0.05*k_{\chi\chi}}{4\pi} \Delta\dot{\chi} \end{cases} \quad (\text{A6.11})$$

Bump stop

The same modelling method is used for these bump stops as the ones from the motor bogie in car bodies A and B.

Traction rods

The same modelling method is used for these traction rods as the ones from the motor bogie in car bodies A and B.

Lateral damper

The same dampers are used for both the vertical and lateral damping. The lateral dampers are hence modelled in the same way and with the same damping constant.

Slewing ring

The slewing ring is used so that the upper frame and lower frame can yaw freely relative to the each other. This slewing ring is slightly smaller than the one used between car body A/B and the bolster beam. The slewing ring is modelled as a zero length spring and damper. The coupling used to model is *p_lin36* with the following values.

$$\begin{cases} \mathbf{F}_k = \begin{bmatrix} 15e6 & 0 & 0 & 0 & 0 & 0 \\ 0 & 15e6 & 0 & 0 & 0 & 0 \\ 0 & 0 & 15e6 & 0 & 0 & 0 \\ 0 & 0 & 0 & 15e6 & 0 & 0 \\ 0 & 0 & 0 & 0 & 15e6 & 0 \\ 0 & 0 & 0 & 0 & 0 & 0 \end{bmatrix} \begin{bmatrix} \Delta x \\ \Delta y \\ \Delta z \\ \Delta\varphi \\ \Delta\chi \\ \Delta\psi \end{bmatrix} + \begin{bmatrix} 0 \\ 0 \\ F0_z \\ 0 \\ 0 \\ 0 \end{bmatrix} \\ \mathbf{F}_c = \begin{bmatrix} \frac{0.4k_{xx}}{4\pi} & 0 & 0 & 0 & 0 & 0 \\ 0 & \frac{0.4k_{yy}}{4\pi} & 0 & 0 & 0 & 0 \\ 0 & 0 & \frac{0.4k_{zz}}{4\pi} & 0 & 0 & 0 \\ 0 & 0 & 0 & \frac{0.4k_{zz}}{4\pi} & 0 & 0 \\ 0 & 0 & 0 & 0 & \frac{0.4k_{zz}}{4\pi} & 0 \\ 0 & 0 & 0 & 0 & 0 & 0 \end{bmatrix} \begin{bmatrix} \Delta\dot{x} \\ \Delta\dot{y} \\ \Delta\dot{z} \\ \Delta\dot{\varphi} \\ \Delta\dot{\chi} \\ \Delta\dot{\psi} \end{bmatrix} + \begin{bmatrix} 0 \\ 0 \\ 0 \\ 0 \\ 0 \\ 0 \end{bmatrix} \end{cases} \quad (\text{A6.12})$$

The stiffness in yawing is set to zero so that the upper and lower frame can rotate freely relative to each other.

Primary suspension

The stiffness of the chevron springs mounted between the wheel and lower frame could not be found. The chevron springs are small compared to the primary suspension on the motor bogies. Due to this, it is assumed that they are relatively stiff. They are modelled in the same way as the chevron springs for the motor bogies. The values of the spring and damping coefficient can be seen below.

$$\left\{ \begin{array}{l} \mathbf{F}_k = \begin{bmatrix} 50e6 & 0 & 0 & 0 & 0 & 0 \\ 0 & 50e6 & 0 & 0 & 0 & 0 \\ 0 & 0 & 50e6 & 0 & 0 & 0 \\ 0 & 0 & 0 & 0 & 0 & 0 \\ 0 & 0 & 0 & 0 & 0 & 0 \\ 0 & 0 & 0 & 0 & 0 & 0 \end{bmatrix} \begin{bmatrix} \Delta x \\ \Delta y \\ \Delta z \\ \Delta \varphi \\ \Delta \chi \\ \Delta \psi \end{bmatrix} + \begin{bmatrix} 0 \\ 0 \\ F0_z \\ 0 \\ 0 \\ 0 \end{bmatrix} \\ \mathbf{F}_c = \begin{bmatrix} \frac{0.2k_{xx}}{20\pi} & 0 & 0 & 0 & 0 & 0 \\ 0 & \frac{0.2k_{yy}}{20\pi} & 0 & 0 & 0 & 0 \\ 0 & 0 & \frac{0.2k_{zz}}{20\pi} & 0 & 0 & 0 \\ 0 & 0 & 0 & 0 & 0 & 0 \\ 0 & 0 & 0 & 0 & 0 & 0 \\ 0 & 0 & 0 & 0 & 0 & 0 \end{bmatrix} \begin{bmatrix} \Delta \dot{x} \\ \Delta \dot{y} \\ \Delta \dot{z} \\ \Delta \dot{\varphi} \\ \Delta \dot{\chi} \\ \Delta \dot{\psi} \end{bmatrix} + \begin{bmatrix} 0 \\ 0 \\ 0 \\ 0 \\ 0 \\ 0 \end{bmatrix} \end{array} \right. \quad (\text{A6.13})$$

Wheel rings and wheel hubs

The wheel rings are attached to wheel hubs with the coupling type *p_lin36*. The wheel hubs are attached to the lower frame with the same coupling. The couplings for a freely rotated wheel differ from the ones in the motor bogies and can be seen below.

$$\left\{ \begin{array}{l} \mathbf{F}_k = \begin{bmatrix} 50e6 & 0 & 0 & 0 & 0 & 0 \\ 0 & 50e6 & 0 & 0 & 0 & 0 \\ 0 & 0 & 50e6 & 0 & 0 & 0 \\ 0 & 0 & 0 & 0 & 0 & 0 \\ 0 & 0 & 0 & 0 & 0 & 0 \\ 0 & 0 & 0 & 0 & 0 & 0 \end{bmatrix} \begin{bmatrix} \Delta x \\ \Delta y \\ \Delta z \\ \Delta \varphi \\ \Delta \chi \\ \Delta \psi \end{bmatrix} + \begin{bmatrix} 0 \\ 0 \\ 0 \\ 0 \\ 0 \\ 0 \end{bmatrix} \\ \mathbf{F}_c = \begin{bmatrix} \frac{0.2k_{xx}}{4\pi} & 0 & 0 & 0 & 0 & 0 \\ 0 & \frac{0.2k_{yy}}{4\pi} & 0 & 0 & 0 & 0 \\ 0 & 0 & \frac{0.2k_{zz}}{4\pi} & 0 & 0 & 0 \\ 0 & 0 & 0 & 0 & 0 & 0 \\ 0 & 0 & 0 & 0 & 0 & 0 \\ 0 & 0 & 0 & 0 & 0 & 0 \end{bmatrix} \begin{bmatrix} \Delta \dot{x} \\ \Delta \dot{y} \\ \Delta \dot{z} \\ \Delta \dot{\varphi} \\ \Delta \dot{\chi} \\ \Delta \dot{\psi} \end{bmatrix} + \begin{bmatrix} 0 \\ 0 \\ 0 \\ 0 \\ 0 \\ 0 \end{bmatrix} \end{array} \right. \quad (\text{A6.14})$$

Notice that the pitch value is set to zero, which will allow the wheels to rotate freely.

A6.5 – M31, guidance of lower frame

As was explained in the description chapter car bodies A and B will rotate the lower frames on car body C. In GENSYS this is modelled by applying a yaw moment on this frame. An angle difference between the car bodies is needed to determine the yaw moment. This angle can be calculated by taking the yaw angle difference between the car bodies, see the calculations below.

$$\begin{cases} \Delta_{AC,\psi} = esys_{A,\psi} + lsys_{A,\psi} + bsys_{A,\psi} - (esys_{C,\psi} + lsys_{C,\psi} + bsys_{C,\psi}) \\ \Delta_{BC,\psi} = esys_{A,\psi} + lsys_{A,\psi} + bsys_{A,\psi} - (esys_{C,\psi} + lsys_{C,\psi} + bsys_{C,\psi}) \end{cases} \quad (A6.15)$$

Due to the way of defining coordinate systems in GENSYS the yaw difference of all three types of coordinate system must be calculated to get the yaw angle difference between two car bodies. The calculations of the desired angles for the lower frame (LF) can be seen below.

$$\begin{cases} \Delta_{LF,AC,\psi} = S_r \Delta_{AC,\psi} + lsys_{C,\psi} + bsys_{C,\psi} - (lsys_{LF,AC,\psi} + bsys_{LF,AC,\psi}) + E_r \\ \Delta_{LF,BC,\psi} = S_r \Delta_{BC,\psi} + lsys_{C,\psi} + bsys_{C,\psi} - (lsys_{LF,BC,\psi} + bsys_{LF,BC,\psi}) + E_r \end{cases} \quad (A6.16)$$

Here S_r is the steering ratio. This ratio controls how much the lower frame shall steer. The calculations of this ratio can be seen in *Appendix 2*. E_r is an error ratio and this factor can be added if errors in the adjustments exist. The variable can be changed if simulations with poorly angled lower frames are of interest. The yaw moment is finally added by using the equations below.

$$\begin{cases} M_{LF,AC,\psi} = \Delta_{LF,AC,\psi} * M_\psi \\ M_{LF,BC,\psi} = \Delta_{LF,BC,\psi} * M_\psi \end{cases} \quad (A6.17)$$

Where the series flexibility value M_ψ is:

$$M_\psi = 19e6 \text{ [Nm/rad]} \quad (A6.18)$$

The size of the series flexibility was discussed with Ingemar Persson and then estimated. The value is probably a little bit too high if considerations are taken to all the serial coupled flexibilities. A decision was made to be satisfied with this value.

A6.6 – M32, Oscillation dampers

The oscillation dampers are modelled as non-linear viscous dampers. The damping characteristics were given in [12]. The sub couplings and values used for these dampers are presented in the next subchapter.

A6.7 – M32, motor bogie couplings

The wheels are attached to the beam via the wheel/beam coupling. The beams are attached to the bogie with eight primary suspensions. The bogie is then attached to the car body by the secondary suspension, two longitudinal, two lateral dampers and two lateral bump stops. An illustration of the couplings can be seen in figure A6.7.

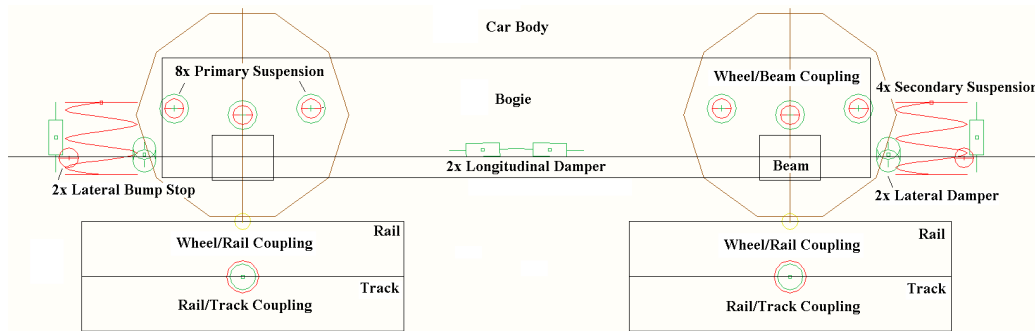


Figure A6.7 – The couplings on trailer and motor bogies. The figure shows how the different components are connected to each other.

Secondary suspension

The secondary suspension consists of four springs and four vertical dampers. The secondary springs are not the same on the motor bogie compared to the trailer bogie. The springs on the motor bogie have lower shear stiffness. These springs have been modelled as solid rubber tubes. The finite element method has been used to calculate the different stiffnesses, where the calculations can be seen in *Appendix 8*. The springs have been modelled with the coupling $k3_l$. The result of the FEM calculations can be seen below.

$$\mathbf{F}_{k,\text{motor}} = \begin{bmatrix} 0.1e6 & 0 & 0 \\ 0 & 0.1e6 & 0 \\ 0 & 0 & 0.65e6 \end{bmatrix} \begin{bmatrix} \Delta x \\ \Delta y \\ \Delta z \end{bmatrix} + \begin{bmatrix} 0 \\ 0 \\ F0_z \end{bmatrix} \quad (\text{A6.19})$$

The secondary springs attached between car body C and the trailer bogie are standard coil springs. The theory and calculations of the stiffnesses can be seen in *Appendix 3*. The results can be seen below.

$$\mathbf{F}_{k,\text{trail}} = \begin{bmatrix} 0.207e6 & 0 & 0 \\ 0 & 0.207e6 & 0 \\ 0 & 0 & 0.567e6 \end{bmatrix} \begin{bmatrix} \Delta x \\ \Delta y \\ \Delta z \end{bmatrix} + \begin{bmatrix} 0 \\ 0 \\ F0_z \end{bmatrix} \quad (\text{A6.20})$$

The vertical dampers have non-linear damping characteristics, however the characteristic is assumed to be piecewise linear. The values have been given from a previously performed SIMPACK modelling of a tram similar to M32 [12]. The characteristics can be seen in figure A6.8.

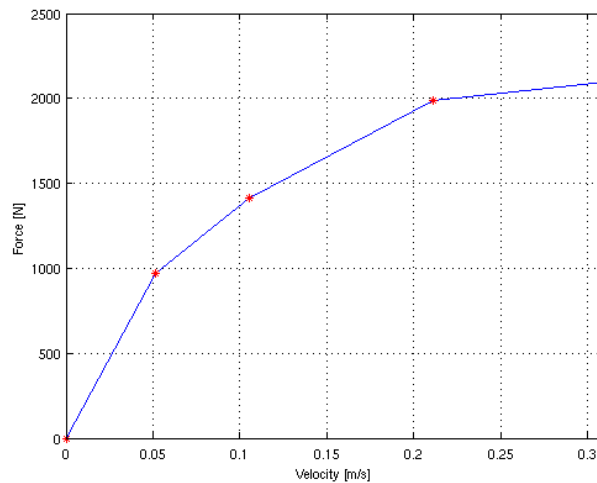


Figure A6.8 – The damping characteristic of the dampers used on model M32.

Depending on how fast the dampers are compressed/extent, the force will vary. The dampers have been modelled with the asymmetric non-linear coupling p_nlin_s . The damping constants are shown in table A6.1 below.

Table A6.1 – The values used for the part wise linear damping characteristics.

Velocity [m/s]	Force [N]	Damping constant [Ns/m]
0-0.051	0-983.63	19.3e3
0.051-0.105	983.63-1428.51	8.2e3
0.105-0.211	1428.51-1998.05	5.4e3
0.211-2.000	1998.05-3966.12	1.1e3

Lateral and longitudinal dampers

The lateral and longitudinal dampers attached between the bogies and car bodies are of the same sort. These are larger in size compared to the vertical dampers. Information about characteristics has not been found. It is assumed that these dampers have the same characteristic as the vertical dampers presented above.

Primary suspension

The primary suspension on M32 consists of rubber springs. There is a total of eight springs on each bogie and these are attached between the wheel beam and bogie, one on each side of one wheel. The coupling p_lin36 is used to model the rubber springs. The stiffness and damping coefficients used are presented below.

$$\left\{ \begin{array}{l} \mathbf{F}_k = \begin{bmatrix} 20e6 & 0 & 0 & 0 & 0 & 0 \\ 0 & 20e6 & 0 & 0 & 0 & 0 \\ 0 & 0 & 5e6 & 0 & 0 & 0 \\ 0 & 0 & 0 & 0 & 0 & 0 \\ 0 & 0 & 0 & 0 & 0 & 0 \\ 0 & 0 & 0 & 0 & 0 & 0 \end{bmatrix} \begin{bmatrix} \Delta x \\ \Delta y \\ \Delta z \\ \Delta \varphi \\ \Delta \chi \\ \Delta \psi \end{bmatrix} + \begin{bmatrix} 0 \\ 0 \\ F0_z \\ 0 \\ 0 \\ 0 \end{bmatrix} \\ \mathbf{F}_c = \begin{bmatrix} \frac{0.2k_{xx}}{4\pi} & 0 & 0 & 0 & 0 & 0 \\ 0 & \frac{0.2k_{yy}}{4\pi} & 0 & 0 & 0 & 0 \\ 0 & 0 & \frac{0.2k_{zz}}{4\pi} & 0 & 0 & 0 \\ 0 & 0 & 0 & 0 & 0 & 0 \\ 0 & 0 & 0 & 0 & 0 & 0 \\ 0 & 0 & 0 & 0 & 0 & 0 \end{bmatrix} \begin{bmatrix} \Delta \dot{x} \\ \Delta \dot{y} \\ \Delta \dot{z} \\ \Delta \dot{\varphi} \\ \Delta \dot{\chi} \\ \Delta \dot{\psi} \end{bmatrix} + \begin{bmatrix} 0 \\ 0 \\ 0 \\ 0 \\ 0 \\ 0 \end{bmatrix} \end{array} \right. \quad (\text{A6.21})$$

It is assumed that the springs have linear characteristics and the coefficients are estimated. The values of the primary suspension on tram M31 are known. It is also known that the M32 springs are very stiff compared to the chevron springs used as a primary suspension on M31 i.e. the stiffnesses are higher on M32 compared to M31.

Wheel/beam coupling

The wheels are attached to the beams by a journal box. This coupling will allow the wheels to rotate freely relative to the beams. This type of coupling is relative stiff and the values used are presented below.

$$\left\{ \begin{array}{l} \mathbf{F}_k = \begin{bmatrix} 50e6 & 0 & 0 & 0 & 0 & 0 \\ 0 & 50e6 & 0 & 0 & 0 & 0 \\ 0 & 0 & 50e6 & 0 & 0 & 0 \\ 0 & 0 & 0 & 0 & 0 & 0 \\ 0 & 0 & 0 & 0 & 0 & 0 \\ 0 & 0 & 0 & 0 & 0 & 0 \end{bmatrix} \begin{bmatrix} \Delta x \\ \Delta y \\ \Delta z \\ \Delta \varphi \\ \Delta \chi \\ \Delta \psi \end{bmatrix} \\ \mathbf{F}_c = \begin{bmatrix} \frac{0.2k_{xx}}{20\pi} & 0 & 0 & 0 & 0 & 0 \\ 0 & \frac{0.2k_{yy}}{20\pi} & 0 & 0 & 0 & 0 \\ 0 & 0 & \frac{0.2k_{zz}}{20\pi} & 0 & 0 & 0 \\ 0 & 0 & 0 & 0 & 0 & 0 \\ 0 & 0 & 0 & 0 & 0 & 0 \\ 0 & 0 & 0 & 0 & 0 & 0 \end{bmatrix} \begin{bmatrix} \Delta \dot{x} \\ \Delta \dot{y} \\ \Delta \dot{z} \\ \Delta \dot{\varphi} \\ \Delta \dot{\chi} \\ \Delta \dot{\psi} \end{bmatrix} \end{array} \right. \quad (\text{A6.22})$$

Bump stop

The bump stops are modelled in the same way as the ones on model M31. The difference is that they do not come in contact with the bogie before a lateral displacement of 10 cm compared to 2cm on M31. The lateral displacement stop is obtained from [12].

Appendix 7 – Coupling commands used in GENSYS

In this *appendix* two tables are presented. The tables can be seen as a summary of the different coupling types used between components on tram vehicles M31 and M32. The first table A7.1 represents the tram model M31.

Table A7.1 – Summary of the different coupling types used between components on M31 model

Couplings between car bodies					
Coupling	Number	Modelled as	Mass 1	Mass 2	Coupling subcommand
Joint	1	Spring and damper	Car body A	Car body C	p_lin36
Joint	2	Spring and damper	Car body B	Car body C	p_lin36
Coupling	Number	Modelled as	Mass 1	Mass 2	Coupling subcommand
Oscillation damper	1	Damper	Car body A	Car body C	c
Oscillation damper	2	Damper	Car body B	Car body C	c
Couplings between car bodies and bolster beam					
Coupling	Number	Type of coupling	Mass 1	Mass 2	Coupling subcommand
Slewing ring	1	Spring and damper	Car body A	Bolster beam A	p_lin36
Slewing ring	2	Spring and damper	Car body B	Bolster beam A	p_lin36
Couplings on bogies under car A and B					
Coupling	Number	Type of coupling	Mass 1	Mass 2	Coupling subcommand
Hour glass spring	1	Spring	Bolster beam A	Bogie A	k3_l
Hour glass spring	2	Spring	Bolster beam A	Bogie A	k3_l
Hour glass spring	3	Spring	Bolster beam B	Bogie B	k3_l
Hour glass spring	4	Spring	Bolster beam B	Bogie B	k3_l
Coupling	Number	Type of coupling	Mass 1	Mass 2	Coupling subcommand
Vertical damper	1	Damper	Bolster beam A	Bogie A	c
Vertical damper	2	Damper	Bolster beam A	Bogie A	c
Vertical damper	3	Damper	Bolster beam B	Bogie B	c
Vertical damper	4	Damper	Bolster beam B	Bogie B	c
Coupling	Number	Type of coupling	Mass 1	Mass 2	Coupling subcommand
Bump stop	1	Non linear spring	Bolster beam A	Bogie A	p_nlin_s
Bump stop	2	Non linear spring	Bolster beam B	Bogie B	p_nlin_s
Coupling	Number	Type of coupling	Mass 1	Mass 2	Coupling subcommand
Traction rod	1	Spring and damper	Bolster beam A	Bogie A	k and c
Traction rod	2	Spring and damper	Bolster beam A	Bogie A	k and c
Traction rod	3	Spring and damper	Bolster beam B	Bogie B	k and c
Traction rod	4	Spring and damper	Bolster beam B	Bogie B	k and c
Coupling	Number	Type of coupling	Mass 1	Mass 2	Coupling subcommand
Lateral damper	1	Damper	Bolster beam A	Bogie A	c
Lateral damper	2	Damper	Bolster beam B	Bogie B	c
Coupling	Number	Type of coupling	Mass 1	Mass 2	Coupling subcommand
Chevron spring	1	Spring and damper	Bogie A	Axle 1	p_lin36
Chevron spring	2	Spring and damper	Bogie A	Axle 1	p_lin36
Chevron spring	3	Spring and damper	Bogie A	Axle 2	p_lin36
Chevron spring	4	Spring and damper	Bogie A	Axle 2	p_lin36
Chevron spring	5	Spring and damper	Bogie B	Axle 5	p_lin36
Chevron spring	6	Spring and damper	Bogie B	Axle 5	p_lin36
Chevron spring	7	Spring and damper	Bogie B	Axle 6	p_lin36
Chevron spring	8	Spring and damper	Bogie B	Axle 6	p_lin36
Couplings on frames under car C					
Coupling	Number	Type of coupling	Mass 1	Mass 2	Coupling subcommand
Coil spring	1	Spring	Car body C	Upper frame 1	k3_l
Coil spring	2	Spring	Car body C	Upper frame 1	k3_l
Coil spring	3	Spring	Car body C	Upper frame 1	k3_l
Coil spring	4	Spring	Car body C	Upper frame 1	k3_l
Coil spring	5	Spring	Car body C	Upper frame 2	k3_l
Coil spring	6	Spring	Car body C	Upper frame 2	k3_l
Coil spring	7	Spring	Car body C	Upper frame 2	k3_l
Coil spring	8	Spring	Car body C	Upper frame 2	k3_l

Coupling	Number	Type of coupling	Mass 1	Mass 2	Coupling subcommand
Vertical damper	1	Damper	Car body C	Upper frame 1	c
Vertical damper	2	Damper	Car body C	Upper frame 1	c
Vertical damper	3	Damper	Car body C	Upper frame 2	c
Vertical damper	4	Damper	Car body C	Upper frame 2	c
Coupling	Number	Type of coupling	Mass 1	Mass 2	Coupling subcommand
Anti-pitch bar	1	Spring and damper	Car body C	Upper frame 1	k and c
Anti-pitch bar	2	Spring and damper	Car body C	Upper frame 2	k and c
Coupling	Number	Type of coupling	Mass 1	Mass 2	Coupling subcommand
Bump stop	1	Non linear spring	Car body C	Upper frame 1	p_nlin_s
Bump stop	2	Non linear spring	Car body C	Upper frame 2	p_nlin_s
Coupling	Number	Type of coupling	Mass 1	Mass 2	Coupling subcommand
Traction rod	1	Spring and damper	Car body C	Upper frame 1	k and c
Traction rod	2	Spring and damper	Car body C	Upper frame 1	k and c
Traction rod	3	Spring and damper	Car body C	Upper frame 2	k and c
Traction rod	4	Spring and damper	Car body C	Upper frame 2	k and c
Coupling	Number	Type of coupling	Mass 1	Mass 2	Coupling subcommand
Lateral damper	1	Damper	Car body C	Upper frame 1	c
Lateral damper	2	Damper	Car body C	Upper frame 2	c
Coupling	Number	Type of coupling	Mass 1	Mass 2	Coupling subcommand
Slewing ring	1	Spring and damper	Upper frame 1	Lower frame 1	p_lin36
Slewing ring	2	Spring and damper	Upper frame 2	Lower frame 2	p_lin36
Coupling	Number	Type of coupling	Mass 1	Mass 2	Coupling subcommand
Primary suspension	1	Spring and damper	Upper frame 1	Lower frame 1	p_lin36
Primary suspension	2	Spring and damper	Upper frame 1	Lower frame 1	p_lin36
Primary suspension	3	Spring and damper	Upper frame 2	Lower frame 2	p_lin36
Primary suspension	4	Spring and damper	Upper frame 2	Lower frame 2	p_lin36
Couplings on wheels and axles					
Coupling	Number	Type of coupling	Mass 1	Mass 2	Coupling subcommand
Rubber rings	1	Spring and damper	Axle and hub 1	Wheel ring 1	p_lin36
Rubber rings	2	Spring and damper	Axle and hub 1	Wheel ring 2	p_lin36
Rubber rings	3	Spring and damper	Axle and hub 2	Wheel ring 3	p_lin36
Rubber rings	4	Spring and damper	Axle and hub 2	Wheel ring 4	p_lin36
Rubber rings	9	Spring and damper	Axle and hub 5	Wheel ring 9	p_lin36
Rubber rings	10	Spring and damper	Axle and hub 5	Wheel ring 10	p_lin36
Rubber rings	11	Spring and damper	Axle and hub 6	Wheel ring 11	p_lin36
Rubber rings	12	Spring and damper	Axle and hub 6	Wheel ring 12	p_lin36
Coupling	Number	Type of coupling	Mass 1	Mass 2	Coupling subcommand
Rubber rings	5	Spring and damper	Wheel ring 5	Wheel hub 5	p_lin36
Rubber rings	6	Spring and damper	Wheel ring 6	Wheel hub 6	p_lin36
Rubber rings	7	Spring and damper	Wheel ring 7	Wheel hub 7	p_lin36
Rubber rings	8	Spring and damper	Wheel ring 8	Wheel hub 8	p_lin36

The complete couplings on tram vehicle M32 can be seen in table A7.2.

Table A7.2 – Summary for the different coupling types used between components on M32 model

Couplings Between car bodies					
Coupling	Number	Type of coupling	Mass 1	Mass 2	Coupling subcommand
Joint	1	Spring and damper	Car body A	Car body B	p_lin36
Joint	2	Spring and damper	Car body A	Car body B	p_lin36
Joint	3	Spring and damper	Car body B	Car body C	p_lin36
Joint	4	Spring and damper	Car body B	Car body C	p_lin36
Joint	5	Spring and damper	Car body C	Car body D	p_lin36
Joint	6	Spring and damper	Car body C	Car body D	p_lin36
Joint	7	Spring and damper	Car body D	Car body E	p_lin36
Joint	8	Spring and damper	Car body D	Car body E	p_lin36
Coupling	Number	Type of coupling	Mass 1	Mass 2	Coupling subcommand
Oscillation damper	1	Damper	Car body A	Car body B	c
Oscillation damper	2	Damper	Car body A	Car body B	c
Oscillation damper	3	Damper	Car body B	Car body C	c
Oscillation damper	4	Damper	Car body B	Car body C	c
Oscillation damper	5	Damper	Car body C	Car body D	c
Oscillation damper	6	Damper	Car body C	Car body D	c
Oscillation damper	7	Damper	Car body D	Car body E	c
Oscillation damper	8	Damper	Car body D	Car body E	c
Couplings between bogies					
Coupling	Number	Type of coupling	Mass 1	Mass 2	Coupling subcommand
Secondary spring	1	Spring	Car body A	Bogie 1	k3_1
Secondary spring	2	Spring	Car body A	Bogie 1	k3_1
Secondary spring	3	Spring	Car body A	Bogie 1	k3_1
Secondary spring	4	Spring	Car body A	Bogie 1	k3_1
Secondary spring	5	Spring	Car body C	Bogie 2	k3_1
Secondary spring	6	Spring	Car body C	Bogie 2	k3_1
Secondary spring	7	Spring	Car body C	Bogie 2	k3_1
Secondary spring	8	Spring	Car body C	Bogie 2	k3_1
Secondary spring	9	Spring	Car body E	Bogie 3	k3_1
Secondary spring	10	Spring	Car body E	Bogie 3	k3_1
Secondary spring	11	Spring	Car body E	Bogie 3	k3_1
Secondary spring	12	Spring	Car body E	Bogie 3	k3_1
Coupling	Number	Type of coupling	Mass 1	Mass 2	Coupling subcommand
Vertical damper	1	Damper	Car body A	Bogie 1	p_nlin_s
Vertical damper	2	Damper	Car body A	Bogie 1	p_nlin_s
Vertical damper	3	Damper	Car body A	Bogie 1	p_nlin_s
Vertical damper	4	Damper	Car body A	Bogie 1	p_nlin_s
Vertical damper	5	Damper	Car body C	Bogie 2	p_nlin_s
Vertical damper	6	Damper	Car body C	Bogie 2	p_nlin_s
Vertical damper	7	Damper	Car body C	Bogie 2	p_nlin_s
Vertical damper	8	Damper	Car body C	Bogie 2	p_nlin_s
Vertical damper	9	Damper	Car body E	Bogie 3	p_nlin_s
Vertical damper	10	Damper	Car body E	Bogie 3	p_nlin_s
Vertical damper	11	Damper	Car body E	Bogie 3	p_nlin_s
Vertical damper	12	Damper	Car body E	Bogie 3	p_nlin_s
Coupling	Number	Type of coupling	Mass 1	Mass 2	Coupling subcommand
Lateral damper	1	Damper	Car body A	Bogie 1	p_nlin_s
Lateral damper	2	Damper	Car body A	Bogie 1	p_nlin_s
Lateral damper	3	Damper	Car body C	Bogie 2	p_nlin_s
Lateral damper	4	Damper	Car body C	Bogie 2	p_nlin_s
Lateral damper	5	Damper	Car body E	Bogie 3	p_nlin_s
Lateral damper	6	Damper	Car body E	Bogie 3	p_nlin_s
Coupling	Number	Type of coupling	Mass 1	Mass 2	Coupling subcommand
Longitudinal damper	1	Damper	Car body A	Bogie 1	p_nlin_s
Longitudinal damper	2	Damper	Car body A	Bogie 1	p_nlin_s
Longitudinal damper	3	Damper	Car body C	Bogie 2	p_nlin_s
Longitudinal damper	4	Damper	Car body C	Bogie 2	p_nlin_s

Longitudinal damper	5	Damper	Car body E	Bogie 3	p_nlin_s
Longitudinal damper	6	Damper	Car body E	Bogie 3	p_nlin_s
Coupling	Number	Type of coupling	Mass 1	Mass 2	Coupling subcommand
Primary suspension	1	Spring and damper	Bogie 1	Wheel beam 1	p_lin36
Primary suspension	2	Spring and damper	Bogie 1	Wheel beam 1	p_lin36
Primary suspension	3	Spring and damper	Bogie 1	Wheel beam 1	p_lin36
Primary suspension	4	Spring and damper	Bogie 1	Wheel beam 1	p_lin36
Primary suspension	5	Spring and damper	Bogie 1	Wheel beam 2	p_lin36
Primary suspension	6	Spring and damper	Bogie 1	Wheel beam 2	p_lin36
Primary suspension	7	Spring and damper	Bogie 1	Wheel beam 2	p_lin36
Primary suspension	8	Spring and damper	Bogie 1	Wheel beam 2	p_lin36
Primary suspension	9	Spring and damper	Bogie 2	Wheel beam 3	p_lin36
Primary suspension	10	Spring and damper	Bogie 2	Wheel beam 3	p_lin36
Primary suspension	11	Spring and damper	Bogie 2	Wheel beam 3	p_lin36
Primary suspension	12	Spring and damper	Bogie 2	Wheel beam 3	p_lin36
Primary suspension	13	Spring and damper	Bogie 2	Wheel beam 4	p_lin36
Primary suspension	14	Spring and damper	Bogie 2	Wheel beam 4	p_lin36
Primary suspension	15	Spring and damper	Bogie 2	Wheel beam 4	p_lin36
Primary suspension	16	Spring and damper	Bogie 2	Wheel beam 4	p_lin36
Primary suspension	17	Spring and damper	Bogie 3	Wheel beam 5	p_lin36
Primary suspension	18	Spring and damper	Bogie 3	Wheel beam 5	p_lin36
Primary suspension	19	Spring and damper	Bogie 3	Wheel beam 5	p_lin36
Primary suspension	20	Spring and damper	Bogie 3	Wheel beam 5	p_lin36
Primary suspension	21	Spring and damper	Bogie 3	Wheel beam 6	p_lin36
Primary suspension	22	Spring and damper	Bogie 3	Wheel beam 6	p_lin36
Primary suspension	23	Spring and damper	Bogie 3	Wheel beam 6	p_lin36
Primary suspension	24	Spring and damper	Bogie 3	Wheel beam 6	p_lin36
Coupling	Number	Type of coupling	Mass 1	Mass 2	Coupling subcommand
Bump stop	1	Non linear spring	Car body A	Bogie 1	p_nlin_s
Bump stop	2	Non linear spring	Car body A	Bogie 1	p_nlin_s
Bump stop	3	Non linear spring	Car body C	Bogie 2	p_nlin_s
Bump stop	4	Non linear spring	Car body C	Bogie 2	p_nlin_s
Bump stop	5	Non linear spring	Car body E	Bogie 3	p_nlin_s
Bump stop	6	Non linear spring	Car body E	Bogie 3	p_nlin_s
Couplings between wheels and wheel beams					
Coupling	Number	Type of coupling	Mass 1	Mass 2	Coupling subcommand
Journal box	1	Spring and damper	Wheel 1	Wheel beam 1	p_lin36
Journal box	2	Spring and damper	Wheel 2	Wheel beam 1	p_lin36
Journal box	3	Spring and damper	Wheel 3	Wheel beam 2	p_lin36
Journal box	4	Spring and damper	Wheel 4	Wheel beam 2	p_lin36
Journal box	5	Spring and damper	Wheel 5	Wheel beam 3	p_lin36
Journal box	6	Spring and damper	Wheel 6	Wheel beam 3	p_lin36
Journal box	7	Spring and damper	Wheel 7	Wheel beam 4	p_lin36
Journal box	8	Spring and damper	Wheel 8	Wheel beam 4	p_lin36
Journal box	9	Spring and damper	Wheel 9	Wheel beam 5	p_lin36
Journal box	10	Spring and damper	Wheel 10	Wheel beam 5	p_lin36
Journal box	11	Spring and damper	Wheel 11	Wheel beam 6	p_lin36
Journal box	12	Spring and damper	Wheel 12	Wheel beam 7	p_lin36

Appendix 8 – Calculation of the secondary springs for M32

The shear stiffness of the secondary suspension spring for the motor bogies has been calculated by using the finite element method in the software ANSYS. The geometry of the spring was given by measuring the spring. Measurements of compression force vs deformation have been done earlier by SP [25]. The characteristics of the secondary spring can be seen in figure A8.1 below.

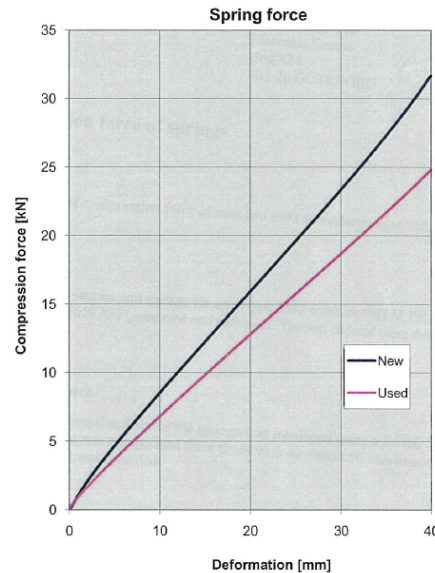


Figure A8.1 – Results of the force vs displacement measure on a new and used secondary spring. The spring is attached in between the car body and bogie on tram vehicle M32.

On the horizontal axis the compression deformation is shown, and on the vertical axis the spring compression force is shown. The blue curve represents the characteristics for a new secondary spring and the red curve the characteristics for a used spring. The spring characteristics are almost linear and the result of the stiffness from the report is shown below.

$$\begin{cases} k_{new} = 0.77 \text{ kN/mm} \\ k_{old} = 0.65 \text{ kN/mm} \end{cases} \quad (\text{A8.1})$$

For the FE-analysis it is assumed that the stiffness of the spring is linear in compression and hence also has the same behaviour for pure shear loads. The linear characteristic in compression is almost true according to the SP compression test and figure A8.1. The material of the spring is rubber and this gives a Poisson's ratio of $\nu = 0.5$. Due to that the Poisson's ratio and the stiffness of the spring is known, an iteration procedure can be used to calculate the Young's modulus. For the analysis the Poisson's ratio was set to $\nu = 0.499$. The reason for this is due to convergence problems and the assumption of a linear elastic model. The shear modulus will go to infinity when the Poisson's ratio goes to 0.5. A vertical force of 19.5 kN was applied on the top surface of the spring. According to the stiffness characteristics for an old spring the deformation from this force should be

$$\Delta_{old} = F_v/k_{old} = 19.5/0.65 = 30 \text{ mm} \quad (\text{A8.2})$$

The Young's modulus was iterated during some analyses to get the right deformation. The results of the analyses can be seen in figure A8.2 below.

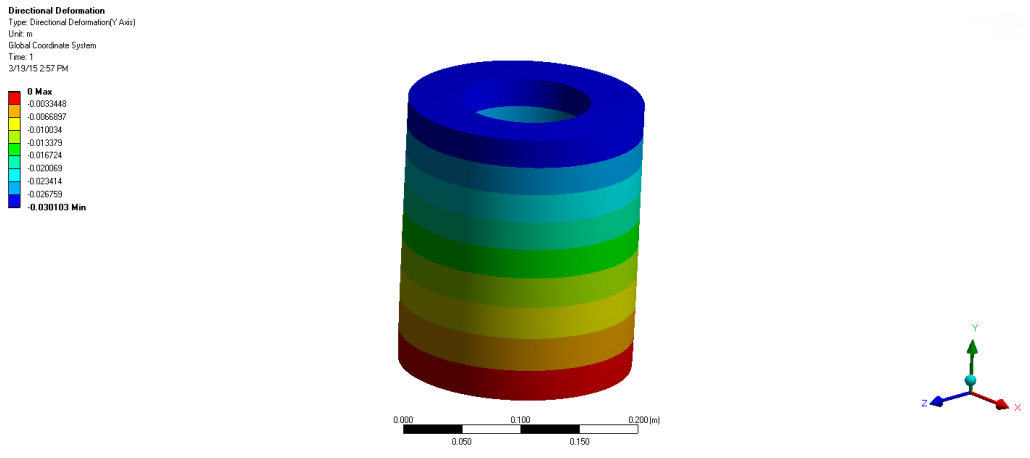


Figure A8.2 – The vertical direction deformation of the rubber spring.

A convergence analysis was also done for the secondary spring. The size of the elements was decreased a couple of times until the results of the deformation did not differ that much. A combination of sufficient result precision and reasonable computation time gave the mesh size according to figure A8.3 below.



Figure A8.3 – The mesh size used for the rubber spring.

The result of the Young's modulus is

$$E = 6.797 \text{ MPa} \quad (\text{A8.3})$$

The Young's modulus for a rubber stretches in-between 1-10 MPa [26]. The iterated value of the Young's modulus is in that range and can be considered as reasonable. This value was used for the shear stiffness analysis. A new analysis was done to obtain the shear stiffness of the spring. A horizontal load of 500 N was applied on the top surface of the spring. Furthermore, a new boundary condition on the same surface was applied to get a pure shear displacement. The deformation of the applied force can be seen in figure A8.4.

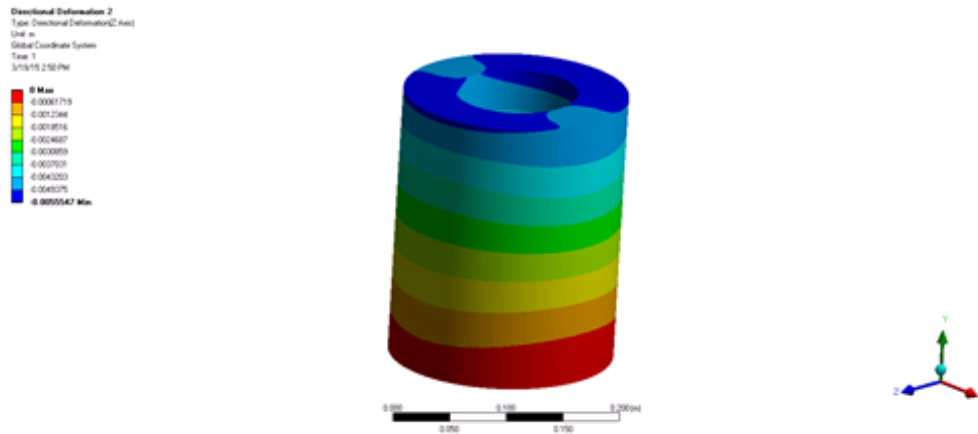


Figure A8.4 – The horizontal direction deformation for the rubber spring.

The applied force of 500 N and a shear displacement of 5.55 mm on the top surface gave the shear stiffness

$$k_s = 0.09 \text{ kN/mm} \approx 0.1 \text{ kN/mm} \quad (\text{A8.4})$$

As mentioned in the report, the trailer bogie uses coil springs (CS) as secondary suspension. The shear stiffness of these springs was calculated to be

$$k_{s,CS} = 0.21 \text{ kN/mm} \quad (\text{A8.5})$$

According to GS, the shear stiffness should be higher for the coil springs compared to the rubber ones. The FEM analysis gave this result and the value of the rubber spring can be assumed to be reasonable.

The method used to calculate the shear stiffness can be discussed. There are different ways to solve the problem and some may be better than the method used here. Although calculations of the shear stiffness was only a small part of the work and spending much time for the FEM analysis was not desirable. A decision was made to be satisfied with the given results. The shear and compression stiffness was used in GENSY when modelling the rubber spring.

A revision document written by Ansaldobreda shows that the shear stiffness of this rubber spring is below a maximum goal value of [27]:

$$k_{a,goal} = 0.14 \text{ kN/mm} \quad (\text{A6.6})$$

This fact supports the results from the FEM analysis performed on the spring. Furthermore, the FE analysis is done on a used spring. This means that the shear stiffness of the spring should be lower than the maximum goal value.